Contributions of information theory and compressed sampling to spectrum monitoring

Lap Luat Nguyen

To cite this version:

Lap Luat Nguyen. Contributions of information theory and compressed sampling to spectrum monitoring. Electronics. Université de Bretagne occidentale - Brest, 2020. English. NNT : 2020BRES0024 . tel-03373105

HAL Id: tel-03373105

https://theses.hal.science/tel-03373105

Submitted on 11 Oct 2021

DOCTORAT
BRETAGNE
LOIRE / MATHSTIC

Université de Bretagne Occidentale

THÈSE DE DOCTORAT DE

L'UNIVERSITÉ DE BRETAGNE OCCIDENTALE

ÉCOLE DOCTORALE N° 601
Mathématiques et Sciences et Technologies
de l'Information et de la Communication
Spécialité : Télécommunications

Par
Lap Luat NGUYEN

« Apports de la théorie de l'information et de l'échantillonnage compressé pour la surveillance du spectre »

« Contributions of Information Theory and Compressed Sampling to Spectrum Monitoring »

Thèse présentée et soutenue à Brest, le 10/06/2020
Unité de recherche : Lab-STICC, CNRS, UMR 6285, F-29200, Brest

Rapporteurs avant soutenance :

Salah BOURENNANE	Professeur des universités, Ecole Centrale de Marseille
Yannis POUSSET	Professeur des universités, Université de Poitiers

Composition du Jury :

Président :	Marion BERBINEAU	Directeur de Recherche, Université Gustave Eiffel
Examinateur :	Gilles BUREL	Professeur des universités, Université de Bretagne Occidentale
Dir. de thèse :	Roland GAUTIER	Maître de Conférences Hors Classe, HDR, Université de Bretagne Occidentale
Encadrant :	Anthony FICHE	Maître de Conférences, Université de Bretagne Occidentale
	Salah BOURENNANE	Professeur des universités, Ecole Centrale de Marseille
	Yannis POUSSET	Professeur des universités, Université de Poitiers

Invité(s) :

Laurent CHAPEL	Responsable projets, Syrlinks - CESSON-SEVIGNE
Guy JESTIN	Responsable du laboratoire de Conversion de Signal, DGA MI - BRUZ

CONTENTS

ACKNOWLEDGEMENT

Foremost, I would like to convey my deeply gratitude to my director of thesis, Assoc. Prof. Roland GAUTIER, for his direction, teaching and encouragement during my PhD research. Accompanied with his enthusiasm, his advises in my professional and personal life helped me to open a new gate of my life. Lastly, his good virtues remain in my mind for all my career and my life.

Besides, I cannot find a word to express my profound gratitude to my supervisor, Assoc. Prof. Anthony FICHE, who has accompanied me from the beginning of my study. His help, his advice, his supports and his encouragements became my motivation, for every single day, to pursuit my research. All the memories, the souvenirs, the working time and life time in France and in United States, I will keep in my heart. A great thanks to my teacher, my colleague and my friend as well.

Also, I am grateful to the all the professors of UBO Brest and IUT Quimper - Lab-STICC/CACS/COM team. Especially, to Prof. Emanuel RADOI and Prof. Gilles BUREL, who have donated their priceless comments and advice to my works and played an important role to my thesis project. Moreover, the assists of Assoc. Prof. El-Houssain BAGHIOUS, Assoc. Prof. Roua YOUSSEF and Assoc. Prof. Mélanie MARAZIN are that what I could not repay. I really appreciate.

In addition, I would like to thank Prof. Duy H. N. Nguyen in San Diego State University for treating me so kind during my stay in San Diego. His enthusiasm, his advice, his help and his knowledge have contributed to the completion of this project. Moreover, my appreciation conveys to the TRAN family in San Diego, for how kind they are to treat me.

I would like to thank the committee of my thesis for their encouragement, insightful comments, and constructive questions.

Last but not least, a thankful sentence to my family, for everything.

LIST OF FIGURES

LIST OF TABLES

RÉSUMÉ

Apports de la théorie de l'information et de l'échantillonnage compressé pour la surveillance du spectre

Depuis quelques années, l'explosion des technologies sans fil (communications mobiles, Internet des Objets, etc.) a entrainé une saturation des ressources spectrales disponibles. C'est le cas notamment pour les communications mobiles où le spectre fréquentiel doit être partagé entre des utilisateurs de plus en plus nombreux. L'une des idées pour faire face à ce problème est d'utiliser les bandes sous licence non occupées sans perturber l'utilisateur primaire [1]. Il est alors indispensable de surveiller le spectre afin de détecter les bandes de fréquences occupées et donc celles non occupées.

Pendant longtemps, la surveillance de spectre Radio-Fréquence (RF) a été basée sur le théorème de Shannon-Nyquist [2,3] tel que la fréquence d'échantillonnage des convertisseurs analogiques numériques (CAN) soit égale au moins au double de la fréquence maximale du support fréquentiel du signal. En pratique, cette méthode est difficilement utilisable dans le cas où l'on souhaite surveiller un spectre large-bande (typ. $F_{Nyq} > 6$ GHz) car la fréquence d'échantillonnage dépasserait très largement les caractéristiques des CANs du marché. Récemment des techniques par échantillonnage sous-Nyquist appelée également acquisition compressée, introduites par Candès [4], ont été développées afin de répondre à ce problème. Ces techniques sont efficaces dès lors que le signal est parcimonieux, c'est-à-dire que seulement une portion relativement faible des sous-bandes du support fréquentiel est active.

Le but de cette thèse a été dans un premier temps de dresser un état de l'art sur les techniques d'acquisition compressé innovantes afin de surveiller un spectre radiofréquence et de choisir le système le plus pertinent en termes de fréquence d'échantillonnage, bande passante et d'implémentation. D'après nos connaissances, le système répondant le mieux à ces contraintes est le Modulated Wideband Converter (MWC) introduit par Mishali et Eldar [5–7]. Dans un second temps, nous nous sommes intéressés à la compensation des défauts de la chaine analogique introduite par le MWC en situation réelle.

La thèse est composée de quatre chapitres où les deux premiers chapitres correspondent

à un état de l'art des techniques utilisées lors de l'acquisition compressé et notamment le MWC et les deux derniers chapitres présentent les contributions de la thèse.

Le premier chapitre présente la théorie de l'acquisition compressée. Tout d'abord, la problématique d'allocation des ressources spectrales en prenant comme exemple la France est présentée en s'appuyant sur l'exemple de la radio cognitive. Le but de la radio cognitive est de surveiller les bandes de fréquences non utilisées et de les attribuer à des utilisateurs secondaires. Traditionnellement, le théorème de Nyquist-Shannon est utilisée afin d'échantillonner convenablement un signal. L'inconvénient avec ce théorème est que la fréquence d'échantillonnage dépasserait très largement les caractéristiques des CANs du marché pour une acquisition très large bande instantanée sans avoir recours à une méthode de balayage fréquentiel par sous bandes. Pour faire face à cette limitation, des techniques dites d'acquisition compressée ont été introduites dans le but de faire l'acquisition d'un signal à partir de peu d'échantillons sous la contrainte que ce signal soit parcimonieux. Un système d'acquisition compressée se décompose en deux étapes : l'acquisition et la reconstruction. Une liste non exhaustive de systèmes physiques d'acquisition sous-Nyquist a été établie comprenant en outre l'échantillonnage non uniforme [8], le démodulateur aléatoire [9, 10] et le MWC. Notre choix s'est porté sur le MWC pour plusieurs raisons. Tout d'abord, il s'agit d'un système permettant de détecter plusieurs bandes spectrales au contraire du démodulateur aléatoire. De plus, l'échantillonnage non uniforme a comme inconvénient rédhibitoire la nécessitée d'échantillonner en respectant le critère de Nyquist. Une fois l'acquisition du signal obtenue en sortie du MWC, il est possible de reconstruire le signal d'origine à partir d'algorithmes gloutons tel que l'Orthogonal Matching Pursuit [11] retenu dans cette thèse.

Le chapitre 2 présente les aspects théoriques du MWC, le choix des paramètres garantissant de bonnes performances de reconstruction et aborde son implémentation. Le système physique du MWC est un système avec M voies en parallèle dont chacune est constituée d'un mélangeur, d'un embrouilleur de séquence de longueur L avec une fréquence de répétition F_p, d'un filtre passe-bas de largeur F_s et d'un CAN de fréquence d'échantillonnage F_s, où $(F_s/2) << F_{Nyq}$. Derrière ce modèle physique, Mishali et Eldar ont développé un modèle mathématique équivalent [6, 7] permettant de mettre le problème de reconstruction du signal d'origine sous la forme d'une équation qu'il est possible de résoudre à l'aide du formalisme de la théorie de l'acquisition compressée. En pratique, il est impossible de prendre une grande valeur de M car cela impliquerait d'avoir M embrouilleurs, M mélangeurs, M filtres et M CANs, ce qui est relativement coûteux et complexe à mettre en œuvre. Théoriquement, il est possible de contourner d'un point de vue mathématique cette contrainte en introduisant au niveau du modèle équivalent un facteur d'augmentation artificielle q du nombre de voies. Le principe va consister à construire à partir des M signaux de sortie échantillonnés à $F_s = qF_p$, q signaux échantillonnés à F_p. Virtuellement, tout va donc se passer comme si on avait qM signaux de sortie échantillonnés à $F_s = F_p$ au lieu d'avoir M signaux échantillonnés à $F_s = qF_p$. D'un point de vue matriciel, une des conditions nécessaires pour que l'on arrive à reconstruire le signal d'origine est que le nombre de voies actives s soient strictement inférieures à la taille du vecteur de sortie de MWC qui vaut qM.

Il est à noter que les séquences d'embrouillage de longueur L ont un rôle clé dans l'architecture du MWC puisque c'est elles qui vont permettre de mélanger judicieusement l'information en bande de base afin d'être en mesure de la retrouver même lors de l'échantillonnage dit sous-Nyquist. Dans la littérature, plusieurs critères sont utilisés pour choisir les séquences tels que la propriété isométrique restreinte (Restricted Isometry Property (RIP)) [12–15] ou la cohérence [16]. Nous avons fait le choix de la cohérence pour sa souplesse et sa facilité d'implémentation. Ensuite, plusieurs types de séquences ont été utilisés pour le système MWC tels que les séquences de Gold [17], Kasami [18], Hadamard [19], pseudo-aléatoires, etc. Le choix du type de séquences s'est porté sur les séquences pseudo-aléatoires pour des raisons technologiques lors de l'implémentation de la génération de ces séquences.

Une étude a été réalisée sur les paramètres clés permettant d'affirmer qu'il est possible de reconstruire correctement le signal d'origine. L'augmentation du nombre d'échantillons permet d'améliorer le taux de bonne reconstruction du spectre d'origine. En effet, la résolution fréquentielle est plus fine ce qui permet alors de détecter des émetteurs de largeur de bande étroites. Il a également été prouvé en simulation que la largeur de bande cumulée des émetteurs dans une même sous-bande active permettait d'obtenir des meilleures performances de reconstruction puisque l'information du signal est prépondérante par rapport à celle du bruit. Un autre paramètre à prendre en compte est la discrimination entre deux émetteurs proches. Le pouvoir de discrimination entre deux émetteurs est de l'ordre de la résolution fréquentielle et les performances dépendent uniquement du rapport signal à bruit.

De plus, le modèle MWC théorique fait l'hypothèse que tous les composants analogiques sont idéaux. Or en pratique cette hypothèse n'est plus vérifiée. Les mélangeurs peuvent introduire des effets non linéaires comme des harmoniques non désirées ou bien de la gigue. Les filtres passe-bas peuvent engendrer des atténuations, des problèmes de déphasage et du repliement de spectre. Les CANs peuvent générer des erreurs lors de l'étape de quantification qui peuvent éventuellement se répercuter lors de la reconstruction. Les séquences pseudo-aléatoires sont une succession rectangulaire de + ou -1. La forme des séquences peut être modifiée et il arrive également que les séquences soient désynchronisées entre elles. La matrice théorique de mélange ou de mesure utilisée lors de la reconstruction n'est plus correcte ce qui engendre de mauvaises performances.

Un état de l'art a également été réalisé pour recenser les prototypes d'acquisition compressée basés sur le MWC dont la majorité proviennent des inventeurs du MWC. La première version date de 2009 [20] avec $M = 4$, $q = 3$, $L = 108$, une largeur de bande de 2 GHz et une fréquence $F_s = 70$ MHz permettant d'avoir un taux de 14% par rapport à celui de Nyquist. La conception de la carte est assez lourde car l'ensemble des composants a dû être dimensionné les uns par rapport aux autres afin de prendre en compte l'ensemble des défauts de la chaine analogique. Une correction de cette carte a été réalisée en 2010 en introduisant une méthode de compensation des filtres passe-bas [21]. Une deuxième carte a été dimensionnée en 2014 [22] avec $M = 3$, $q = 5$, $L = 135$, une largeur de bande de 6 GHz et une fréquence $F_s = 120$ MHz permettant d'avoir un taux de 6% par rapport à celui de Nyquist. Une méthode de calibration a été proposée afin de prendre en compte les défauts de la chaine analogique dans la matrice de calibration [22]. La version la plus récente date de 2018 avec $M = 4$, $q = 5$, $L = 305$ [23], une largeur de bande de 6 GHz et une fréquence $F_s = 120$ MHz permettant d'avoir un taux de 8% par rapport à celui de Nyquist.

En 2019, l'équipe CACS/COM du lab-STICC a développé un prototype d'acquisition compressée basé sur le MWC. Le nombre de voies physiques M égal 4, le facteur d'augmentation artificielle du nombre de voies q a été fixé à 7, la taille des séquences L vaut 96, la largeur de bande a surveillée est égale à 1 GHz et la fréquence d'échantillonnage des convertisseurs F_s vaut 72 MHz. Ces paramètres permettent d'avoir un taux de 29% par rapport à celui de Nyquist et de détecter l'équivalent de 6 émetteurs symétriques ou regroupements d'émetteurs sous les conditions qu'ils occupent chacun une largeur de bande maximale $B = 9$ MHz et que celle de parcimonie au niveau des sous bandes du modèle équivalent soit vérifiée. La solution technologique retenue pour générer les séquences pseudo-aléatoires est un FPGA pour sa souplesse d'utilisation puisqu'il est possible de régénérer à la volée différents jeux de séquence. Chaque voie est constitué d'un mélangeur M1-008 de chez MArki, d'un filtre passe-bas SXLP-36+ de chez Mini-Circuits avec une fréquence de coupure à -3 dB de 40 MHz. L'acquisition des signaux est réalisée à partir d'un oscilloscope DSO90404A de chez Agilent. Pour la synchronisation des séquences, il a été indispensable d'insérer une carte ZX180-HPC VITA 57.1 connecté au trigger externe de l'oscilloscope. Une méthode de calibration (pas encore publiée) a également été proposée par l'équipe avec l'avantage de n'utiliser qu'un seul signal de calibration au lieu d'une centaine dans [22]. La méthode proposée est donc moins lourde à mettre en œuvre.

Le chapitre 3 concerne l'implémentation des filtres passe-bas dans un système MWC. En effet, le système MWC théorique suppose que tous les composants de la chaine analogique sont idéaux. Le terme filtre passe-bas idéal signifie que la réponse fréquentielle du gain est une porte, tandis que la réponse fréquentielle de la phase est nulle. Or un filtre réel est caractérisé par une réponse fréquentielle non plate du gain pour la bande passante, une bande de transition peu sélective qui va introduire des repliements de spectre lors de l'échantillonnage et une réponse fréquentielle en phase non nulle ce qui va alors apporter des modifications par rapport à la matrice de mélange théorique. Une première étude a été réalisée en simulation afin de proposer une méthode de compensation permettant de corriger les défauts introduits par des filtres classiques (Butterworth, Chebyshev I et II, Bessel). Une première méthode de compensation a été proposée où l'on suréchantillonne légèrement après le filtrage passe-bas, puis on applique un filtrage numérique afin d'éliminer le repliement de spectre, suivi d'un rééchantillonnage à la fréquence F_s et terminé par une compensation d'amplitude. Les performances en reconstruction sont très inférieures à celles obtenues avec le filtre idéal car les filtres réels introduisent des déphasages qui modifient alors la matrice de mélange. Par conséquent, la deuxième méthode de compensation a pour but d'effectuer une compensation de la phase après l'échantillonnage à F_s. Les performances de reconstruction se rapprochent de celles obtenues avec le filtre idéal ce qui prouve qu'il est indispensable de corriger la phase. Une compensation globale prenant en compte la correction du gain et de la phase a donc été proposée et a prouvé son efficacité en simulation car les performances de reconstruction sont quasi identiques à celles obtenues avec le filtre idéal. Pour prouver la pertinence de cette méthode de compensation, des tests ont été réalisés sur un filtre réel SXLP-36+ [24] en simulation et en pratique en supposant que l'ensemble des autres composants de la chaine analogique sont idéaux.

Le dernier chapitre aborde l'introduction des méthodes de quantification faible nombre de bits appliquées au MWC. Un état de l'art des différentes technologies des convertisseurs (approximation successives, pipeline, $\Sigma\Delta$) a été réalisé dans le contexte du

MWC. L'avantage des convertisseurs faible nombre de bits est d'être bon marché, d'avoir une basse consommation (intéressant pour les systèmes embarqués) et d'avoir une partie hardware simple. La principale contrainte des convertisseurs faible nombre de bits est l'erreur de quantification entre l'entrée et le signal de sortie quantifié. Pour diminuer l'erreur de quantification, il est possible de suréchantillonner le signal à l'entrée du convertisseur d'un facteur m. Il faut faire attention à la valeur de m choisie car le but du MWC est de faire l'acquisition d'un signal à un taux très inférieur à celui de Nyquist. Plusieurs convertisseurs faible nombre de bits ont été simulés, comme le convertisseur $\Sigma\Delta$ et le convertisseur uniforme Gaussien, et comparés au cas idéal. Les résultats ont permis d'arriver à un compromis entre le facteur de suréchantillonnage, le nombre de bits et le type de convertisseurs, tout en conservant des performances acceptables.

INTRODUCTION

Motivation: Spectrum sensing in Cognitive radio, Cellular network and Internet-of-things

In the context of rapid increase in wireless technology, it triggers the explosion of users who need wireless in daily life. Consequently, the demands for high data rate and ubiquitous wireless applications also grow significantly, it involves the lack of frequency bands to serve these demands. In mobile communications, the bandwidth of cellular networks has to be shared for all users, and the number of users never stops growing while the bandwidth is always limited. The frequency resource is exploited by providing a license, it will determine how much spectrum that is used based on the license of this given band [25]. Mainly because of this, it is seemingly impossible to compromise with the growing demands of wireless applications. One of the ideas to deal with this problem is to use the licensed wireless channel without affecting its owner [1]. Therefore, the term "Spectrum Sensing" [26–28] is now introduced to wireless systems in order to identify the occupied frequency bands, beside the capability of operating in a lot of different channels. It means that the goal of such new radio architectures is to operate on wideband spectrum and to detect multiple transmitted signals among many idle channels. As a result, the wideband processing system will have a potential benefit to practical applications.

One of the applications which needs wideband monitoring is cognitive radio network [29, 30]. While the frequency bands which are allocated for cellular network are nonstop using, the other bands for other applications are using inefficiently. For example, a radio channel can only broadcast their news within a few fixed hours of the day, then the rest of the day this channel will be vacant. In order to exploit this channel efficiently, other devices may be allowed to operate on this frequency band while it is vacant. This strategy is based on the definition of the cognitive network [1]. According to [31, 32], the cognitive radio has ability to detect available channels and deploy its transmissions to enable more communications and improve radio operating behavior [32]. Figure 1 shows an example of cognitive radio network structure. The network structure [33] can be considered as two groups of users. The primary users who have license and authority to access the network and exploit their spectrum bands. While the cognitive radio users do not have authority to access these spectrum bands, however, the spectrum band can be shared to the cognitive radio users based on cognitive radio principle. It helps to exploit the spectrum efficiently. The cognitive radio users can communicate each other in multi-hop ad-hoc communications or with their own infrastructure. To do this, the cognitive radio applications need to learn the environment (spectrum sensing), and every actions depend on their sensing results. This network contributes to solve the problem of the inefficient use of the spectrum resources. Thus, the system in cognitive radio network has to operate in wideband spectrum (to sense and detect). The cognitive radio system also has the capability of collecting the signal in different channels and detecting different vacant channels.

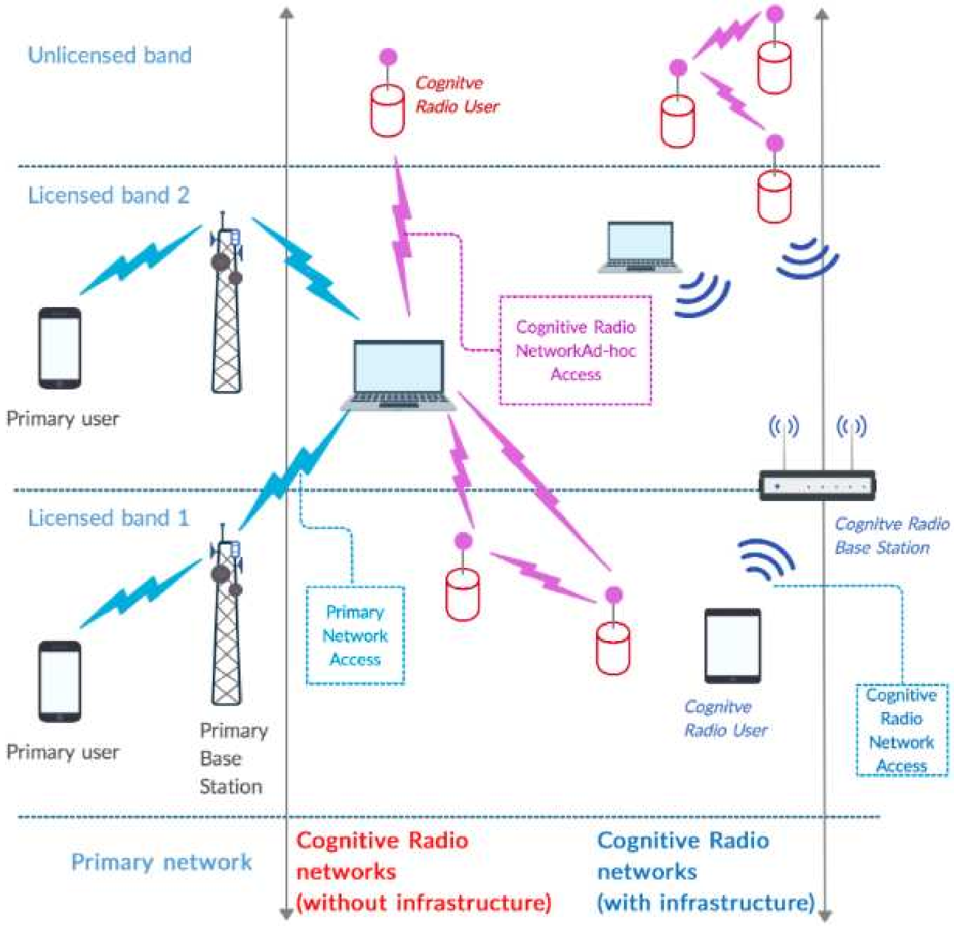

Figure 1 – Cognitive radio network structure.

One of the concerns in cognitive radio is the interference with other users, it is to ensure that the system has the ability to avoid the interference. Therefore, the parameters of interest have been proposed with respect to useful signal or interference as following [34]:

1. Central frequency, bandwidth, power level.
2. Transmission time, direction-of-arrival and localization.
3. Modulation (AM/FM/etc.) and protocol (WiFi, Bluetooth, etc.).

Another application is cellular networks where the frequency band is nonstop used. In one cell of a mobile network, the spectrum is shared for every user in this cell. The frequency band is used not only for calling data but also for a huge number of applications which need data transfer as well. In order to save and efficiently use the spectrum resources, the base stations are zoned so that the frequency band is reused at two non-adjacent base stations. However, the cell size will be reduced to serve the spectrum for the demand of high data rate of users, then, the number of users in the cell must be reduced too. While the demand of high data rate is growing day by day, the solution of small cell size is no longer practical [35]. Hence, the idea of using licensed bands as secondary users and deploying wideband sensing in cellular networks becomes a promising solution.

Moreover, there are some civilian/defense applications of spectrum sensing that can be implemented in real life. For instance, it is important to monitor and detect potential hi-tech threads in military areas such as drones around a nuclear power plant. Indeed, a drone can easily fly over the security fences and transfer weapons/explosives into the plant or track the secret operation/information. If the threads are undetected, they could bring a great danger to a large location. Another real application of wideband spectrum monitoring is to detect a lost tourist in the sea or the desert. When there is a huge number of boats concentrating on one vacation location, it is very difficult to determine one vanishing person at sea. Thus, one of the solutions is a sensing system which can monitor the wide spectrum and detect the small bandwidth occupation. Based on the cellphone signal, the monitoring system can detect that signal in a wide area and can determine the location of the victim. By this way, the applications of wideband sensing and monitoring will bring many practical benefits in many different fields and it would become a motivation to deploy the wideband sensing/monitoring system to real life. A final example among different possible solutions for spectrum sensing concerns the Internet-of-Things (IoT) such as Smart Wearable, Smart Home, Smart City, Connected Car, Health

Care, etc, in which a lot of wireless devices need to share a specific spectrum. In unlicensed or free spectrum, it can be saturated for high access demand, while other spectrum bands are idle or vacant, but cannot be used. The cognitive IoT is attractive since its ability to connect everything, share information to each device in the network and auto-make intelligent decisions or share information to humans in many applications. In this context, the cognitive radio networks and spectrum sensing for IoT applications are proposed to re-use the licensed spectrum which is not assigned to an owner or is not being used by its owner. To do that, the IoT devices need to have the cognitive capacities. Then, the spectrum sensing is an essential function in the IoT applications [36]. In the narrower scale, the IoT network needs to coexist with other networks in the unlicensed spectrum. To deploy a massive IoT application with a massive number of devices, an efficient spectrum sensing is required [37] only in unlicensed band. Moreover, the IoT is now considered as a Low Power Wide Area (LPWA) network since it usually consists in deploying low power wireless devices over a wide area network. Since the conventional or non-cellular wireless technologies can connect up to a few hundred meters maximum, then to have a long range IoT network, the trend of utilizing cellular networks for IoT networks and applications is a potential solution. Beside the long range connectivity, the LPWA network also offers some benefits such as ultra low power operation, low cost, scalability and Quality-of-Service [38]. Some of common IoT standards are being deployed in cellular network such as SIGFOX [39], LoRaWAN [40] (operate on sub-GHz) and NB-IoT [41] (coexists with LTE network). Because of the adaptation to the cellular network, the frequency bands of these standards are sub-GHz. For the NB-IoT standard, the transmitter bandwidth is 180 kHz and the spacing between transmitters is 15 kHz. The bandwidth of LoRaWAN standard is 125-500 kHz while it is 200 kHz in SIGFOX. The parameters of these standards are presented in Table 1 [42].

Technology	NB-IoT	LoRaWAN	SIGFOX
Frequency (MHz)	In-band LTE carrier, or within LTE guard bands, or standalone in re-farmed GSM spectrum	Regional sub-GHz bands	Regional sub-GHz bands
Downlink (DL) Bandwidth	180 kHz (15 kHz sub-carrier spacing)	125 kHz, 500 kHz	Base station listening bandwidth: 200 kHz, 100 Hz UL channels; 600 Hz DL channels
Uplink (UL) Bandwidth	Single-tone: 180 kHz (3.75 kHz or 15 kHz spacing) or Multitone: 180 kHz (15 kHz sub-carrier spacing)	125, 250, 500 kHz	
Maximum range/Coverage	∼164 dB	∼150-157 dB	∼146-162 dB

Table 1 – Parameters of NB-IoT, LoRaWAN and SIGFOX standards.

Consequently, blindly detecting these narrow bandwidths among a very large sensed wideband signal seems to be an attractive challenge. Likewise, the energy efficiency of IoT network is also a concern. The optimal power transmission allocation method is proposed to improve the dynamic spectrum sensing and data throughput [43]. In addition to energy efficiency for spectrum sensing, some key parameters such as frequency resolution, the bandwidth and spacing between sensing subbands have also been studied [44].

Methods and solutions

To apply wideband spectrum sensing to real life, there are numerous methods which are proposed in literature. In practice, the wideband input signal needs to be digitally converted to adapt with the post processing or formats of the post-hardware/software. Theoretically, the conversion rate, or Nyquist sampling rate, must respect the Nyquist-Shannon theorem [2, 3], in which the sampling rate is at least twice the input bandwidth to achieve a perfect reconstruction. The commercial analog-to-digital converters (ADCs) currently on the market are not able to reach the huge bandwidth required by such spectrum sensing applications, which are usually up to several tens of GHz. For information, the best ADCs used today (for example in high-end oscilloscopes with instantaneous bandwidth close to 10 GHz) are at an extremely high-cost, energy consuming and a mass of data generating requirement. To store and process the output of such ADCs, it consequently needs very fast Random Access Memories (RAMs) and processors, which are also high consuming. They are totally incompatible to the low-cost and low consumption embedded applications for IoT or cognitive radio networks.

In spectrum sensing, the transmitted signals are unknown (blind spectrum detection) and there are only a few narrow bands which contain useful information presenting behind that wide spectrum. Furthermore, digital conversion of the whole wideband signal will lead to a waste of hardware resources and energy. The requirements to have a huge resource to process and store wideband signal data are impossible to satisfy. To deal with this major challenge, plenty of research has been proposed to sample a wideband signal under the Nyquist rate, so-called sub-Nyquist sampling methods [45–47], in both theory and applications. Although in literature, a high number of research relates to this field, there are only three methods which are considered as possible and closest to the problem of sub-Nyquist sampling and the thesis perspectives. Various approaches have opened a new vision in the spectrum monitoring framework where the broadband digitization is not accessible by the conventional hardware. This will bring benefits of increasing processing range, minimizing complexity and reducing energy consumption in a sampling and monitoring wideband system.

The first one of the methods is multicoset sampling [48]. By using this method, the reconstruction scheme is expanded with the goal to detect the signal whose band locations are unknown. This method is developed based on compressed sampling technology, aiming to seek the transmitted signal from a wide dedicated area of spectrum. This method also brings a theory of lower sampling rate which is much less than Nyquist rate currently, while ensuring a good reconstruction for a wideband signal.

The second method is random demodulator [9, 10]. This is a system combining a random number of generators, a mixer, an accumulator/lowpass filter and an ADC. For the purpose to deal with sparse and band-limited signal, sparse input signal is multiplied with a pseudo-random sequence, then filtered to acquire the filtered signal which will be sampled at a lower rate relatively. The advantage of the random demodulator method encapsulates in reducing the sampling rate.

Modulated Wideband Converter (MWC) [5] is a system which blindly processes the signal in the case of sparse and wide spectrum. For operating this scheme, input signal is sampled at a lower rate than Nyquist rate. For sampling, a multi-subband signal is processed by multiplying with a periodic waveform and low-pass filtering before sampling. The goal of this operation is to capture this signal in baseband with a mix of several subbands. By taking into account the advantages of analog mixers, beside the functions of low pass filter and the ADC, this scheme brings an opportunity of applying a new technology for wideband monitoring into practice [6]. To the best of our knowledge, the MWC is recognized as the most successful and realistic solution to specify this thesis issues: sampling and reconstructing a wideband signal. In order to reconstruct the original spectrum from MWC output and sensing matrix, Compressed Sampling framework [12, 13] allows us to recover a signal sampled at below the Nyquist rate, however, must respect some conditions for the input signal and system components. In practice, the MWC can be deployed with non-ideal lowpass filters and achieves high performance of reconstruction [49, 50]. As well, a low-bit ADC with non-uniform quantization method has been demonstrated to perform better than uniform quantization at a moderate oversampling factor [51].

In recent years, the Compressed Sensing (CS) is a rapidly growing subject which has considerable attractions in many fields such as signal processing, image processing, applied mathematics, and computer science. In the scope of this thesis, only the application of CS in signal processing is focused. CS provides a structure for sensing and compressing a finite length vector input. The output of CS, which is compressed, has a reduction in length significantly compared to the signal input. In this thesis, the CS is applied to solve the problem of sensed wideband signal; the output of the sub-Nyquist sampling system is considered compressible, since its length is reduced notably compared to the wideband input. The input signal in CS is assumed sparse to ensure a correct reconstruction. The sparsity, in this study, is considered as the sparse active subbands in a wideband input signal. Generally, the CS is handled in two steps: choosing a sensing matrix and taking the measurement vector (output) from the sparse input vector. Finally, the sparse input vector is recovered from the measurement vector. This thesis aims to exploit the state-of-art of the MWC and CS technology, to monitor and detect the wideband spectrum, without any knowledge of the input signal and its frequency support. The illustration of CS in this thesis scope is shown in Figure 2, in which χ is the wideband input signal, y is the compressed version of χ and the output of the sub-Nyquist sampling system also. The sensing matrix is Φ. The problem is how to recover the wideband input signal correctly. Since the theoretical sub-Nyquist sampling system is based on ideal components (mixers, lowpass filters and ADCs) to guarantee the perfect reconstruction, the goal of this thesis is to study the imperfections of components and to produce a robust prototype of sub-Nyquist sampling scheme based on CS. Consequently, solutions to overcome these imperfections and approach the ideal components in theoretical performances need to be proposed as well.

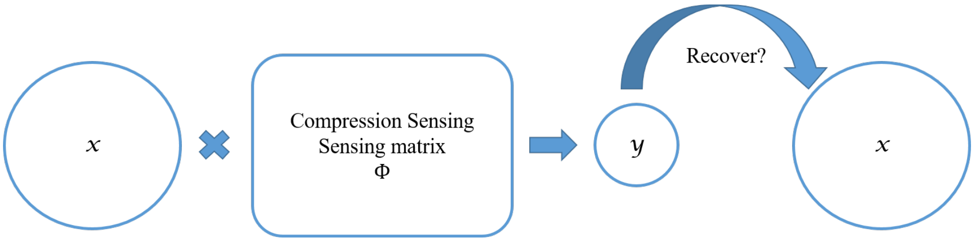

Figure 2 – Compressed Sensing concept.

Thesis organization

In Chapter 1, the framework of CS is introduced. By firstly introducing the traditional sampling technique (Nyquist-Shannon theorem), the analysis of the very first sub-Nyquist sampling scheme is made and compared to the traditional sampling one. In this chapter, some preliminary models are analyzed and compared such as Multicoset, Random Demodulator and the MWC. The rest of this chapter shows two common reconstruction algorithms: ℓ_1-minimization and greedy algorithms.

In Chapter 2, the MWC is examined to have the overview of this system. The main goal of this sub-Nyquist sampling system is to sample an unknown wideband signal at a sub-Nyquist rate. This system consists of a multi-physical channels, each channel comprises a mixer, a lowpass filter and an ADC. There are two conditions to ensure the correct reconstruction from the MWC output: the input signal must be sparse and all the MWC components (mixer, lowpass filter and ADC) must be ideal. To go further in details of the MWC, an equivalent model and the MWC condition are investigated. Beside that, this chapter also presents some pre-processing methods to detect the number of active subbands from the wideband input signal and a criteria to choose a correct mixing sequences set. The MWC can apply to many applications, thus this chapter presents a study on the impacts of transmitter signal key parameters on the IoT spectrum sensing and reconstruction. The key parameters of a wideband signal such as frequency resolution, the bandwidths of the sensed transmitters, and the frequency spacing between active subbands are analyzed. Especially, the spectrum detection of LoRaWAN 868EU (one of the common IoT standards), is simulated and evaluated with the MWC. These impacts are assessed based on the correct reconstruction and false alarm rates. At last, another study on some prototypes of the MWC are shown. Moreover, the imperfections of MWC components such as mixers, lowpass filters, ADCs and their impacts on the spectrum reconstruction are pointed out. To obtain a correct signal reconstruction, a calibration method in literature developed by Technion [22] is shown. In another approach, this chapter proposes a new calibration method using only one calibrating signal to the MWC, compared to multiple calibrating signals in referenced method [22]. The proposed calibration method can be deployed in the MWC prototype designed by our laboratory (Lab-STICC). At last, the spectrum reconstructions from this prototype are shown with different Signal-to-Noise Ratios (SNRs).

To deploy the MWC system into practice and produce a prototype of this system, Chapter 3 focuses on the implementation of non-ideal lowpass filter which is one of the main imperfections of the MWC. A post-processing method is proposed to obtain an equivalent real lowpass filter output close to the ideal one. For comparison and analysis, this chapter also investigates some common types of lowpass filter such as Butterworth, Chebyshev type I and II, Bessel. The next part illustrates the spectrum reconstructions by applying these types of real filter and the post-processing method to the MWC when the lowpass filter is simulated by such types of common filters. Simulations with different physical parameters of the MWC are presented. To extend the study to practice, this chapter also implements a commercial off-the-shelf (COTS) lowpass filter SXLP-36+ to the MWC. The COTS filter is firstly modeled and characterized. By applying the proposed post-processing method, the reconstruction performances based on the experimental MWC system signals are analyzed in function of the SNR. This chapter brings an opportunity to deploy a MWC system in practice with COTS components.

Chapter 4 extends the research to non-ideal ADC. By assuming that the mixer and the lowpass filter are ideal, this chapter studies the impact of non-ideal ADC on the spectrum reconstruction. With the goal focused on: low cost, low power consumption, low complexity and easy to implement on communications, low-bit ADC is taken into account (1-bit). In this chapter, some quantizing methods are compared: peak-to-peak quantizing, optimal Gaussian source quantizing and $\Sigma\Delta$ quantizing. This study also proposes a trade-off between oversampling factor, number of bits and type of quantizers.

To sum up the contributions of this thesis, a brief summary is shown in the last chapter.

Chapter 1

COMPRESSED SENSING/COMPRESSED SAMPLING

Theoretically, to avoid losing information when converting a signal from analog to digital, the sampling rate must be at least twice the bandwidth of the signal, according to Nyquist/Shannon theorem [2, 3]. This sampling rate, also called Nyquist rate, is not suitable to certain applications whose signal bandwidth is extremely high such as high resolution image and video processing [52], radar sensing [53] or wideband cognitive radio signal processing [54]. The Nyquist sampling in such applications becomes significantly high so that the conventional Analog-to-Digital Converters (ADCs) cannot meet.

Increasing sampling rate of a converting hardware is not a simple problem, it is related to increasing cost and power consumption. Consequently, a new method is proposed in literature to capture and present a compressible version of the wide-bandwidth signal. The compressed version of the signal is at a sampling rate typically 30% under the Nyquist rate. This method is called Compressed Sensing.

1.1 Cognitive radio, Spectrum Sensing and Compressed Sensing concepts

The spectrum is always limited, however, the demands of using radio spectrum are non-stop raising. The spectrum resources are controlled and managed by policies or regulations of each country, for example, the Federal Communications Commission (FCC) in the US [55] or the Directorate for Spectrum Control (DSC) in France (Agence nationale des fréquences (ANFR)) [56]. Figure 1.1 shows an example of spectrum allocation in France from 3 kHz to 275 GHz [57], most of the spectra for services and applications are allocated in national incorporating. The allocations concern the classification of the primary user and the secondary user, to improve the efficient utilization of the spectrum.

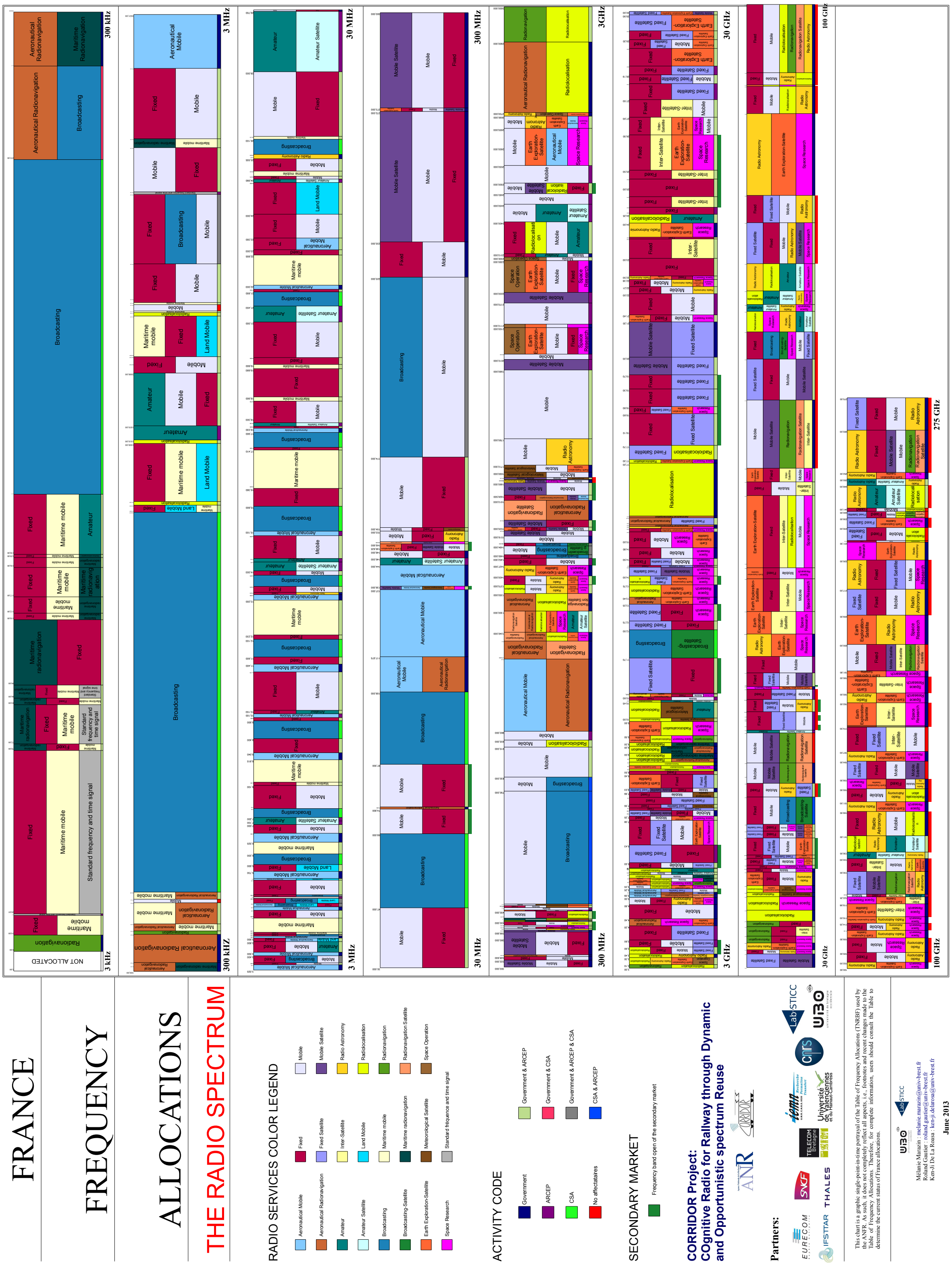

This chart is a graphic single-point-in-time portrayal of the Table of Frequency Allocations (TNRBF) used by the ANFR. As such, it does not completely reflect all aspects, i.e., footnotes and recent changes made to the Table of Frequency Allocations. Therefore, for complete information, users should consult the Table to determine the current status of France allocations.

Mélanie Marazin : melanie.marazin@univ-brest.fr
Roland Gautier : roland.gautier@univ-brest.fr
Ken-Ji De La Roasa : ken-ji.delarosa@univ-brest.fr

June 2013

Figure 1.1 – Spectrum allocation in France from 3 kHz to 275 GHz.

The spectrum is allowed to be used for those who are authorised, in other words, who keep the license. Nevertheless, the spectra are used inefficiently according to research in [27]. It stated that there is a maximum 85% of utilisation for the allocated spectrum in the US. Also, the FCC reported that some allocated channels are used frequently while the others are usually idle [58]. As explained in the previous section, the cognitive radio network [30, 32] is proposed as a solution for the efficient spectrum utilization. It allows the secondary users, without license, to use the wireless channel as long as the primary users (licensed users) are unaffected. When the channels are not used by the primary users, they are called spectrum holes. One of the main functions of cognitive radio is to detect spectrum holes [59], as in Figure 1.2 [26, 28].

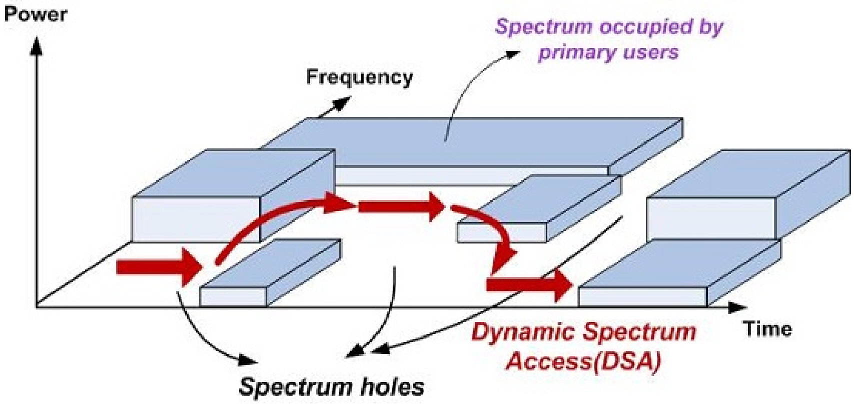

Figure 1.2 – Cognitive radio - spectrum sensing concept [26, 28].

To detect the spectrum holes, the cognitive radio network needs to know where the spectrum occupations of primary users are, thus, the spectrum sensing concept is considered as the key process of cognitive radio, followed by decision process and action process [60, 61]. Hence, once the spectrum sensing process is performed correctly, it leads to a right decision making and a right action taking after [62]. Due to the wide detecting range demand of the cognitive radio, spectrum sensing applications need to sense in a wide frequency band. The wide-bandwidth input signal is an issue that the sampling hardware needs to deal with.

1.1.1 Nyquist-Shannon theorem

In communications field, sampling theorem is a condition described by Harry Nyquist and Claude Shannon [2, 3], to be able to convert a band limited signal (continuous-time) into a digital sequence (discrete in time) samples. This method is also called Nyquist-Shannon theorem. The theorem can be simply understood as: The sampling frequency should be at least twice the maximum bandwidth of the signal, to not lose information contained in the signal. Mathematically,

$$F_s \geq 2B \tag{1.1}$$

with F_s the sampling frequency, B the bandwidth of the signal, can be considered as the highest frequency which is contained in the signal, and $F_{Nyq} = 2B$ is also called Nyquist rate.

Back to the context of spectrum sensing, in case the sensed signal raises up to several tens GHz, it will lead to the problem that the sampling rate overcomes the capability of a conventional sampling hardware. As explained above, a sampling hardware is able to reach up to several GHz sampling, however, it requires an extra power consumption, a high memory to store the output sample, and certainly a high cost to deploy. In real life applications, it is impossible to implement such a system for a huge quantity of devices necessary for the largest number of users. Consequently, methods need to be proposed to reduce the sampling rate, at sub-Nyquist rate without loss of information.

1.1.2 Papoulis generalized sampling

A very first method which was proposed in 1977 by Papoulis [63], is a generalized multichannel scheme to sample a bandlimited signal at sub-Nyquist rate. Considering that the Nyquist rate of wideband input is equal M times the ADC sampling rate F_s. In this scheme, M converters are deployed in parallel. At each channel, the bandlimited signal is sampled at a sub-Nyquist rate F_s. Thus, the sum of all channels sampling rate is equal to the Nyquist rate. This method is also called uniform interleaved sampling method.

The uniform interleaved sampling scheme provides a solution to deal with the exceeding sampling rate of a converter. Although this model is not considered as a Compressed Sensing scheme, it provides a basic overview of Compressed Sensing methods. To implement a uniform interleaved sampling scheme, a multiple-delay method is applied as in Figure 1.3, to reduce the Nyquist sampling rate F_{Nyq}.

To fully collect all samples of signal $x(t)$, the output of the second channel must come later than the output of the first channel, a T_s/M time space and so on for the other

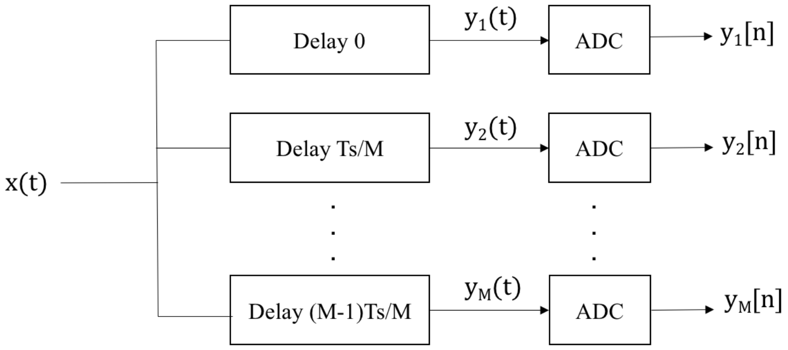

Figure 1.3 – Uniform sampling system.

channels. After that, all samples are multiplexed to have a digital output of signal $x(t)$. By taking care of this delay, this system sampling rate operates as if it is multiplied by M times, that is to say MF_s.

Nevertheless, to deal with wideband signal sampling, an ADC needs to face with two constraints:

- Nyquist sampling theorem (ADC sampling rate must be equal to input signal Nyquist rate),
- ADC input bandwidth (ADC bandwidth must be equal to input signal bandwidth).

Comparing these two constraints of a sampling system, the approach of this scheme can solve the limitation of the ADC sampling rate, however, it cannot solve the problem of the limited bandwidth of the ADCs which is generally equal to a value close to F_s. It does not fully meet the requirements of a Compressed Sampling scheme.

1.1.3 Compressed Sensing

The term Compressed Sensing, or Compressed Sampling (CS), is firstly introduced by [4,12]. It is valuable for the wideband spectrum sensing perspectives by reducing sampling rate. The reconstruction from sub-Nyquist samples, which applies CS, must respect the sparsity assumption, it means sparse active channels which occur in a wideband signal. Some real applications nowadays are built based on the framework of CS recently while the literature of this field is represented in thousands of references. Three main fields which use this technology are wireless communications, image and video processing [16]. Especially, the innovation of wireless applications tends to sense the spectrum in a large area, while desired signals usually present in some sparse channels. The meaning of CS is to handle sparse signals with a guarantee that the signal is recovered at a high probability.

In signal processing, the CS method should be considered two main stages: compressed signal acquisition stage and signal reconstruction stage. The compressed signal acquisition stage provides digital data by ADC, and choosing a suitable analog to digital converting method is also a problem in this case owing to two limitations of ADC bandwidth (ADC bandwidth must be equal to input signal bandwidth) and Nyquist sampling theorem (sampling frequency must be equal to Nyquist rate). To make it clear, Figure 1.4 introduces a general scheme of a CS device with M parallel channels.

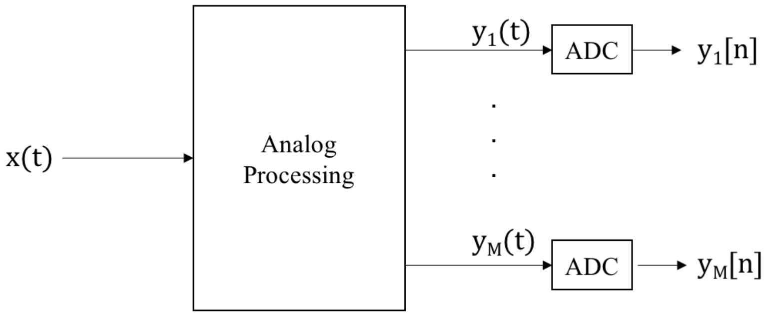

Figure 1.4 – General scheme of a CS device with M parallel channels.

This scheme is proposed to process a wide frequency band analog signal $x(t)$ which contains all the useful subbands and noise. The idea of this sampling scheme is to sample a signal at Nyquist rate which exceeds the sampling rate of a normal ADC M times. Instead of using one converter, M converters are implemented to sample the wideband signal. By copying the signal to M sub-channels, each sub-channel is also sampled by an ADC with a sampling period T_s, then $F_s = 1/T_s$ the sampling frequency of ADCs. Generally, this scheme is called multi channel sampling (except Random Demodulator, which consists of only one channel, will be explained in next the part). The key point is how to reduce the sampling rate, in other words, reduce the bandwidth of the informative part of an interest $y_i(t)$, from the wideband input signal $x(t)$. It depends on the analog processing step beforehand.

1.1.4 Compressed Sampling of sparse signal

A signal $x(t)$ is called sparse in some representation bases or dedicated bases, if and only if there is a small number of non-zero components in the well chosen representation base. Assuming that signal $x(t)$ has d-dimension and s number of non-zero elements, whereas $s \ll d$.

Let us denote $\mathbf{P} = [\mathbf{p}_1; \mathbf{p}_2; \cdots; \mathbf{p}_N]$ the measurement matrix, where vector $\mathbf{p}_i$ $(i \in [1, N])$ has the same size with input vector $\mathbf{x}$ and the size of measurement matrix $\mathbf{P}$ is $N \times d$. The measurement $\mathbf{y}$ is calculated by

$$\mathbf{y} = \mathbf{P}\mathbf{x}. \tag{1.2}$$

The term of compression is explained as, the size of vector $\mathbf{y}$ is $N \times 1$, it is much smaller than vector $\mathbf{x}$ $(d \times 1)$. That is to say, instead of sampling the signal $\mathbf{x}$ at a high rate and then compressing its sampled data, the data of $\mathbf{x}$ can be sensed directly in its compressed form $\mathbf{y}$, and sampled at a lower rate. The last part is a brief introduction about compressed sampling reconstruction methods. Figure 1.5 shows an illustration of the CS equation with the size of $\mathbf{x}$, $\mathbf{P}$ and $\mathbf{y}$.

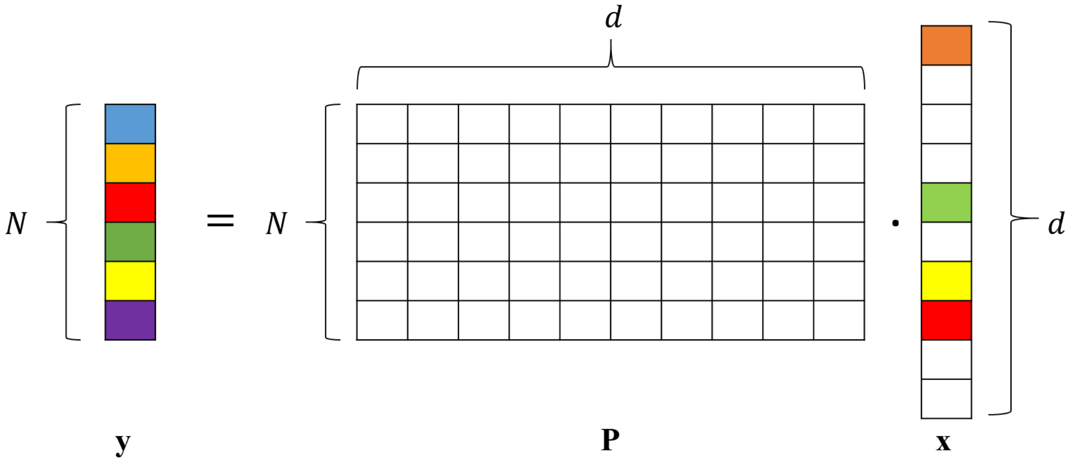

Figure 1.5 – Illustration of CS equation.

1.1.5 Compressed Sensing applications

The exceeding Nyquist rate causes many troubles in storage and process or transmission. Besides, with current systems in market, increasing sampling rate will increase cost, especially, in some applications which need high speed ADC such as high resolution radars [64] or medical scanners [16], the sampling rate of these systems cannot satisfy the demand of applications. Thus, CS allows us to face this situation with sub-Nyquist ADC rate. For instance, a sparse representation of a digital image highly compressed which is sampled below the Nyquist rate can be well-reconstructed by applying CS. Nevertheless, in the context of sparse wireless signal processing and neglecting some fields of image and video processing, there are some important factors which need to be taken into account, the retaining of relevant information from CS acquisition methods and the existence of noise are always important.

The traditional spectrum scanning/sensing methods are limited to the scan time and hardware complexity [65–70]. Moreover, these methods are also restricted to hundreds of MHz, while the demand of applications would increase to several tens of GHz. Besides, the energy consumption of these traditional systems is also in a higher demand. The implementation of CS for spectrum sensing has contributed to address such issues as energy consumption, scan time and hardware complexity. Especially, the approaches of CS in this field have expanded the range of sensing bandwidth up to several GHz. It significantly reduces the energy consumption, less than 50 times compared to the traditional method, and scan time is faster which only needs 4.4 μs for each span of scanning [71].

In photography, the CS is also deployed in a sensor of a mobile phone camera. This application can reduce the energy per image in the image acquisition process [72]. Another implementation as a single-pixel camera [73], the image quality can be improved by a number of repeated snapshots which are randomly taken from a grid. This implementation can ignore the lens of a camera while requiring a part data from a conventional image [74]. Moreover, CS can be used in applications of facial recognition [75].

Due to an enormous application of CS nowadays, this study focuses only on spectrum sensing application, a main process of cognitive radio. The next sections of this chapter present some particular sub-Nyquist sampling methods and the last part explains some common reconstruction methods of the CS technique.

1.2 Sub-Nyquist schemes for cognitive radio

A CS acquisition system is a combination of techniques that acquires a wideband signal in an economical manner, while all the useful information is stored and processed. As in the previous section, sampling methods must satisfy the two constraints: ADC rate and ADC bandwidth. Consequently, this section introduces some methods which exist in practice and should be considered as the premises to come up with a new approach in the wideband monitoring system.

1.2.1 Non-uniform interleaved sampling: Multicoset sampling

Similar to uniform interleaved sampling, non-uniform interleaved sampling [8] is proposed to handle the problem of sampling rate. However, the delays in this model are not regular in comparison with the uniform interleaved sampling, as shown in Figure 1.6.

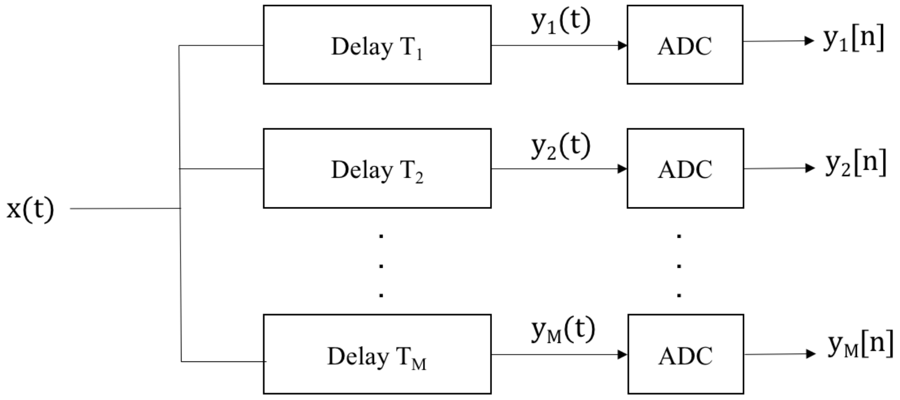

Figure 1.6 – Non-uniform interleaved sampling system.

As in the uniform interleaved sampling, by taking the delay very well, the sampling rate is considered to be reduced since it does not need to sample the entire analog signal. Nevertheless, this scheme also has the problem of input signal bandwidth. The advantage of this scheme is simpler than the uniform interleaved sampling, since the exact delay time to synchronize outputs is not necessary.

One of the methods which is developed based on non-uniform and interleaved sampling model is multicoset sampling [46, 48], this scheme is shown in Figure 1.7.

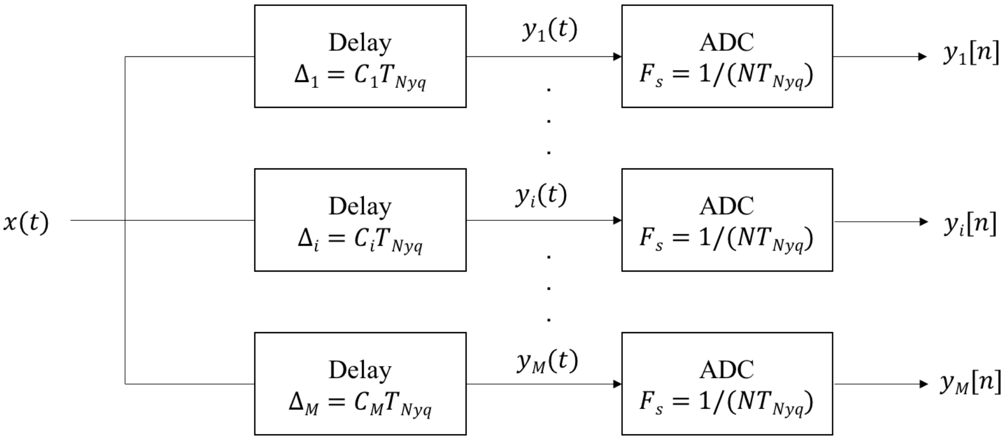

Figure 1.7 – Multicoset sampling scheme.

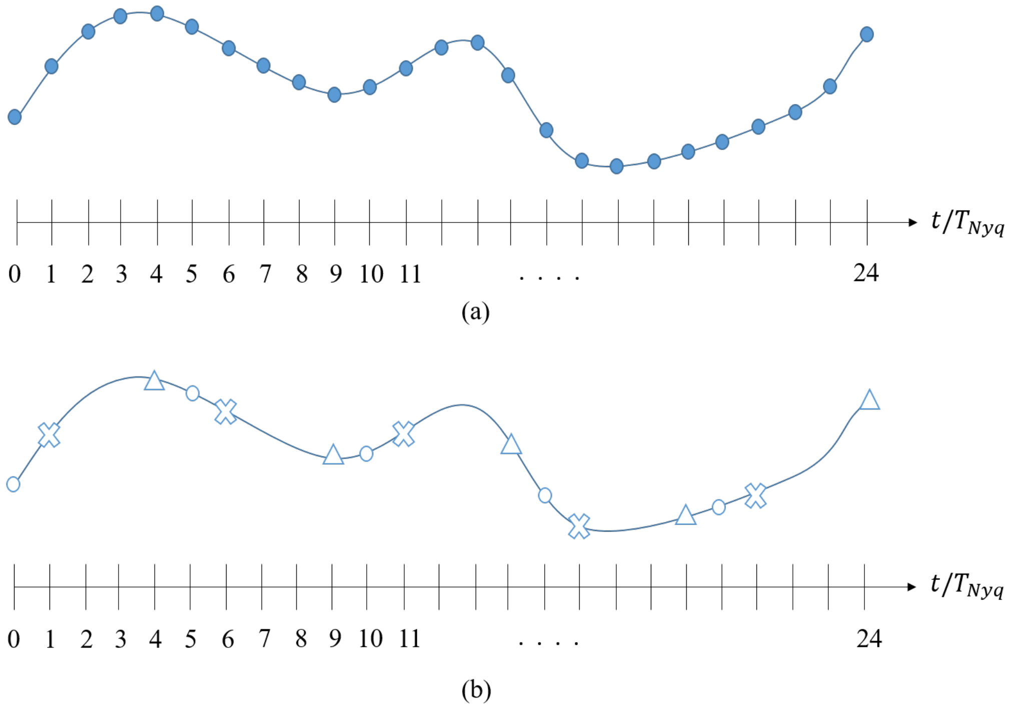

(a)

(b)

Figure 1.8 – (a) Samples at Nyquist rate. (b) Samples at multicoset sampling scheme.

A wideband input signal $x(t)$ with sparse subbands is split into M channels. At each channel, a Δ_i time delay is applied with a fixed coefficient $C_i T_{Nyq}$. Let us assume that N_e is the number of samples at Nyquist rate, then the Nyquist grid is divided into N blocks, with the cosets C_i (ordered integer) such that $0 \leq C_1 < ... < C_i < ... < C_M < (N_e - 1)/N$. At each block of N, only one sample which corresponds to the value of coset C_i^{th} is kept.

For example, if $C_i^{th} = 3$, then the 3^{rd} sample in that block is kept. Thus, at one channel of multicoset sampling scheme, there will be totally N samples which are kept. By doing so, the sampling rate of the ADCs is obviously reduced to a factor of N ($F_s = F_{Nyq} \times N$). The principle of the multicoset sampling scheme is to select $M \times N$ samples among N_e samples. Theoretically, if the number of channels of this scheme can increase such as $N \times M = N_e$, there will be no information lost and this scheme can be considered as sampling at Nyquist rate. It is impossible, however, to increase the number of physical channels in practice because it costs a high price to provide and combine a huge amount of devices as in Figure 1.7. A comparison between samples at Nyquist rate and samples at multicoset sampling scheme is depicted in Figure 1.8. In this example, the coset coefficients are taken $C_1 = 0$, $C_2 = 1$ and $C_3 = 4$.

The advantages of this method are a simple deployment into practice and a sampling rate reduction, then a conventional ADC can meet this rate. Nevertheless, the time delay in many different cosets cannot be deployed accurately. It will lead to a bad reconstruction once the delay is unpredictable. Moreover, this multicoset sampling scheme requires ADCs at low rate but in large bandwidth. It is difficult to process the signal with a large bandwidth in practice, even in before or after reconstruction. The shift elements are also an issue of this scheme, due to the difficulty of maintaining accurate time delays between ADCs [23].

1.2.2 Random Demodulation

Random Demodulator

The Random Demodulator [9,10], is a combination of one mixer, one integrator or one lowpass filter and one ADC. This scheme is depicted in Figure 1.9.

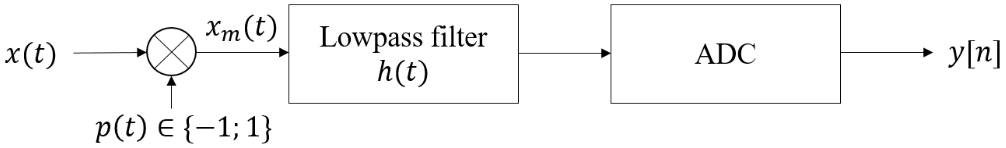

Figure 1.9 – Random Demodulator scheme.

The wideband signal $x(t)$, with sparse active subbands, is firstly multiplied with a mixing sequence $p(t)$ by a mixer. The mixing sequence alternates between -1 and $+1$ at Nyquist rate or higher [10]. This sequence is referred to as a chipping sequence, to provide the $p(t)$ continuous-time demodulation signal. Then, the mixer produces a modulated signal $x_m(t)$. Obviously, the mixing sequence can shift the spectrum of input signal from high frequency band to lower frequency band, by smearing the tone of the input across the whole spectrum. Thus, the modulated spectrum of the active subbands in $x_m(t)$ can be captured by a lowpass filter since all the spectrum information is now turned down in the low frequency band. The ADC of this scheme can work on a normal rate because the bandwidth of the input signal is reduced by the lowpass filter. The advantage of this method is that the sampling rate is reduced significantly, compared to the Nyquist rate. The second point is that the bandwidth of the ADC input is also reduced by the lowpass filter. Because the input is sparse, thus the irrelevant information should be eliminated, rather than sampling and reconstructing it.

Nevertheless, this scheme has some drawbacks that make it difficult to deploy in practice. The pseudo-random number generator needs to operate at Nyquist rate. In spectrum sensing applications, the Nyquist rate usually raises up to tens of GHz. Consequently, the conventional pseudo-random number generator devices cannot adapt to this rate. Moreover, the sensing matrix which is based on $p(t)$ (developed in Chapter 2) becomes too large (in dimension). This assumption cannot adapt for real time processing applications [76].

Modulated Wideband Converter

The MWC [5–7] scheme relies on a multi-branch of Random Demodulators, however, the fundamentals are a little different. The MWC scheme and processing stages are featured in Figure 1.10, which include the MWC physical scheme, a pre-processing stage to estimate the number of active subbands, and the reconstruction stage. This scheme is explained in detail in Chapter 2.

Generally, the MWC consists of M physical channels. Each channel has one mixer, one analog filter and one ADC. The wideband signal $x(t)$ is first mixed with a sequence $p_i(t)$ as in Random Demodulator. This mixing sequence can be any sequence which has good properties in communications such as Gold [17, 71], Zadoff-Chu [77] or Kasami [18], etc. The choice of a suitable mixing sequence and the study on the MWC will be detailed in Chapter 2. The cutoff frequency of lowpass filter is chosen $F_c = F_s/2$ for convenience, with $F_s << F_{Nyq}$ is the sampling rate of a conventional ADC. The sampling frequency in this scheme is uniform.

The MWC can solve the problem of the wideband input bandwidth and the sampling

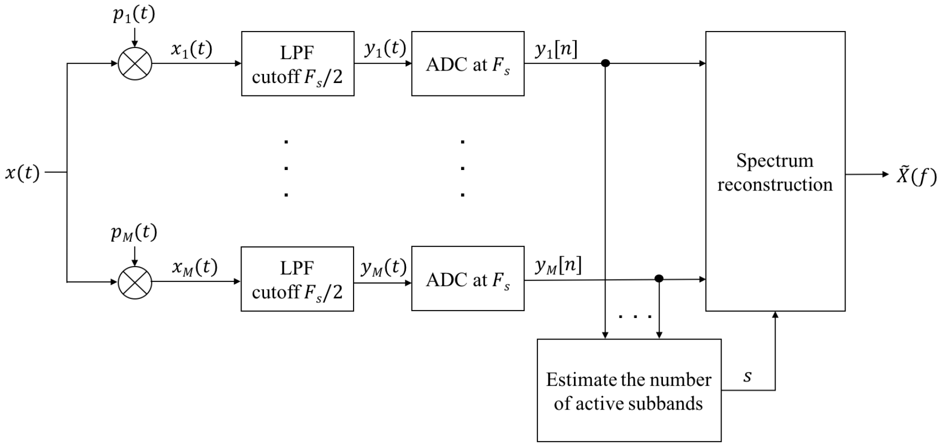

Figure 1.10 – The MWC scheme and processing stages.

rate. The advantages of this scheme is the implementation by commercial off-the-shelf (COTS) devices. It is more practical than the Random Demodulator because it can detect more active subbands than one. The drawback of this scheme is that it is based on the theoretical assumption of analog components, to ensure the correct reconstruction of the wideband input signal. Nevertheless, it is proved that the MWC non-ideal analog devices imperfections can be compensated to approach the ideal case by applying some post-processing schemes. It is possible to study some analog components imperfection, independently of the others (lowpass filter in Chapter 3, ADC in Chapter 4) or to implement a calibration method to estimate the correct sensing matrix.

1.2.3 Comparison

Generally, the potential methods such as Multicoset Sampling, Random Demodulator and MWC are possible to deploy to practice. Otherwise, they also have their drawbacks.

As depicted above, the Random Demodulator has only one physical channel, then by the help of the mixing sequence, it can detect a single discrete multitone. In fact, a sensed signal always contents a number of harmonics, then it makes this scheme is not practical [78]. The multicoset, on the other hand, has better reconstruction of multiband signal since it comprises a multi-channel scheme. Nevertheless, as introduced above, this scheme is difficult to deploy because of two limitations. First, the wide bandwidth of the signal is a big constraint of this scheme since the analog components need to work with such bandwidth. Second, the accurate time shift is also hard to maintain [79]. Due to these two limitations, the multicoset sampling seems to be hard to deploy in practice. Besides, the MWC can sample a wideband signal at sub-Nyquist rate. This scheme has good performance in multiband signal as well and by the proposed architecture, this can be deployed by commercial analog components [23, 50]. The MWC allows the ADCs to operate at a uniform rate and there is no limitation of time shift. The analog signal in this scheme is filtered at baseband, then the analog components just need to work with baseband signal, better than the multicoset sampling which deals with the wide-bandwidth signal. The limitations of this scheme are based on the impacts of the analog devices. By combining a chain of analog devices, then it increases the complexity and increases the impact of analog devices too [80]. At last, the comparisons is summarized in Table 1.1.

	MWC	**Random Demodulator**	Multicoset
Signal model	Multiband	Sparse Harmonic	Multiband
ADC bandwidth requirement	Baseband	Baseband	Nyquist bandwidth
Hardware design	Pros: - ADCs operate synchronously. Cons: - Difficult (multi-chains of analog devices, imperfections). - High rate mixing sequence.	Pros: - Simple. Cons: - High rate mixing sequence. - Analog devices imperfections.	Cons: - Difficult (multi physical channels). - Accurate time shift requirement.

Table 1.1 – Comparison table of three possible sub-Nyquist sampling methods.

1.3 Reconstruction algorithm CS

There are plenty of approaches to reconstruct a sparse input vector in the framework of CS in the literature. In this section, two common and natural reconstruction algorithms are considered: ℓ_1 minimization algorithm [81, 82] and greedy algorithm [83].

1.3.1 ℓ_1-minimization algorithms

From Equation 1.2, the measurement vector $\mathbf{y}$ is known, the input signal $\mathbf{x}$ is unknown, however, with the knowledge of sparsity of $\mathbf{x}$. A sparse input signal $\mathbf{x}$ can be recovered by solving the optimization problem

$$\hat{\mathbf{x}} = \min\{\|\mathbf{x}\|_0 : \mathbf{P}\mathbf{x} = \mathbf{y}\}. \tag{1.3}$$

The pseudo-norm $\|\mathbf{x}\|_0$ represents the number of non-zeros in vector $\mathbf{x}$ [82]. Mathematically, the optimization problems have no general algorithm to solve. The traditional algorithm to search for the root of an optimization function cannot ensure that whether this root is the global optimal. Nevertheless, the benefit of convex optimization with some specific characteristics of local optimal and global optimal can help solving the optimization problem. Because the $\|\cdot\|_0$ objective function is non-convex, then it is very difficult to solve by applying the convex optimization. Consequently, an alternative model is to replace $\|\cdot\|_0$ by $\|\cdot\|_1$ and a computationally tractable model has form

$$\hat{\mathbf{x}} = \min\{\|\mathbf{x}\|_1 : \mathbf{P}\mathbf{x} = \mathbf{y}\}. \tag{1.4}$$

This approach is so-called basic pursuit [84]. The problem ℓ_0-minimization problem can share common solutions with ℓ_1-minimization in a condition that $\mathbf{x}$ is sparse enough [82]. In practice, the system is always in case of noisy and undetermined signal sparsity. The undetermined sparsity and noisy signal can be referred to as the signal that contains a small number of elements in significant magnitude, the rest of elements are not necessarily exactly zero but in small magnitude. The extension of the CS approach can recover such a signal under these constraints as well. The ℓ_1-minimization model can be solved with the stability results and its extension form as

$$\hat{\mathbf{x}} = \min\{\|\mathbf{x}\|_1 : \|\mathbf{P}\mathbf{x} - \mathbf{y}\|_2 \leq \epsilon\}. \tag{1.5}$$

The ϵ is being determined by the noise or quantization levels. The existing methods to solve this problem are in [85–87].

1.3.2 Greedy algorithms

Generally, the equation of reconstruction process can be presented in the form

$$\mathbf{y} = \mathbf{P}\mathbf{x}. \tag{1.6}$$

Noting that:

- $\mathbf{x}$ the vector input signal which has the form of sparsity,
- $\mathbf{y}$ the vector which contains samples from compressed acquisition (measurement vector),
- $\mathbf{P}$ the measurement matrix (also called sensing matrix).

The size of each vector and matrix should be denoted

— d the length of $\mathbf{x}$,

— N the length of $\mathbf{y}$,

— $N \times d$ the size of matrix $\mathbf{P}$,

— s number of nonzero elements in $\mathbf{x}$.

It is observed that the length of $\mathbf{x}$ must be greater than $\mathbf{y}$ because of compression, then $d > N$. Moreover, the number of nonzero elements in $\mathbf{x}$ is much less than the number of elements of $\mathbf{x}$, that is to say $s \ll d$. Thus, the condition $d > N > s$ is obtained.

However, in practice the received signal always includes the noise

$$\mathbf{y} = \mathbf{P}\mathbf{x} + \mathbf{b}, \tag{1.7}$$

where $\mathbf{b}$ a vector of noise.

In parallel with the ℓ_1-minimization algorithms, the greedy algorithms are based on greedy/iterative methods for solving this problem. The principle of reconstruction is to search $\mathbf{x}$ from $\mathbf{y}$. The method to solve this problem [88] has proposed the idea of pursuit and it has brought many efficiencies. To reach the vector solution, the process is divided into many iterations. At each iteration, the vector $\mathbf{x}$ is redefined by adding nonzero components and the criterion is re-estimated. This idea can improve the criterion after each iteration. The optimal vector solution to stop the iteration, however, is unknown. It means that there is no guarantee or probability to know where the iterative algorithm should stop. Thus, these methods which propose the optimal solution to stop the iterations and obtain an optimize vector solution $\mathbf{x}$, are called greedy or iterative methods [89][90].

One of the greedy algorithms is Orthogonal Matching Pursuit (OMP) [11], which is considered as the most common method, thanks to its probability of optimum and theoretical expectations. In the next chapter, the introduction of the MWC principles, the method to determine number of active subbands, and the reconstruction methods such as Orthogonal Matching Pursuit, Compressive Sampling Matching Pursuit (CoSaMP) [91] and Iterative Hard Thresholding (ITH) [92, 93] are presented, dedicated for the specific MWC output to recover the spectrum of signal input $x(t)$.

Orthogonal Matching Pursuit: OMP

This algorithm is proposed to recover sparse signals [11]. The advantage of this method is simple not only in mathematical view but also in technical view. It is also categorized as a greedy algorithm. Suppose that the matrix $\mathbf{P}$ has size $N \times d$ and N measurements of vector $\mathbf{y}$ are known. The principle of this algorithm is step by step described as.

1. In the first iteration, the unknown vector $\mathbf{x}$ is assumed to have only null elements. Then, the column $\mathbf{P}_j$ of matrix $\mathbf{P}$, which is most correlated to the measurement vector $\mathbf{y}$, is searched.
2. At each iteration, the updated solution vector is found by adding nonzero components to the previously obtained vector $\mathbf{x}$, so that to minimize the norm of the residual vector $\mathbf{r} = \mathbf{x} - \mathbf{P}_j\mathbf{y}$, which measures the reconstruction error.
3. The iterations are stopped when s non-zero elements are added.

The description of OMP in mathematical view:

1. Firstly, the column of measurement matrix $\mathbf{P}$, called $\mathbf{P}_j$, is found by

$$\mathbf{P}_j = \arg\max_{\mathbf{P}_i \in \mathbf{P}} |\langle \mathbf{x}, \mathbf{P}_i \rangle| \quad i \in [s, d].$$

2. The next step is, the vector solution $\hat{\boldsymbol{x}}$ should be found (where $\hat{\boldsymbol{x}}$ is considered as the estimation vector of $\mathbf{x}$):

$$\hat{\boldsymbol{x}} = \arg\min_{\hat{\boldsymbol{x}} \in \mathbb{R}} \left\| \mathbf{y} - \mathbf{P}_j \times \hat{\boldsymbol{x}} \right\|.$$

   The entry of the non-zero element $\mathbf{z}_j$ in vector $\mathbf{z}$ is predicted based on $\hat{\boldsymbol{x}}$.

3. Lastly, the calculation of residual $\mathbf{r} = \mathbf{y} - \mathbf{P}_j \times \hat{\boldsymbol{x}}$ is taken, since the residual $\mathbf{r}$ is the prediction of remained elements of vector $\mathbf{z}$ regarding the columns of measurement matrix $\mathbf{P}$.
4. The algorithm is repeated until the residual is small enough (maybe there is no non-zero element in the vector residual) or $\hat{\boldsymbol{x}}$ is small enough.

Compressive Sampling Matching Pursuit: CoSaMP

The Compressive Sampling Matching Pursuit (CoSaMP) [91] allows more than one zero component to be added into the vector solution. This method uses the same algorithm as OMP and its principles as in follows

1. Firstly, the number of columns of matrix $\mathbf{P}$ (αs columns) is searched, which are the most correlated with the vector $\mathbf{r}_{k-1}$ (as for OMP, the correlation can be estimated

simply by calculating the absolute value of the cosine of the angle between each pair of vectors).

2. Then, the number of these columns is added into vector solution $\hat{\boldsymbol{x}}_{k-1}$, the vector $\hat{\boldsymbol{x}}_k$ is thus obtained.
3. The number of non-zero components in vector solution is re-estimated: $\hat{\boldsymbol{x}}_k = \mathbf{P}_k\mathbf{y}$
4. If the number of non-zero components is greater than s, there are only s strongest components that will be kept in the vector solution. The other non-zero components will be canceled.
5. The residual vector will be re-estimated: $\mathbf{r}_k = \mathbf{y} - \mathbf{P}_k\hat{\boldsymbol{x}}_k$.
6. The iteration is stopped when the norm of the residual vector falls below a certain threshold.

There is a difference between CoSaMP and OMP in that the number of αs non-zero components is added at each iteration (instead of one in OMP). As a result, CoSaMP requires fewer measurements than OMP. However, it is more difficult to apply CoSaMP into practice than OMP because of the exceeding number of non-zeros s in the vector solution.

Iterative Hard Thresholding: IHT

The basic idea of IHT [92, 93] is evaluated simply in mathematics, which can improve the performance but increase the complexity of the system. The algorithm can be summarized as follows.

1. The algorithm starts with a vector solution of all zero components.
2. The residual is estimated at each iteration.
3. By adding the number of non-zero components, which are related to the residual vector, the vector solution is re-defined.
4. There are only the strongest components which are kept (iterative thresholding).
5. The iteration stops when the norm of the residual vector falls below a certain threshold.

The ITH is considered in two steps. Thus, the entry points for the iteration k are on one hand the matrix $\mathbf{P}$ and the vector $\mathbf{x}$ (fixed elements), and on the other hand the solution vector $\hat{\boldsymbol{x}}_{k-1}$, with the iteration $k-1$ (variable element).

In the first step, the residual is firstly calculated at the iteration $k-1$

$$\mathbf{r}_{k-1} = \mathbf{x} - \mathbf{P} \times \hat{\boldsymbol{x}}_{k-1}.$$

Then, a first estimate of the solution vector at the iteration k is calculated, using the following expression

$$\hat{\boldsymbol{x}}_k^{(d)} = \hat{\boldsymbol{x}}_{k-1} + \mathbf{P}^H \mathbf{r}_{k-1}.$$

Although the calculation is different, the idea of this estimate is the same as OMP. Thus, it is clear that the elements of the vector solution that is added to $\hat{\boldsymbol{x}}_{k-1}$ to form $\hat{\boldsymbol{x}}_k^{(d)}$ that are the scalar products between the residual at the iteration $k-1$ and the columns of the matrix $\mathbf{P}$.

In the OMP method, these scalar products are used just to determine the index of the next non-zero element of the solution vector (its value is calculated in the second step), here it contributes directly to the estimation of the solution vector. This procedure therefore leads to reinforcing the components of the solution vector corresponding to the scalar products, that is to say, to the columns of the matrix $\mathbf{P}$ which are most correlated with the residual at the previous iteration.

In the second step, over the iterations, the s components of the vector $\hat{\boldsymbol{x}}_k^{(d)}$ which are strongest in absolute value need to be taken into account, however, the other components are increasingly strong, this makes the vector being not sparse. Since the scalar products between the residue $\mathbf{r}_{k-1}$ and the columns of the matrix $\mathbf{P}$ are generally non-zero. In order to make the estimation of the solution vector being sparse, a hard thresholding is applied in this step, only the s strongest components in absolute value being conserved, while the others are set to zero.

$$\hat{\boldsymbol{x}}_k = T_s\{\hat{\boldsymbol{x}}_k^{(d)}\}$$

It is noted that this approach is not very complex, since each step is essentially limited to a matrix-vector multiplication. On the other hand, experience shows that this method is not very efficient when the noise is significant.

In the next chapter, the principle of the MWC will be studied. Besides, the next chapter also shows the implementation of this scheme by addressing the imperfections of MWC analog devices and calibration methods.

CHAPTER 2

MWC: FROM THEORY TO PRACTICE

In the literature, there are a lot of approaches in the field of wideband monitoring. Among them, the Modulated Wideband Converter (MWC) proposed in [5], is considered as the most practical sub-Nyquist sampling system, since it has been implemented into analog front-end hardware [6]. The MWC is a multi-physical channel system, each physical channel consists of a chain of mixer, lowpass filter and conventional ADC. This system is a blind detector, without any knowledge of frequency supports of the input signal. To reconstruct the input signal spectrum, this scheme applies the reconstruction methods based on the CS hypothesis, which assumes the input signal to be sparse. Concentrating on the two limitations of a wideband sampling system mentioned in Chapter 1, this scheme can overcome the limitations of analog bandwidth signal and sampling rate of a sensing system. The MWC is considered as a sub-Nyquist sampling system. It should be noted that the MWC system is the patent owned by [94–98].

2.1 Theoretical background

2.1.1 MWC: physical scheme

The block diagram of the MWC is represented in Figure 2.1. The signal $x(t)$ is considered as a multi-band signal, having an unknown, sparse and wideband spectrum. The MWC consists of M physical channels. The input signal is multiplied with pseudo-random mixing sequences $p_i(t)$ $(1 \leq i \leq M)$. The idea of the mixing function $p_i(t)$ is to shift all useful subbands into baseband. Then, the lowpass filter, with the cutoff frequency $F_c = F_s/2$, stores only the baseband input signal content. The signal in this stage is confined in the interval $[-F_s/2; F_s/2]$ width. Let us assume, for convenience, that the ADC converts the filtered signal into the digital domain using a sampling rate of F_s. Then, from the sub-Nyqusit samples of signal $x(t)$, the number of active subbands s is estimated. After that, the spectrum reconstruction method based on the CS hypothesis is applied to search for the spectrum of $x(t)$.

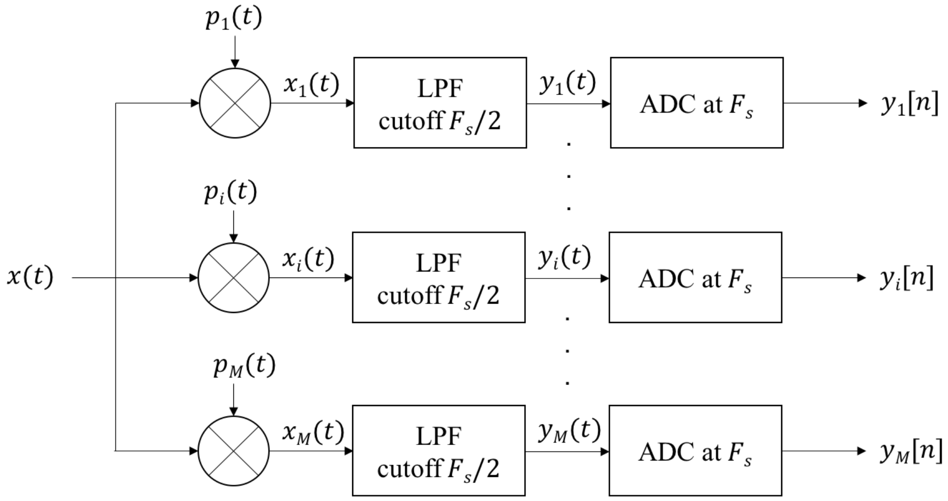

Figure 2.1 – The traditional MWC scheme.

Nevertheless, the choice of correct parameters for each component needs to be taken into account to have a correct process in digital steps after. Firstly, the mathematical equations of the system are summarized as follows. At i^{th} channel, with $1 \leq i \leq M$, $p_i(t)$ plays a role as a mixer. When signal $x(t)$ is split into M channels and then multiplied by $p_i(t)$

$$x_i(t) = p_i(t)x(t), \tag{2.1}$$

and the signal $y_i(t)$ after the lowpass filter reads as

$$y_i(t) = (h * x_i)(t), \tag{2.2}$$

with $h(t)$ the transfer function of the lowpass filter and $*$ the convolution operator. Finally, the digital signal is given by

$$y_i[n] = y_i(nT_s). \tag{2.3}$$

with T_s the sampling period.

In frequency domain, the system equations give

$$X_i(f) = (P_i * X)(f). \tag{2.4}$$

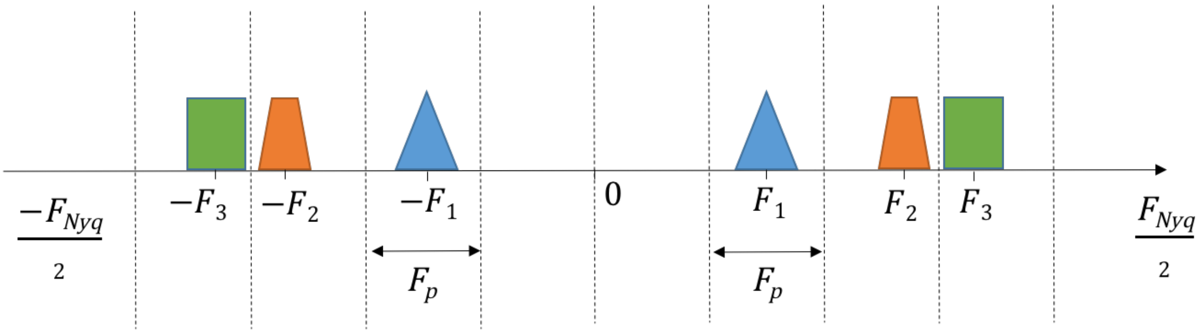

(a) Spectrum of input signal $x(t)$.

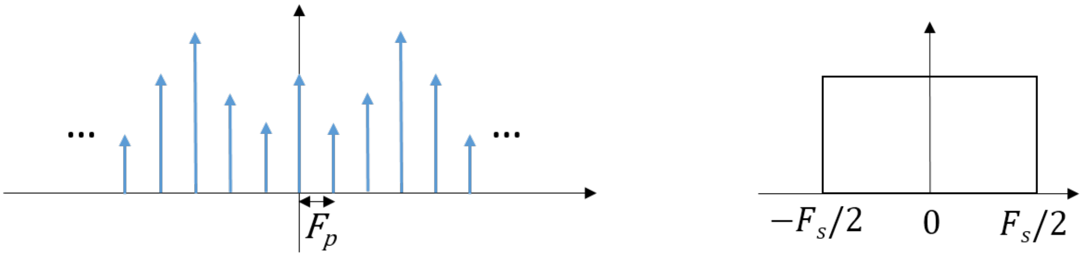

(b) Spectrum of mixing sequence.

(c) Frequency response of lowpass filter.

Figure 2.2 – Spectra of input signal, mixing sequence and frequency response of low pass filter in frequency domain.

$$Y_i(f) = H(f)X_i(f). \tag{2.5}$$

$$\tilde{Y}_i(f) = F_s \sum_{k=-\infty}^{+\infty} Y_i(f - kF_s), \tag{2.6}$$

where $\tilde{Y}_i(f)$ the Fourier transform of a sampling signal $y_i[n]$. The spectrum of input signal $X(f)$, mixing sequence $P_i(f)$ and frequency response $H(f)$ of the low pass filter could be observed in Figure 2.2. By presenting an equivalent model of the MWC, the function of each component will be examined further and in detail in the next part.

2.1.2 MWC: An equivalent model

With the size of matrix $\mathbf{P}$ and lengths of vector $\mathbf{y}$ and $\mathbf{z}$ that are found in Equation 2.15, the MWC system can be depicted by an equivalent scheme [6][7] as in Figure 2.3. In practice, the MWC has M physical channels. When M is a high number, it is difficult to deploy the MWC due to the high-cost and complex system, since each channel has one mixer, one filter and one ADC. It seems to be a constraint to go further in experimental study. Indeed, a prototype of MWC now could be expanded to 4 physical channels [6,22]. In the theoretical point of view, however, the equivalent scheme has the same functions as the MWC scheme but the mathematical expressions are different. Hence, the equivalent model can bring a better study on the MWC and its components.

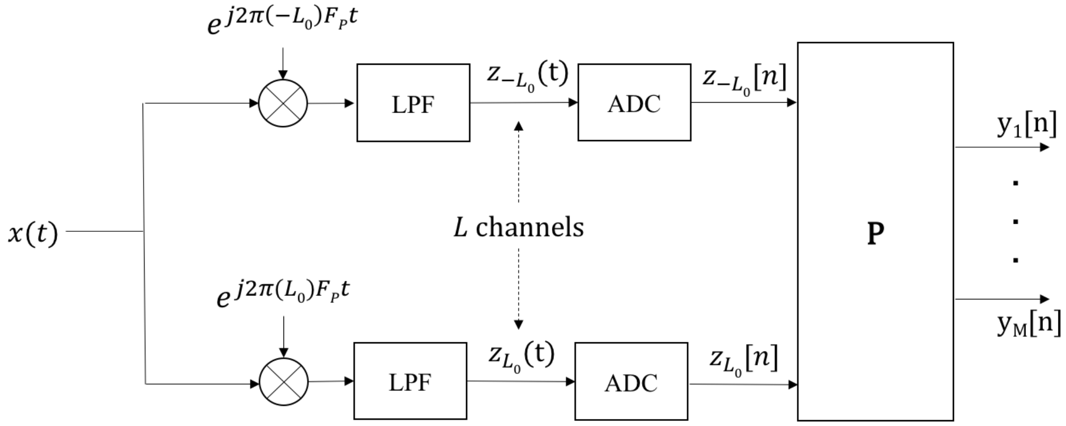

Figure 2.3 – Equivalent scheme of the MWC.

The equivalent scheme will provide exactly the same outputs as MWC because the same transfer functions are used. It is important to note that this scheme is a theoretical model, which cannot be applied in practice. The goal of this model is to deeply understand how the system works by seeking the details of every component such as how many channels M should have exactly. The sampling frequency F_s, sequences $p_i(t)$ and its repetition frequency F_p need to be examined.

Going further in details of each component, at first, supposing that $p_i(t)$ is an arbitrary waveform and it is not periodic. It leads to the infinite sequence of outputs after mixing that cannot be managed. To solve this problem and make it easier, the mixing function $p_i(t)$ is chosen as a periodic pseudo-random waveform, with the period T_p. Consequently, there is a finite output $x_i(t)$ at each physical channel. Suppose that $p_i(t)$ is also set as a piece-wise function with values varying between ± 1. The mixing function $p_i(t)$ is illustrated in Figure 2.4. Moreover, the sampling period of the conventional ADC is T_s. In the Nyquist bandwidth F_{Nyq}, let us denote L the ratio between F_{Nyq} and F_p, with $L = F_{Nyq}/F_p$. It means that in the Nyquist bandwidth, there are L subbands with F_p bandwidth. The goal of the MWC is to detect the active subbands l where the transmitters of input $x(t)$ are located, with $L = 2L_0 + 1$ and $-L_0 \leq l \leq L_0$.

The mixer $p_i(t)$ is periodic with period T_p, then $F_p = 1/T_p$ the repetition frequency

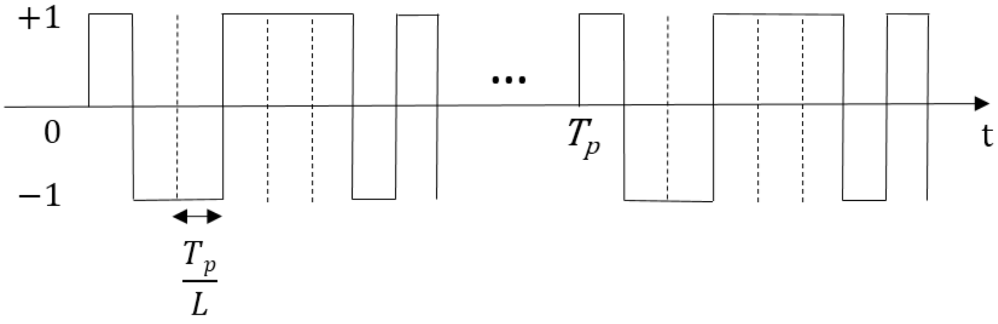

Figure 2.4 – Mixing function $p_i(t)$.

of the mixing function. The main purpose of this function is to shift all the spectrum of input signal into baseband, in frequency domain, function $p_i(t)$ can be written as

$$P_i(f) = \sum_{l=-L_0}^{+L_0} p_{il}\delta(f - lF_p). \tag{2.7}$$

It means that the input spectrum $X(f)$ is shifted a multiple of l of F_p. Figure 2.5 shows an example of the shifted spectra after multiplying with the mixing function in Matlab. In this case, L is taken 96 channels, and $M = 4$, $F_{Nyq} = 1$ GHz.

In time domain, $p_i(t)$ has form

$$p_i(t) = \sum_{l=-L_0}^{+L_0} p_{il}e^{j2\pi lF_pt}, \tag{2.8}$$

in which, p_{il} the Fourier complex coefficient derived from $p_i(t)$.

$$p_{il} = F_p \int_{-T_p/2}^{T_p/2} p_i(t)e^{-j2\pi lF_pt}dt. \tag{2.9}$$

By combining the system equations (Equations 2.4 to 2.6) above, the output of the

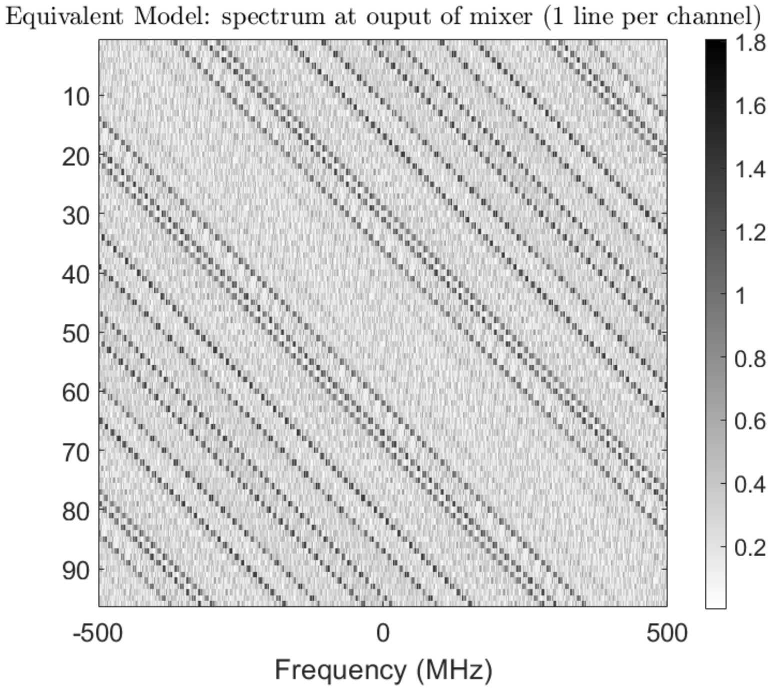

Figure 2.5 – Shifted spectra in the output of the mixer.

MWC in frequency domain is

$$\begin{aligned}\tilde{Y}_i(f) &= F_s \sum_{k=-\infty}^{+\infty} H(f-kF_s)(P_i * X)(f-kF_s) \\ &= F_s H(f-kF_s) \sum_{k=-\infty}^{+\infty} (P_i * X)(f-kF_s).\end{aligned} \tag{2.10}$$

Therefore, with $P_i(f) = \sum_{l=-L_0}^{+L_0} p_{il}\delta(f-lF_p)$, the output $\tilde{Y}_i(f)$ can be rewritten

$$\begin{aligned}\tilde{Y}_i(f) &= F_s H(f-kF_s) \sum_{l=-L_0}^{+L_0} \sum_{k=-\infty}^{+\infty} p_{il} X(f-lF_p-kF_s) \\ &= \sum_{l=-L_0}^{+L_0} p_{il} \left\{ F_s \sum_{k=-\infty}^{+\infty} H(f-kF_s) X(f-lF_p-kF_s) \right\}.\end{aligned} \tag{2.11}$$

The expression $X(f-lF_p-kF_s)$ means that the spectrum of $X(f)$ is shifted in $(l+k)F_s$ (if $F_s = F_p$ is considered), as in Figure 2.6.

For a better explanation, let us denote that $Z_l(f)$ is the signal $X(f)$ which is shifted

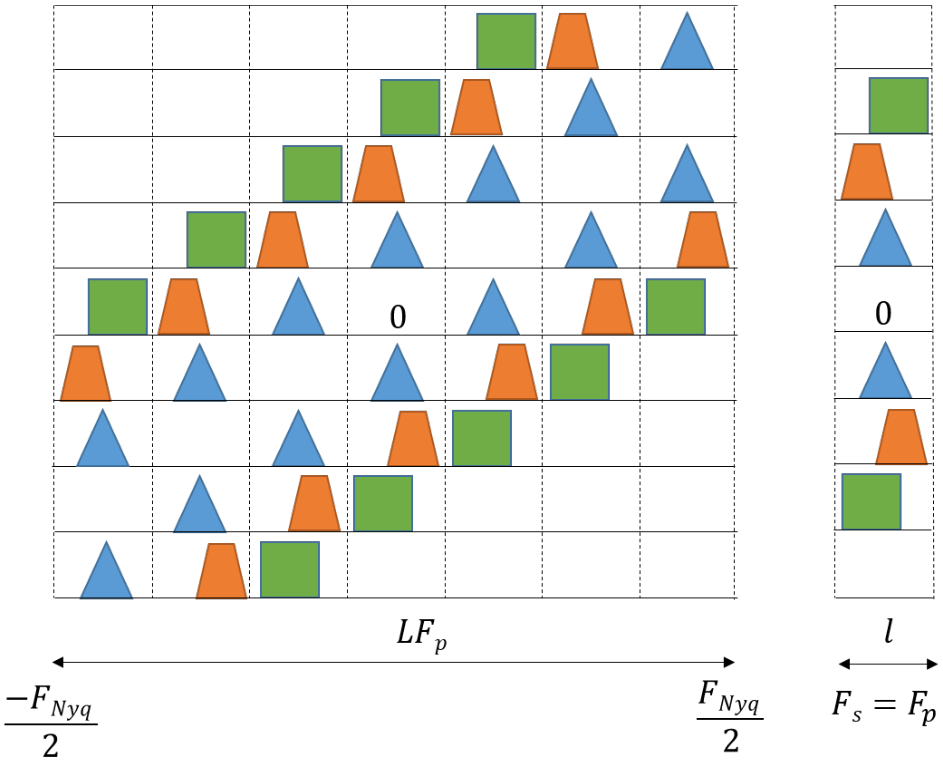

Figure 2.6 – The shifted spectrum and filtered spectrum at baseband.

by lF_p frequency, and $Z_l(f)$ keeps only a width of F_s from baseband after passing filter $H(f)$. Firstly, $Z_l(f)$ has form

$$Z_l(f) = H(f)X(f - lF_p). \tag{2.12}$$

Figure 2.7 illustrates a Matlab example of $Z_l(f)$ which is the shifted spectra of signal $X(f)$ and passed through the lowpass filter with cutoff frequency $F_s = qF_p = 72.9$ MHz.

On the other hand, the system equation $\tilde{Y}_i(f)$ can be rewritten as

$$\begin{aligned}\tilde{Y}_i(f) &= \sum_{l=-L_0}^{+L_0} p_{il} \left\{ F_s \sum_{k=-\infty}^{+\infty} Z_l(f - kF_s) \right\} \\ &= \sum_{l=-L_0}^{+L_0} p_{il} \tilde{Z}_l(f).\end{aligned} \tag{2.13}$$

The expression $F_s \sum\limits_{k=-\infty}^{+\infty} Z_l(f - kF_s)$ is the Fourier transform of the sampling signal $z_l[n]$ with sampling frequency F_s. Finally, the whole system in time domain can be rewritten

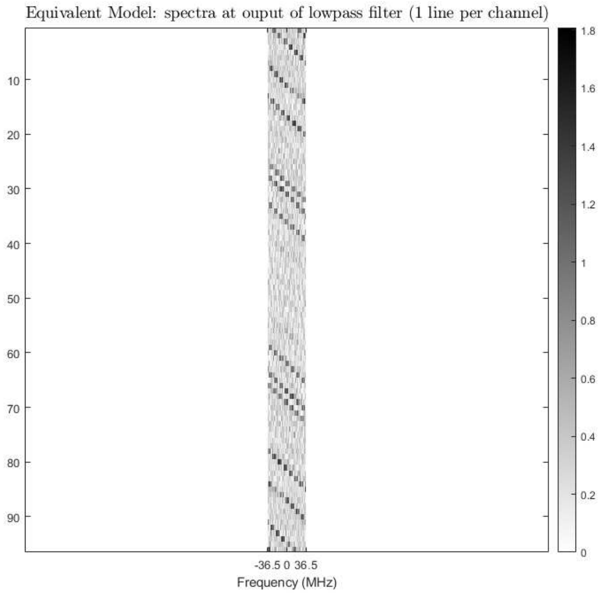

Figure 2.7 – Spectra after lowpass filter.

as

$$y_i[n] = \sum_{l=-\infty}^{+\infty} p_{il} z_l[n]. \tag{2.14}$$

A sensing matrix is formed from the periodic pseudo-random mixing sequences $p_i(t)$, such as $(\mathbf{P})_{il} = p_{il}$ [5]. Vectors $\mathbf{y}$ and $\mathbf{z}$ are formed from signals $y_i[n]$ and $z_l[n]$. The equation of system above can be performed as

$$\mathbf{y} = \mathbf{P}\mathbf{z}. \tag{2.15}$$

The matrix $\mathbf{P}$ could not be infinite because this is a real system. Absolutely, $\mathbf{y}$ is the output of the MWC sampling system, which has M physical channels. Thus, $\mathbf{y}$ has M elements. Then, $(\mathbf{y})_i = y_i[n]$ is a $M \times 1$ vector. As explained above, the limitation of l of z_l varies from $-L_0$ to $+L_0$ with $L = 2L_0 + 1$. Hence, $(\mathbf{z})_l = z_l[n]$ is a $L \times 1$ vector, and L is the maximum number of multiple l certainly. Totally, the size of matrix $\mathbf{P}$ is $M \times L$.

2.1.3 MWC parameter conditions

Parameter constraints

Furthermore, in order to have a good simulating implementation of this system, the response for each component needs to be precise and whether the sample outputs contain all information of the input. If not, the conditions should be posed on the input to ensure a better reconstruction.

In summary, the length of output **y** is M, the length of **z** is L, then the size of matrix **P** is $M \times L$. The mixer performs frequency shifts of $x(t)$ by carrier frequency F_p. Consequently, it is easy to see that $F_s \geq F_p$, with $[-F_s/2; F_s/2]$ signal bandwidth frequency of the lowpass filter. If $F_s < F_p$, the information which is located outside F_s will be eliminated by the filter. From the equation 2.15, based on the sensing matrix **P** the vector **z** will be possibly reconstructed. Thus, the matrix **P** should be invertible or pseudo-invertible, which gives $M \geq L$. Finally, the conditions can be defined by

$$MF_s \geq LF_s = \frac{F_{Nyq}}{F_p} F_s \geq F_{Nyq}. \tag{2.16}$$

Because this is a blind spectrum sensing system while the Nyquist frequency is unable to pre-determine. Thus, this condition is difficult to be satisfied since the sampling frequency of this system has exceeded the Nyquist frequency regarding this condition. That is the reason why an assumption needs to be made: the input signal needs to be sparse. That is to say, the signal **z** contains only a few non-zero elements. It will lead to $M < L$, and from vector **y**, vector **z** can still be recovered. This respects the condition of sparse **z** (in case of insignificant noise). Back to the condition $F_s \geq F_p$, firstly, if $F_s = F_p$, this is a very basic case that the filter can resolve each subband separately. This case, however, happens rarely in practice and it cannot ensure that all real systems have $F_s = F_p$. So, $F_s > F_p$, noting that $F_s = qF_p$.

In principle, at each physical channel of the MWC, there is one transmitter falling in the baseband l^{th} subband. Hence, the higher the number of MWC physical channels M, the larger the number of transmitters able to be detected by the MWC. As explained above, however, the MWC becomes significantly more expensive as M is getting larger. Consequently, a collapsing factor q is proposed to collapse the number of physical channels M. Instead of sampling M physical channels at F_s, the signal will be considered as if $q \times M$ channels sampled at F_p, with $q = F_s/F_p$ [7]. Theoretically, the number of physical channels of the MWC is extended to $q \times M$ channels. Then, the maximum number of transmitters that can be detected by the MWC increases also, up to $s \leq Mq - 1$, with s number of active subbands. Figure 2.8 depicts the extension of the number of MWC channels.

In the equivalent model, the spectrum $X(f)$ is shifted a frequency F_p with every l

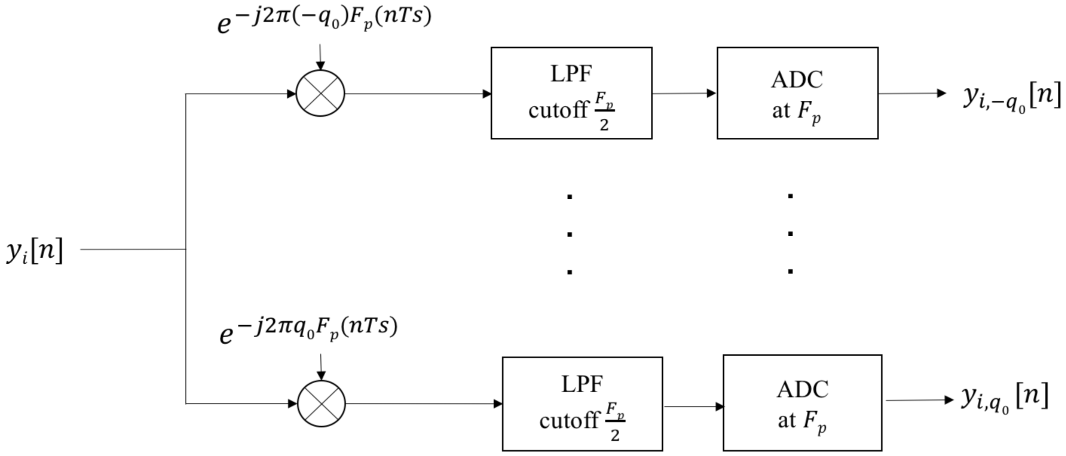

Figure 2.8 – The extension of number of MWC channels.

integer by the mixer. Then

$$X_l(f) = X(f - lF_p). \tag{2.17}$$

After filtering, the input spectrum is

$$Z_l(f) = H(f)X_l(f). \tag{2.18}$$

The spectrum $X_l(f)$ is symmetric, $\forall r \in \mathbb{N}$, it can be rewritten as

$$\begin{aligned} X_l(f + rF_p) =& X(f + rF_p - lF_p), \\ =& X(f - (l - r)F_p), \\ =& X_{l-r}(f). \end{aligned} \tag{2.19}$$

Then with $Z_l(f)$, the same symmetry spectrum should be

$$Z_l(f + rF_p) = Z_{l-r}(f), \tag{2.20}$$

and after sampling:

$$\tilde{Z}_l(f + rF_p) = \tilde{Z}_{l-r}(f). \tag{2.21}$$

The output of the MWC system $y_i[n] = \sum\limits_{l=-L_0}^{+L_0} p_{il} z_l[n]$ has Fourier transform

$$\tilde{Y}_i(f) = \sum_{l=-L_0}^{+L_0} p_{il} \tilde{Z}_l(f). \tag{2.22}$$

Then,

$$
\begin{aligned}
\tilde{Y}_i(f + rF_p) &= \sum_{l=-L_0}^{+L_0} p_{il}\tilde{Z}_l(f + rF_p), \\
&= \sum_{l=max(-L_0,-L_0+r)}^{min(L_0,L_0+r)} p_{il}\tilde{Z}_{l-r}(f), \\
&= \sum_{l=max(-L_0,-L_0-r)}^{min(L_0,L_0-r)} p_{i,l+r}\tilde{Z}_l(f).
\end{aligned} \tag{2.23}
$$

Noting that $\forall r \in \mathbb{N}$, rF_p must be inside $[-F_s/2; +F_s/2]$ (bandwidth of lowpass filter). Consequently, the bandwidth $[-F_s/2; +F_s/2]$ can be divided into q subbands with a width F_p. For the value of r, there are q possible output values of the MWC which can replace M channels $y_i[n]$ sampled at $F_s = qF_p$ by qM channels $y_{i,r}[n]$ sampled at F_p. Each subband can be chosen arbitrarily with a bandwidth $[-F_p/2; +F_p/2]$ and this subband is inside the range $[-F_s/2; +F_s/2]$. If the subband is chosen outside $[-F_p/2; +F_p/2]$, it can be written in the form $f + rF_p$. In summary, there are q subbands in width F_p located in bandwidth $[-F_s/2; +F_s/2]$ (these q subbands inside $[-F_s/2; +F_s/2]$ can be denoted $q = [-q_0; ...; 0; ...; q_0]$).

Back to time domain, the system equation is finally

$$
y_{i,r}[n] = \sum_{l=max(-L_0,-L_0-r)}^{min(L_0,L_0-r)} p_{i,l+r} z_{l,0}[n], \tag{2.24}
$$

Where $z_{l,0}$ represents z_l but it is limited in sub band $[-F_p/2; +F_p/2]$ and is sampled at F_p certainly. The matrix $\mathbf{P_e}$ is a matrix with all elements $p_{i,l+r}$. Then, matrix $\mathbf{P_e}$ is the matrix $\mathbf{P}$ which is shifted to the left r positions when r is positive, and to the right r positions when r is negative. When $r = 0$, the matrix $\mathbf{P}$ is unchanged.

Let us considered all elements $y_{i,r}[n]$ as a vector, denoting $\mathbf{y_e}$, vector $\mathbf{y_e}$ has size qM and it can be expressed by

$$
\mathbf{y_e} = \begin{pmatrix} y_{1,-q_0}[n] & \cdots & y_{M,-q_0}[n] & \cdots\cdots & y_{1,q_0}[n] & \cdots & y_{M,q_0}[n] \end{pmatrix}^T. \tag{2.25}
$$

Considering all elements $z_{l,0}[n]$ as a vector $\mathbf{z_0}$, then this vector has size L

$$
\mathbf{z_0} = \begin{pmatrix} z_{1,0}[n] & \cdots & z_{L,0}[n] \end{pmatrix}. \tag{2.26}
$$

Overall, the signal $y_{i,r}[n]$ can be obtained by shifting the spectrum $y_i[n]$ from rF_p to the left. In the time domain, it can be implemented by multiplying with $e^{-j2\pi rF_p(nT_s)}$. After that, the signal $z_{l,0}[n]$ is collected by filtering at F_p and sampling at F_p. All these processes are illustrated in Figure 2.8. From all steps developed above, a new system can be obtained

$$\mathbf{y_e} = \mathbf{P_e}\mathbf{z_0}, \tag{2.27}$$

where $\mathbf{P_e}$ is the shifted version of matrix $\mathbf{P}$, and $\mathbf{P_e}$ can be written in a short form

$$\mathbf{P_e} = \begin{bmatrix} \mathbf{P_{\text{-}q_0}} \\ \vdots \\ \mathbf{P_{q_0}} \end{bmatrix}. \tag{2.28}$$

In summary, the equivalent system is acquired, so-called an extension system, which includes:

— Vector $\mathbf{y_e}$ has length qM (instead of M).

— Matrix $\mathbf{P_e}$ has size $qM \times L$, a shifted version of matrix $\mathbf{P}$ (size $M \times L$).

— Vector $\mathbf{z_0}$ is unchanged with L components, but it is limited in band $[-F_p/2; +F_p/2]$.

Hence, the system 2.27 is used for the signal reconstruction, by applying the reconstruction methods in Section 1.3.

Sequences sets

The role of the mixing sequence is important in the MWC system. In Figure 2.3 of MWC equivalent model, the sensing matrix $\mathbf{P}$ is built based on the mixing sequences. Thus, a correct sensing matrix leads to a correct reconstruction. Back to the system equation 2.15, to compute the sensing matrix $\mathbf{P}$, the condition $M < L$ and the sparsity of active subbands must be respected as explained in Section 2.1.2. Practically, to find the solution for vector $\mathbf{z}$, there is a condition posed on $\mathbf{P}$ to guarantee that vector $\mathbf{z}$ has a unique solution [16]. The condition is based on the coherence $\mu(\mathbf{P})$ of matrix $\mathbf{P}$. Note that s is the number of nonzero elements in vector $\mathbf{z}$ (active subbands), if

$$s < \frac{1}{2}\left. \quad 1 + \frac{1}{\mu(\mathbf{P})}\right), \tag{2.29}$$

then the sparse vector $\mathbf{z}$ has a unique solution. While $\mu(\mathbf{P})$ is found by

$$\mu\left(\mathbf{P}\right) = \underset{1 \leq i \leq j \leq L}{max} \frac{|\langle \mathbf{P}_i, \mathbf{P}_j \rangle|}{\|\mathbf{P}_i\|_2 \|\mathbf{P}_j\|_2}, \tag{2.30}$$

where the coherence $\mu(\mathbf{P})$ is defined as the largest absolute scalar product between any of the two columns $\mathbf{P}_i$ and $\mathbf{P}_j$ of matrix $\mathbf{P}$ [99][100]. The coherence $\mu(\mathbf{P})$ is always in the range of $\left[\sqrt{\frac{L-M}{M(L-1)}}, 1\right]$, also called Welch's bound [101]. According to the greedy algorithm of reconstruction in Section 1.3, the reconstructed error will be estimated by

$$\|\hat{\mathbf{z}} - \mathbf{z}\|^2 \leq \frac{\epsilon^2}{1 - \mu(k)(2L-1)}. \tag{2.31}$$

for a constant $\epsilon > 0$. Consequently, minimizing the coherence $\mu(\mathbf{P})$ will bring a high probability to find the solution for vector $\mathbf{z}$ and minimize the reconstructed error.

Moreover, some CS studies state that for a specific class of subgaussian random sensing matrix $\mathbf{P}$, the Restricted Isometry Property (RIP) [12–15] ensures that the input vector $\mathbf{z}$ can be reconstructed with high probability from the vector solution $\hat{\mathbf{z}}$ to Equation 1.5, by respecting the guarantee

$$\|\hat{\mathbf{z}} - \mathbf{z}\|_2 \leq \epsilon + \frac{\sigma_s(\mathbf{z})_1}{\sqrt{s}}, \tag{2.32}$$

with ϵ in Equation 1.5 is called the noise or quantization level, or it can be considered as the upper bound on the norm of vector noise, s is number of non-zeros in $\mathbf{z}$, provided by $M = s\log(L/s)$, as explained in Section 1.1.4. Consequently, to have a sensing matrix which satisfies the (δ_s,s)-RIP, if $\mathbf{z}$ with s-sparse and an appropriate small constant δ_s

$$\left(1 - \delta_s\right)\|\mathbf{P}\|_2^2 \leq \|\mathbf{P}\mathbf{z}\|_2^2 \leq \left(1 + \delta_s\right)\|\mathbf{P}\|_2^2. \tag{2.33}$$

The RIP ensures that all subgaussian matrices of $\mathbf{P} \in \mathbb{C}^{M \times L}$ are closed to the isometry and this property keeps the reconstruction stable in the presence of noise. Totally, these main two conditions to guarantee the reconstruction in CS are the lowest coherence of the sensing matrix and RIP. The sensing matrix just needs to satisfy one of them to ensure the reconstruction. In this study, the condition of coherence is used. The next part shows a study on minimizing the coherence $\mu(\mathbf{P})$.

In [102], by comparing the Maximal, Gold [17], Kasami [18] and Hadamard [19] codes, the research states that Gold or Kasami sequences are especially suitable for the MWC.

Nevertheless, in practice, the Gold codes sequences deployed in the MWC [22] have technical limitation on the number of sequences within the code [102], due to the Gold codes generation by FPGA. A study on the choice of mixing code sequences based on the coherence and deployment to the MWC has been made in [34]. By firstly analysing the coherence of circulant matrices which are constructed by Bernoulli [5] and Gold sequences, those are typical in communications and CS. Moreover, this analysis extends to the advanced techniques such as Zadoff-Chu code [103, 104] in time domain, and this technique is compared with a new version of Zadoff-Chu code based real-valued circulant sensing matrix in frequency domain [105]. Compared to the random matrices, the circulant matrix has benefit in the cost of generating, since it needs only one code and then permuted [106]. Thus, the circulant matrix can provide better performance and high level metrics in coherence and isometric properties. In [34], the study also detailed that the Zadoff-Chu-based circulant matrix can perform better than the Gold-based circulant matrix or the others sequences codes such as Bernoulli or random codes. Nevertheless, the problems of generating and applying circulant matrix to the MWC in practice have not been addressed yet. Moreover, the Zadoff-Chu-based circulant matrix can achieve high performance when the ratio M/L is high. In practice, it is hard to deploy high M (due to the increasing cost of analog components) and impossible to attain $M \geq L$ as explained in the MWC conditions above. Consequently, there is an example of MWC implementation by choosing $M = 4$ and $L = 305$, which means $M/L = 1\%$ [22]. In this study, $M = 4$ and $L = 96$ are deployed, which means $M/L = 4\%$, and the pseudo-random sequences with lowest coherence is used. Because in random matrix, the coherence is easy to compute, then, it is possible to generate pseudo-random sequences by the FPGA. The sequences generating in FPGA is detailed in Section 2.3.

In definition, the mixing sequence $p_i(t)$ is a binary sequence of ± 1. Figure 2.9 shows an example of four mixing sequences which correspond to four physical channels of the MWC system and their length is 96 ($M = 4$ and $L = 96$). As mentioned before, the sensing matrix $\mathbf{P}$ is built based on these sequences which has an important role to reconstruct the input signal. Therefore, the set of sequences must have the size of matrix $\mathbf{P}$, which is $M \times L$. It means that there are M binary sequences and each sequence has L elements ± 1, which are applied to the MWC system. The method of choosing a good sequence set is proposed to rely on the lowest coherence of the matrix $\mathbf{P}$.

The pseudo-random sequence is proposed in this study since it is simple to generate. Nevertheless, it is very hard to obtain directly a pseudo-random sequence which has good

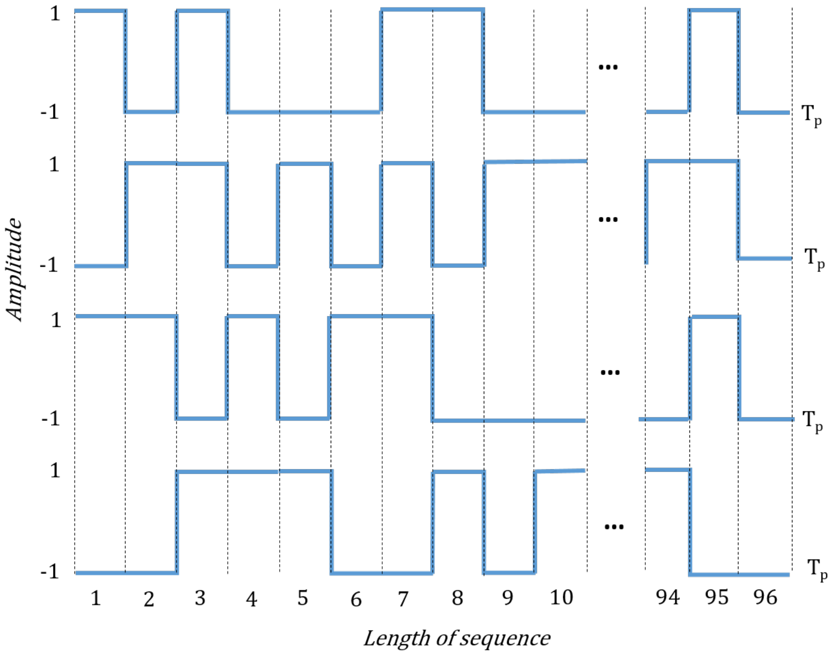

Figure 2.9 – Four mixing sequences correspond to four physical channels of the MWC system, $M = 4$ and $L = 96$.

properties depending on the parameters of the system, since the sequence is generated randomly. By searching one million sets of sequences to find a sequences set which has minimum coherence ($M = 4$ and $L = 96$), Figure 2.10 shows a histogram of these sequences sets and their coherence. In this case, the sequences set, which is considered as the lowest coherence, has the coherence value 0.414.

In fact, the sequences can be generated infinitely to find the minimum coherence but the real applications will not allow to do this owing to the consumption time of each application. Hence, the time to generate these pseudo-random sequences needs to be fixed and depends on the requirements of applications. The problem is to find the compromise between time consuming and low coherence, then, the solution for this problem is a relationship to decide what value of coherence is good enough in a specified time.

It should be noted that in the simulator, the mixers are assumed to be ideal. In practice, however, problems of synchronization can appear and it leads to the degradation of spectrum reconstruction (these problems are detailed in Section 2.3.2). In the next part, a pre-processing step to estimate the number of subbands is presented.

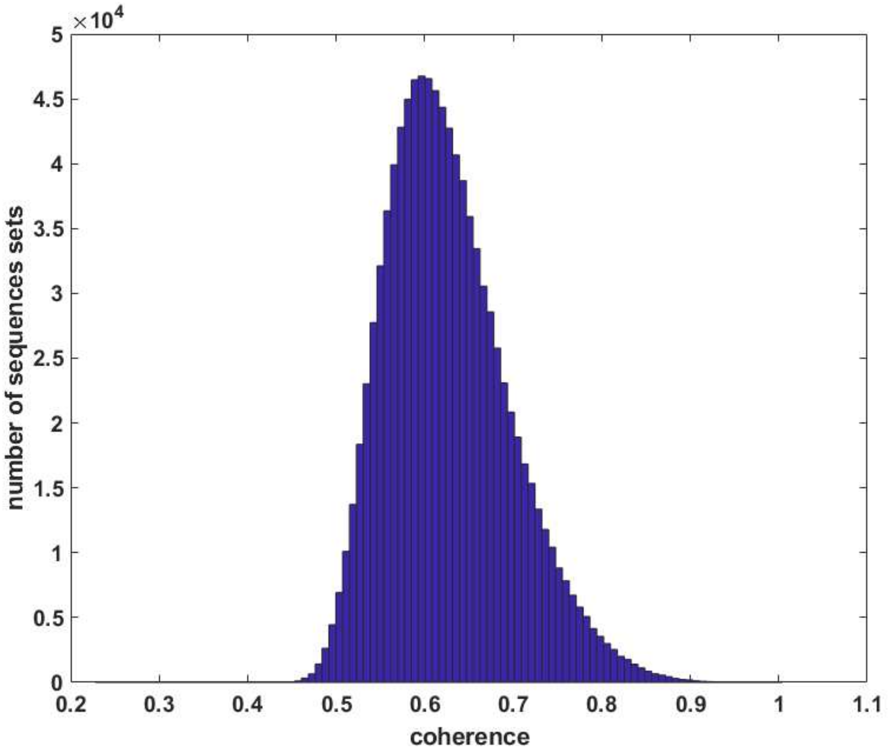

Figure 2.10 – Histogram of criterion to choose a lowest coherent sequences set.

2.1.4 Number of active subbands estimation

As explained in the previous section, in the MWC, the Nyquist bandwidth is divided into L subbands. The active subbands are the subband which the transmitters are located in. In this section, some estimation methods for the number of active subbands are introduced. This task is considered as a pre-processing step in Figure 2.1, before spectrum reconstructing. At the output of the MWC, the vector $y_i[n]$ $(1 \leq i \leq M)$ has N sub-Nyquist samples. Then, this output is considered as a $M \times N$ matrix $\mathbf{y}$, or $qM \times N$ in the case of using collapsing factor q. Similarly, the signal $z[n]$ has N sub-Nyquist sample elements and is considered as a $L \times N$ matrix. The main perspective of the MWC is to seek for $\mathbf{z}$ when the output $\mathbf{y}$ and the sensing matrix $\mathbf{P}$ are known.

The number of active subbands estimation methods are based on the singular values of matrix $\mathbf{y} \in \mathbb{C}^{M\times N}$, or equivalently the associated autocorrelation matrix eigenvalues. Indeed, their variation is directly related to the number of active subbands s. Moreover, there are exactly s non-zero eigenvalues in the noiseless case. In the case of additive white Gaussian noise, all the $M - s$ values which are smaller than the eigenvalues, are equal to the noise variance. In the case of very strong noise, it is difficult to determine exactly the number of active subbands.

The methods Akaike Information Criterion (AIC) [107] and Minimum Description Length (MDL) [108] are easy to adapt with the MWC system for estimating the number of active subbands. The noise is considered as additive white Gaussian noise (AWGN). The number of subbands is determined by the best match between the model and the observation elements of MWC output

$$s = \arg\min_{k}[C(k)], \tag{2.34}$$

where $C(k)$ the cost function related to the log-likelihood of model parameters for $N = k$, with N the number of sub-Nyquist samples of the MWC. The estimators AIC and MDL have been adapted by [109]. Let us denote that P the number of independent realizations of length M. The cost functions in both cases are

$$AIC(k) = -2P(M-k)\log\left[\frac{\prod_{i=k+1}^{M}\lambda_i^{1/(M-k)}}{\frac{1}{M-k}\sum_{i=k+1}^{M}\lambda_i}\right] + 2k(2M-k), \tag{2.35}$$

$$MDL(k) = -P(M-k)\log\left[\frac{\prod_{i=k+1}^{M}\lambda_i^{1/(M-k)}}{\frac{1}{M-k}\sum_{i=k+1}^{M}\lambda_i}\right] + \frac{1}{2}k(2M-k)\log P, \tag{2.36}$$

where $\{\lambda_i\}_{i=1\ldots M}$ the eigenvalues of the autocorrelation matrix (or the square of singular values of the data matrix $\mathbf{y}$) ranked in descending order.

A different method to estimate the number of active subbands is based on the predicted eigen-threshold [110] by estimating the threshold $\{Th_{M-m}\}_{m=1\ldots M-1}$ for each eigenvalue $\{\lambda_{M-m}\}_{m=1\ldots M-1}$. An eigenvalue which is above the threshold is considered as one active subband. The threshold corresponding to each eigenvalue has the expression

$$Th_{M-m} = \left[(m+1)\frac{1+t[P(m+1)^{-1/2}]}{1-t[Pm]^{-1/2}} - m\right] l_{M-m+1}, \tag{2.37}$$

where

$$l_{M-m+1} = \frac{1}{m}\sum_{i=M-m+1}^{M}\lambda_i, m = 1..M, \tag{2.38}$$

with t a fixed parameter according to the desired false alarm probability.

Moreover, another estimation method is based on two discriminant functions [111].

This method analyzes the eigenvalues of the autocorrelation matrix, however, the principle of this method is different to the methods above. In this case, two discriminant functions are defined such as $\{g_1(k)\}_{k=1\ldots M-1}$ and $\{g_2(k)\}_{k=1\ldots M-1}$. The difference of these two functions is to estimate the number of active subbands s when s is the cardinal number of

$$s = \text{card}\,\{k | g_1(k) - g_2(k) > 0\}\,, \tag{2.39}$$

where

$$g_1(k) = \frac{\lambda_{k+1}}{\sum_{i=2}^{M} \lambda_i}, \tag{2.40}$$

$$g_2(k) = \frac{\zeta_k}{\sum_{i=1}^{M-1} \zeta_i}, \tag{2.41}$$

with $\zeta_k = 1 - \alpha(\lambda_k - \mu_k)/\mu_k$, $\mu_k = \frac{1}{M-k} \sum_{i=k+1}^{M} \lambda_i$, $\forall k = 1 \ldots M-1$ and α is calculated by $\alpha \max\limits_k [(\lambda_k - \mu_k)/\mu_k] = 1$. The next section is an introduction of spectrum reconstruction methods.

2.1.5 Input signal reconstruction and performance evaluation

Input signal reconstruction

A sensing matrix is formed from the periodic pseudo-random mixing sequences $p_i(t)$, such as $(\mathbf{P})_{il} = p_{il}$ [5], with $p_{il} = F_p \int_{-T_p/2}^{T_p/2} p_i(t) e^{-j2\pi l F_p t} dt$ the Fourier coefficient derived from $p_i(t)$. Let us denote by $z_l[n]$, $l = 1..L$, the Fourier transform of the multi-subband input signal in the l^{th} subband. Consequently, the system equation [6][7] is $\mathbf{y} = \mathbf{Pz}$, with $\mathbf{P} \in \mathbb{C}^{qM \times L}$. Figure 2.11 shows an illustration of the system equation.

This system equation complies with the CS main constraint $s \leq Mq - 1$, with s is the number of active subbands or the non-zero elements in $\mathbf{z}$. The size of output $\mathbf{y}$ $(q \times M)$ is much smaller than the size of input $\mathbf{z}$ (L elements). The reconstruction principle is to search $\mathbf{z}$ from $\mathbf{y}$, by applying the methods which are presented in Section 1.3.

Performance evaluation

This section introduces the correct reconstruction and false alarm rates to evaluate the performance of spectrum reconstruction. It should be noted that the input bandwidth

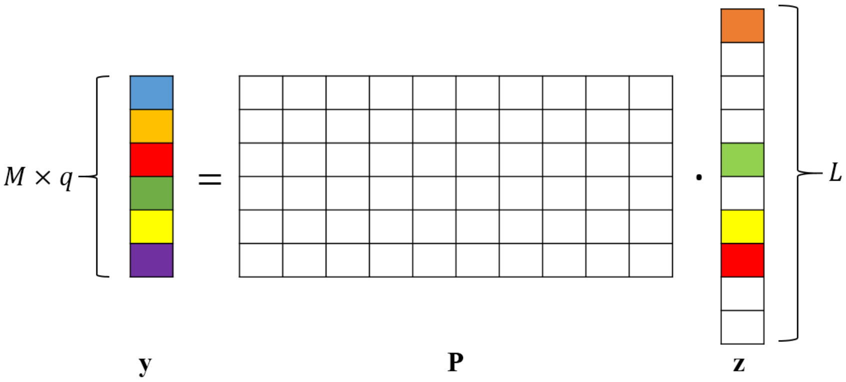

Figure 2.11 – Illustration of the MWC system equation.

$[\frac{-F_{nyq}}{2}; \frac{F_{nyq}}{2}]$ is divided into L subbands, so-called the MWC subbands. In the reconstruction stage, the reconstruction algorithm will recover all the width of one MWC subband if this subband is active. For example, if there is one transmitter which locates (astride) two MWC subbands, there will be two active subbands in this case. Then, after reconstructing the bandwidth of a transmitter, the remaining width of these two MWC subbands is considered as noise.

Let us note that the real subbands are the subbands that we expect, which are considered exactly the same as the input signal; and the detected subbands are what we obtain from the MWC outputs. The performance of correct detection is determined by the correct reconstruction rate P_c. P_c includes the expected activity elements among all the reconstructed activity elements in the reconstructed subbands; and is estimated by the percentage of occupation between the detected and real subbands related to the real subbands occupied by the spectrum

$$P_c = \frac{\%(B_r \cap B_d)}{\%B_r}, \tag{2.42}$$

where B_d the detected subbands and B_r the real subbands occupation. For example, Figure 2.12 illustrates the transmitted real signal B_r and detected signal B_d included false alarms.

The false alarm rate P_f, which evaluates only unexpected transmitters, is defined by the percentage of detected subbands different to real subbands occupation which intersect the complement of the real subbands occupation related to the complement of real subbands occupied by the spectrum. In this case, the noise at each expected subband is

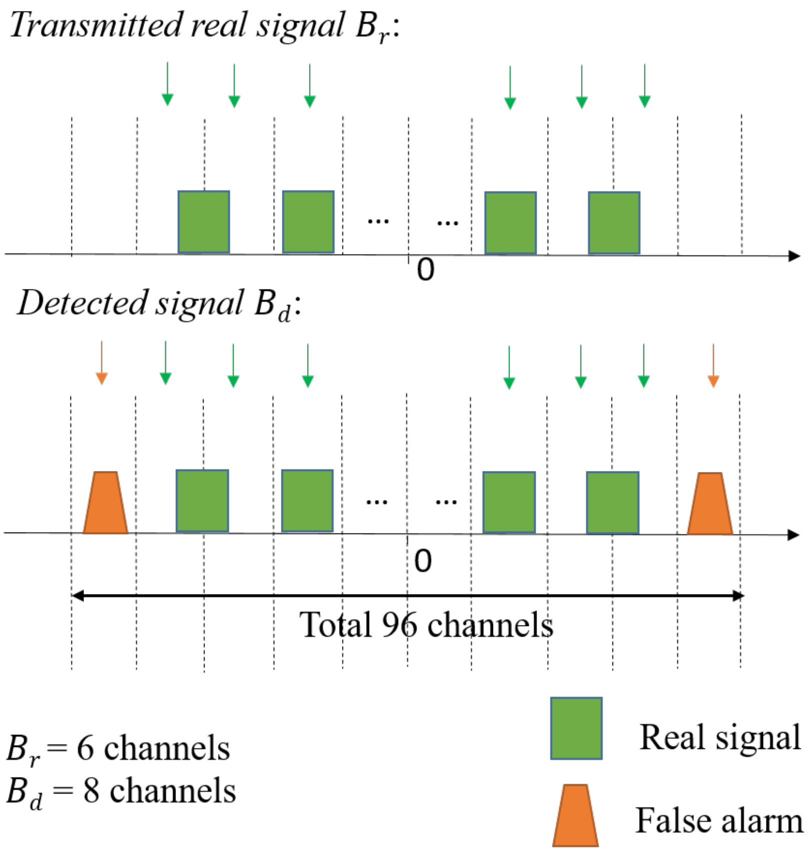

Figure 2.12 – Illustration of transmitted real signal B_r and detected signal B_d.

not taken into account

$$P_f = \frac{\%((B_d \setminus B_r) \cap \bar{B}_r)}{1 - \%B_r}. \tag{2.43}$$

2.2 Transmitter signal key parameters on the CS spectrum reconstruction

This section studies the influence of a wideband signal key parameters on its spectrum reconstruction, and especially for Internet-of-Things (IoT) applications. It should be noted that all the parameters such as the frequency resolution, the bandwidths of the sensed transmitters, and the frequency spacing between their subbands have impacts on the performance of the reconstruction [44]. This section analyzes the impacts of all these key parameters. The spectrum detection of LoRaWAN EU868, one of the IoT standards, is simulated and examined. In the framework of spectrum sensing, the spectrum reconstruction is carried out from the sub-Nyquist samples, and then evaluated based on the correct reconstruction and false alarm rates.

In the simulation, assuming that all the components of the MWC are ideal, the parameters of the MWC are chosen as $M = 4$, $L = 192$, $q = 7$ and $F_{Nyq} = 2$ GHz, so that to have a configuration compatible with LoRaWAN standard. This standard is used in the ISM band. From 867.1 to 868.5 MHz frequency band, the LoRaWAN standard can deploy up to 8 transmitters with 125 kHz bandwidth and 75 kHz guard band (frequency spacing) for each transmitter [112]. This is also an IoT standard deployed in Europe as well as Vietnam.

2.2.1 Minimum bandwidth of one transmitter

For all simulation scenarios with the configuration of the MWC as above, then, the other parameters can be derived: the repetition frequency of mixing function $F_p = F_{Nyq}/L = 10.4$ MHz, the sampling frequency $F_s = q \times F_p = 72.8$ MHz, the cutoff of lowpass filter $F_c = F_s/2 = 36.4$ MHz.

In the first scenario, the number of samples of the wideband input signal sampled at the Nyquist rate is chosen as $N_e = 2^n \times L$, in which 2^n is for the efficiency of fast Fourier transform. Firstly, $n = 11$ is chosen, resulting in $N_e = 393216$ samples. Since $F_s = (q \times F_{Nyq})/L$, then, the sub-Nyquist number of samples at MWC output, which is sampled at F_s, is $N = (q \times Ne)/L = 14336$ samples for each physical channel of the MWC. Overall, the number of samples at MWC output is $N_{total} = N \times M = 57344$ samples. It is easy to observe that the sampling rate is reduced by a factor $r = F_{Nyq}/(F_s \times M) = L/(q \times M)$, and in this case, the sampling rate is reduced 6.9 times at the output of the MWC.

The frequency resolution in this simulation is $R_f = F_{Nyq}/N_e = 5$ kHz. One transmitter is randomly generated in $[0; 1]$ GHz and its bandwidth is changed. Figure 2.13 shows the correct reconstruction and false alarm rates at each SNR level as a function of the transmitter bandwidth B from 5 kHz to 500 kHz. It can be observed in Figure 2.13 that for a small bandwidth 5 kHz, which is equal to the frequency resolution, the correct reconstruction rate is low. This rate increases when the bandwidth increases. For high SNRs (25 and 30 dB), the correct reconstruction rate can approach 100% with input bandwidth more than 250 kHz while there is no false alarm for 30 dB and low false alarm rate for 25 dB (less than 2%). At low SNR = 15 dB, the minimum bandwidth raises up to 380 kHz to achieve 98% of reconstruction, however, the false alarm rate is high for this bandwidth as well.

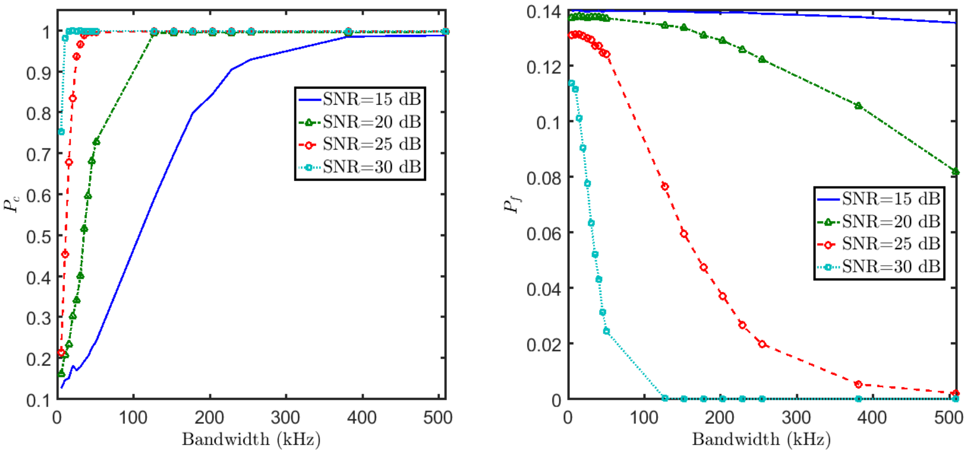

Figure 2.13 – Correct reconstruction and false alarm rates in function of bandwidths at 5 kHz frequency resolution.

It should be noted that in all the simulations, the SNR is evaluated in each active subband of the original spectrum, so that it can be seen as the SNR in the band of interest. Let us denote the SNR in the whole Nyquist bandwidth SNR_{Nyq}. The relationship between these two SNRs is

$$\mathrm{SNR} = \mathrm{SNR}_{Nyq} + 10 \log \left(\frac{F_{Nyq}}{2 \times N_t \times B} \right), \tag{2.44}$$

with N_t the number of transmitters, and $N_t = 1$ for this simulation. At $\mathrm{SNR} = 15$ dB and $B = 380$ kHz, the SNR_{Nyq} in the whole Nyquist bandwidth can be inferred as -19 dB. A very high noise level in the whole Nyquist bandwidth makes the useful subbands to be aliased by the noise. It leads to the overestimation of the number of active subbands s. This explains the reason why at SNR of 15 dB, an incorrect reconstruction and high false alarm can be obtained.

In Figure 2.14, the number of Nyquist samples is reduced to $N_e = 98304$ samples with $n = 9$, which means that the frequency resolution $R_f = 20.3$ kHz in this simulation is larger. It is easy to observe that the performance of correct reconstruction at each SNR is reduced since the number of samples is reduced. Compared to Figure 2.13, the false alarm rate increases at all SNRs and all values of bandwidth. In the first approach, it can be concluded that when more samples are used, the correct reconstruction rate is improved. It means that the resolution frequency is getting better, so that the system can detect a very small bandwidth of the transmitter. To have a better comparison with Figure 2.13, the bandwidth from 0 to 0.5 MHz of Figure 2.14 is shown in Figure 2.15. It can be seen

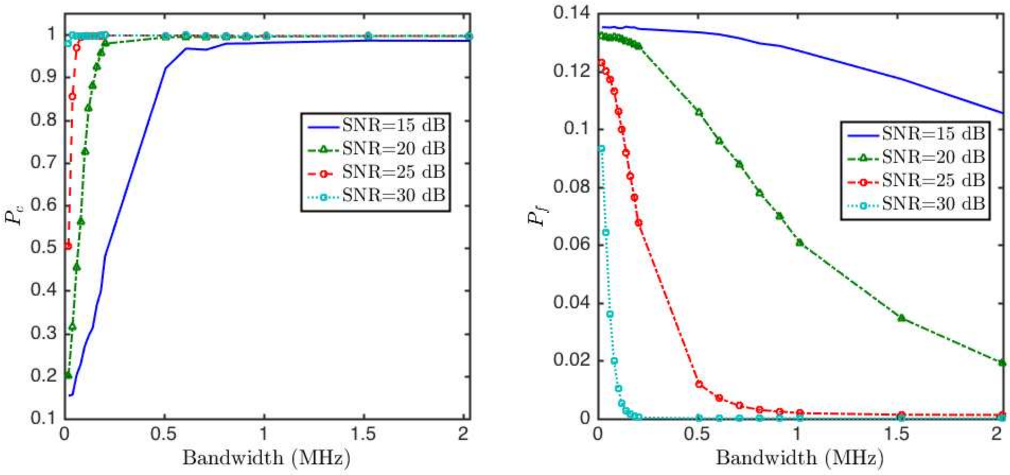

Figure 2.14 – Correct reconstruction and false alarm rates in function of bandwidths at 20.3 kHz frequency resolution.

when less samples are used (larger frequency resolution), the correct reconstruction rates decline for all SNR levels and the false alarm rates increase as well.

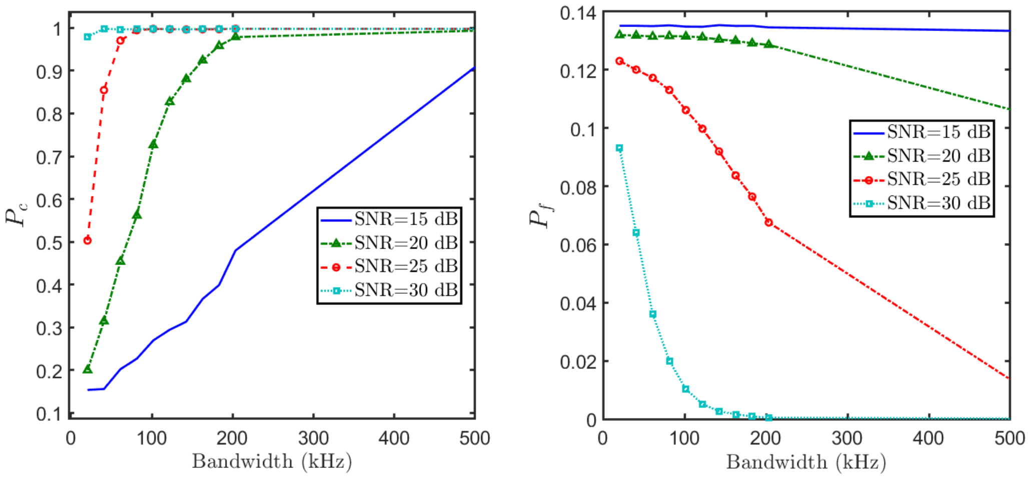

Figure 2.15 – Correct reconstruction and false alarm rates in function of bandwidths at 20.3 kHz frequency resolution with bandwidth from 0 to 0.5 MHz.

2.2.2 Number of transmitters

Number of transmitters and cumulative bandwidth in different active subbands

The goal of this simulation scenario is to examine the number of transmitters in different active subbands, with respect to the sparsity constraint on the number of active subbands $s \leq qM - 1$ [5]. According to the MWC principle, the whole Nyquist bandwidth is divided into L subbands. In this simulation, the number of transmitters $N_t \in [1;5]$ is randomly generated in different active subbands. The number of samples is fixed at $N_{total} = 57344$ samples (equivalent $N_e = 393216$ Nyquist samples). From Figure 2.13, one transmitter with $B = 60$ kHz can be correctly detected at SNR $= 30$ dB. Consequently, the bandwidth of each transmitter in this simulation is chosen as 60 kHz. The MWC configurations are the same as in the previous simulations. The correct reconstruction and false alarm rates are shown in Figure 2.16. To compute the correct reconstruction rate, a threshold is fixed to determine detected transmitters. In this figure, the correct reconstruction rate is reduced when increasing the number of transmitters in the case of high noise levels (SNR $= 15$ and 20 dB).

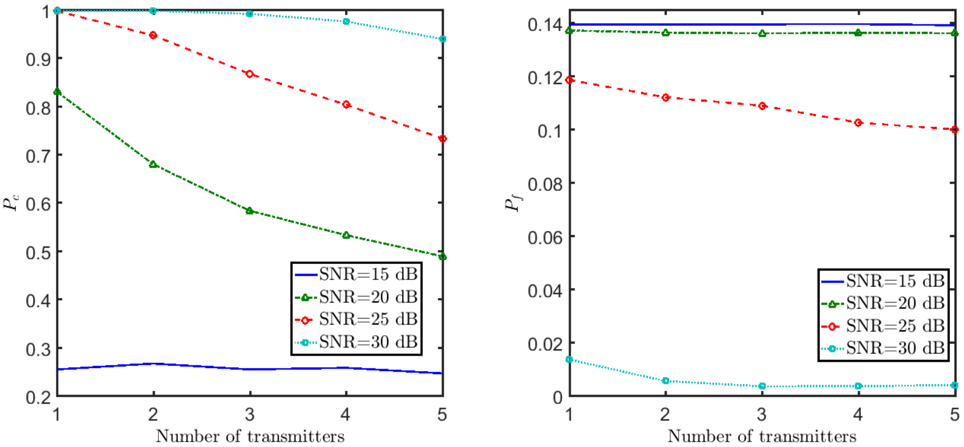

Figure 2.16 – Correct reconstructions and false alarm rates in function of number of transmitters in different active subbands with $B = 60$ kHz and $R_f = 5$ kHz.

The transmitter bandwidths in different subbands in Figure 2.16 are not accumulated. As explained above, when the power of transmitter in one active subband is not significant compared to the noise, for example in case of high noise at Nyquist bandwidth $\text{SNR}_{Nyq} = -20$ dB with 5 transmitters at SNR $= 15$ dB, it leads to a problem that the blind detection system cannot separate the transmitter from the noise.

Number of transmitters and cumulative bandwidth in one active subband

Figure 2.17 presents the correct reconstruction and false alarm rates at each SNR level in function of the number of transmitters in only one active subband. It can be seen that the correct reconstruction rates are high even if one transmitter has narrow bandwidth (60 kHz) except SNR $= 15$ dB. When increasing the number of transmitters (up to 5 transmitters) in one subband, the correct reconstruction rate also increases. From the result of Figure 2.17, the MWC system can detect 3 transmitters with 100% of reconstruction and low false alarm (less than 5%) at SNR of 25 dB, equivalently $\text{SNR}_{Nyq} = -12$ dB.

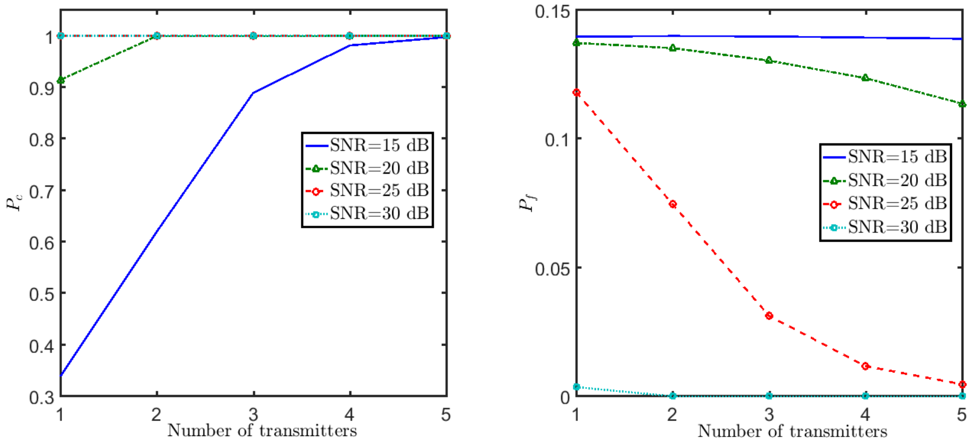

Figure 2.17 – Correct reconstructions and false alarm rates in function of number of transmitters in one active subband with $B = 60$ kHz and $R_f = 5$ kHz.

The formula of SNR_{Nyq} mentioned above shows that the width of detection can be accumulated by the system. If the bandwidth of a transmitter is narrow, more transmitters are needed to satisfy the requirement of signal power that the system can detect correctly. For example in Figure 2.13 and Figure 2.17, for a SNR of 30 dB, the bandwidth 60 kHz will be detected at 100% of reconstruction and no false alarm. Therefore, only one transmitter of 60 kHz is needed in case 30 dB (SNR). At 25 dB, however, 240 kHz of bandwidth is required to be detected correctly and low false alarm (Figure 2.13). Then, it needs up to 4 transmitters of 60 kHz bandwidth (Figure 2.17). It is interesting to observe that at 15 dB, the correct reconstruction rate is high with more than 3 transmitters (Figure 2.17), however, the false alarm rate is high also, it means that the system cannot separate the useful spectra and the noise. One example of spectrum reconstruction is shown in Figure 2.18, where 4 transmitters with 60 kHz bandwidth are generated consecutively at 15 and 30 dB in only one subband [661.4; 671.8] MHz. In this case, for example in Figure 2.18a (SNR = 15 dB), it is difficult to discriminate the transmitters from the reconstructed signal mixed with noise. Moreover, the false alarm rate is equal to 13.9%. In Figure 2.18b (SNR = 30 dB), all transmitters are completely detected without any false alarm. These values correspond to the false alarm rate of one transmitter with 240 kHz bandwidth (Figure 2.13). Figure 2.13 and Figure 2.17 show that the bandwidth of transmitters in one active subband can be accumulated and it leads to a better reconstruction if more bandwidths are accumulated, since the proportion of signal power and noise in that band is enhanced significantly.

2.2.3 Frequency spacing and LoRaWAN spectrum detection application

Minimum frequency spacing

In this section, the frequency spacing of 4 transmitters increases gradually, from $R_f = 5$ kHz to $8R_f = 40$ kHz with $B = 60$ kHz. The transmitters are generated consecutively in only one subband [859.3; 869.7] MHz. We introduce a measurement P_B which corresponds to the correct detection rate of the minimum and maximum frequencies $\{f_{t_{min}}; f_{t_{max}}\}$ of all transmitter bandwidths, with $t \in [1; N_t]$.

Figure 2.19 illustrates the correct detection rate of $\{f_{t_{min}}; f_{t_{max}}\}$ and false alarm rate in function of frequency spacing. At high noise levels (SNR of 15 and 20 dB), the reconstructions are incorrect regardless the frequency spacing between these transmitters is small or large. The high noise makes the detection of power transitions difficultly and leads to an incorrect estimation of couples $\{f_{t_{min}}; f_{t_{max}}\}$. For low noise level, the reconstructions are improved. Thus, perfect reconstruction at 30 dB and high correct reconstruction rates at 25 dB can be obtained, without any false alarm. It can be inferred that the minimum frequency spacing is 5 kHz at SNR = 30 dB with perfect reconstruction and at SNR = 25 dB with high correct reconstruction rate (more than 90%) and no false alarm. Figure 2.20 confirms the simulated results with the spectrum reconstructions at a SNR of 20 and 30 dB. The ability to discriminate between two adjacent transmitters is directly related to the frequency resolution shown in Figure 2.19, and that the performances of reconstruction depend only on the SNR.

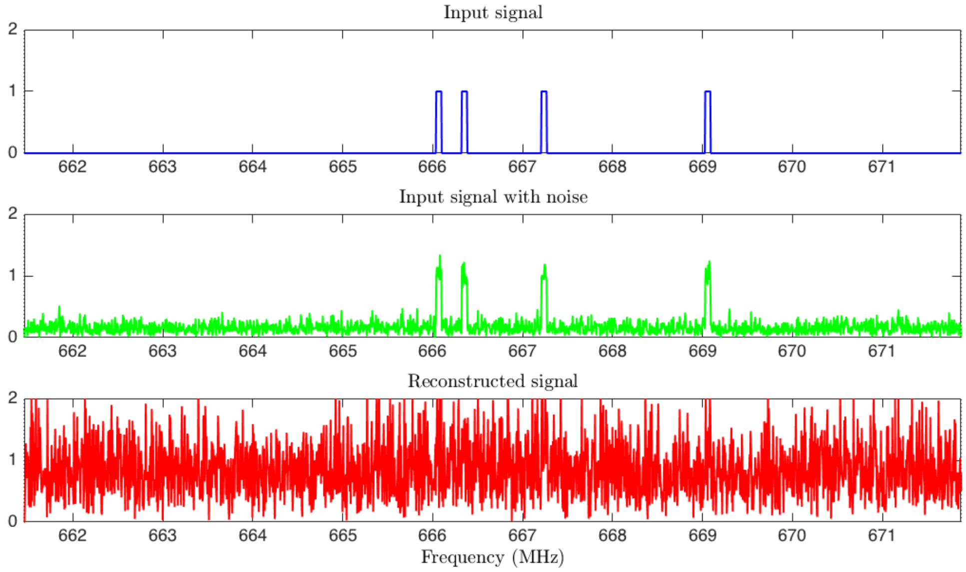

(a) SNR $= 15$ dB

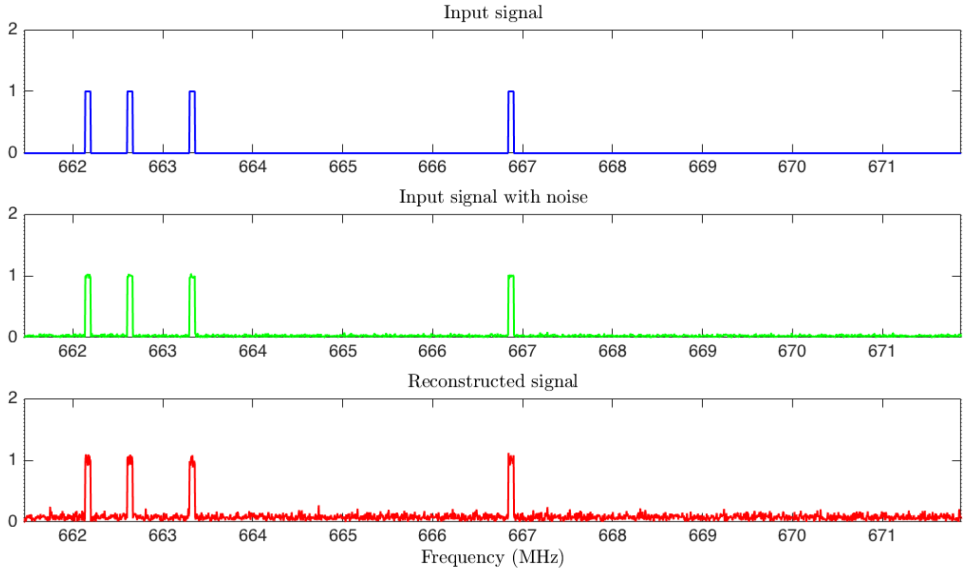

(b) SNR $= 30$ dB

Figure 2.18 – Spectrum reconstructions of 4 transmitters generated in one active subband at SNR of 15 and 30 dB with $B = 60$ kHz and $R_f = 5$ kHz.

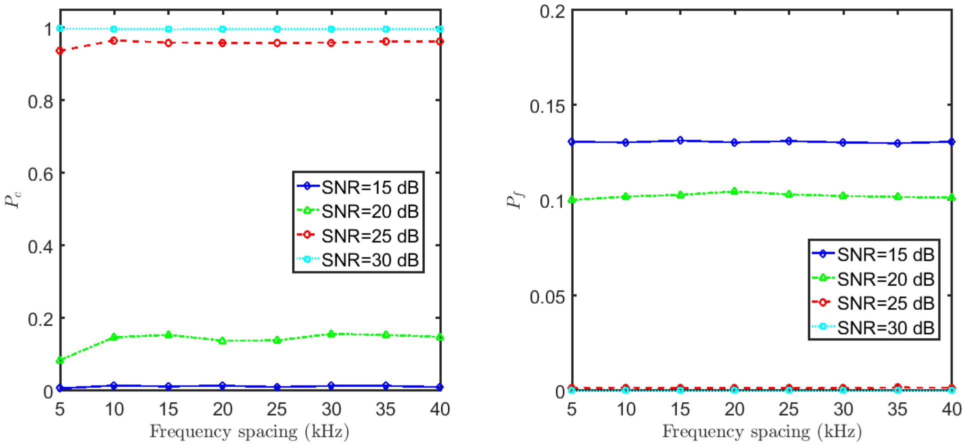

Figure 2.19 – Correct detection rate of all couples $\{f_{t_{min}}; f_{t_{max}}\}$ and false alarm rate in function of frequency spacing with $B = 60$ kHz and $R_f = 5$ kHz.

LoRaWAN spectrum detection application

In this section, the frequency spacing between transmitters in LoRaWAN is studied and the configuration of LoRaWAN standard is simulated to examine the spectrum detection in the IoT applications.

As introduced above, the total bandwidth of all transmitters in LoRaWAN EU868 is equal to $8 \times 0.125 = 1$ MHz. The total sub-Nyquist number of samples is $N_{total} = 57434$ and the Nyquist number of samples is $N_e = 393216$. The correct reconstruction and false alarm rates of LoRaWAN EU868 standard with 8 transmitters from 867.1 to 868.5 MHz is shown in Table 2.1. As the simulation results from previous sections, the correct reconstruction and false alarm rates can approach 100% in the case of SNR $= 30$ dB, corresponding to $\text{SNR}_{Nyq} = 0$ dB. Moreover, there is no correct detection in cases of very high noise SNR $= 15$ and 20 dB, corresponding to $\text{SNR}_{Nyq} = -15$ and -10 dB. Figure 2.21 illustrates one example of LoRaWAN EU868 standard spectrum reconstruction with 30 dB (SNR). The spectra can be obtained with a correct number of transmitters and frequency bands.

Overall, from the simulation results, the number of transmitters, the frequency resolution and the cumulative or non-cumulative bandwidth all cause an impact on the sensed spectrum reconstruction. Nevertheless, the biggest constraint is the noise levels. The intensity of noise determines the correctness of all the spectrum reconstruction in a spectrum sensing system.

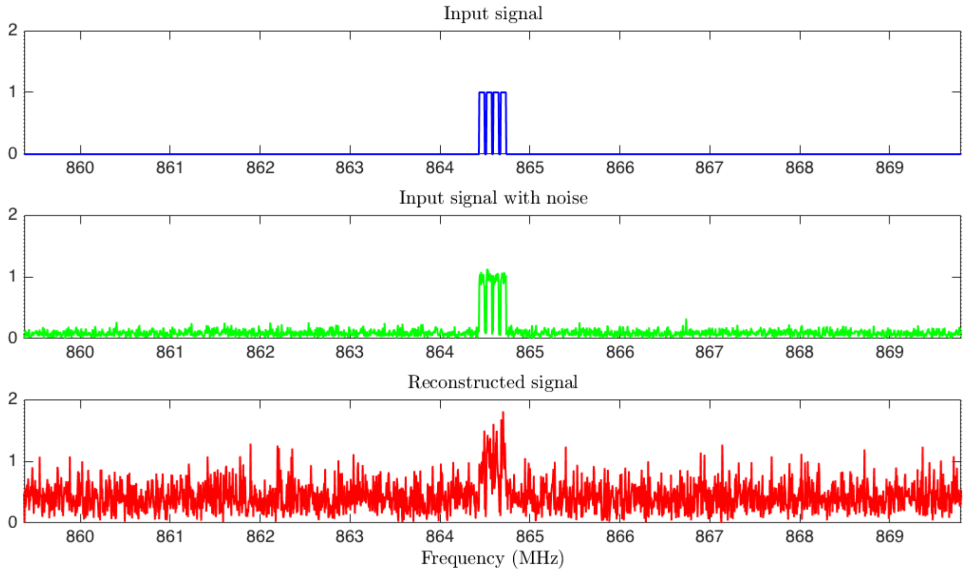

(a) SNR = 20 dB

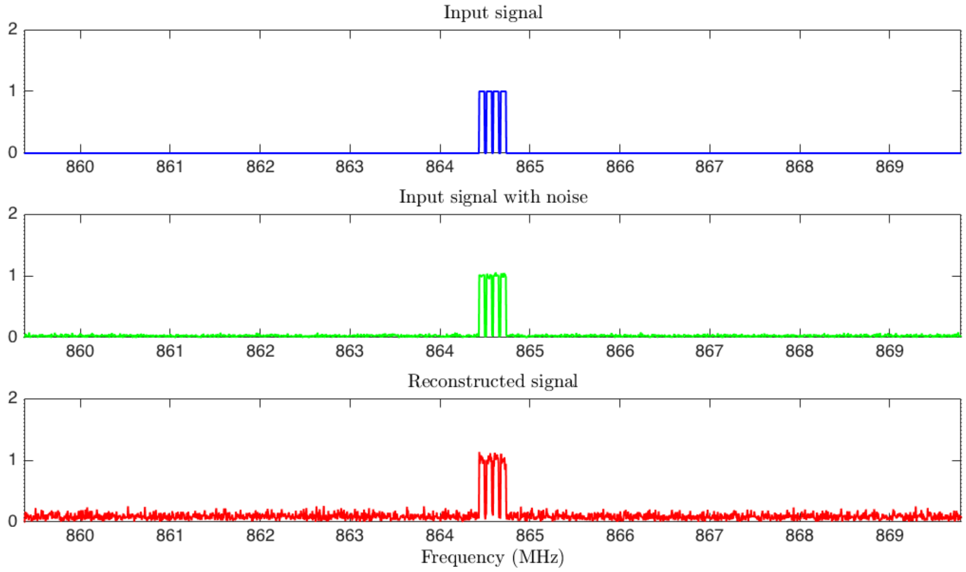

(b) SNR = 30 dB

Figure 2.20 – Spectrum reconstructions of 4 transmitters generated consecutively with frequency spacing 5 kHz at SNR of 20 and 30 dB, $B = 60$ kHz and $R_f = 5$ kHz.

SNR (dB)	15	20	25	30
P_B	0.02	0.25	0.86	1
P_c	0.97	0.93	0.99	1
P_f	0.12	0.004	0	0

Table 2.1 – Correct detection of $\{f_{t_{min}}; f_{t_{max}}\}$, correct reconstruction and false alarm rates of 8 transmitters LoRaWAN in function of SNRs.

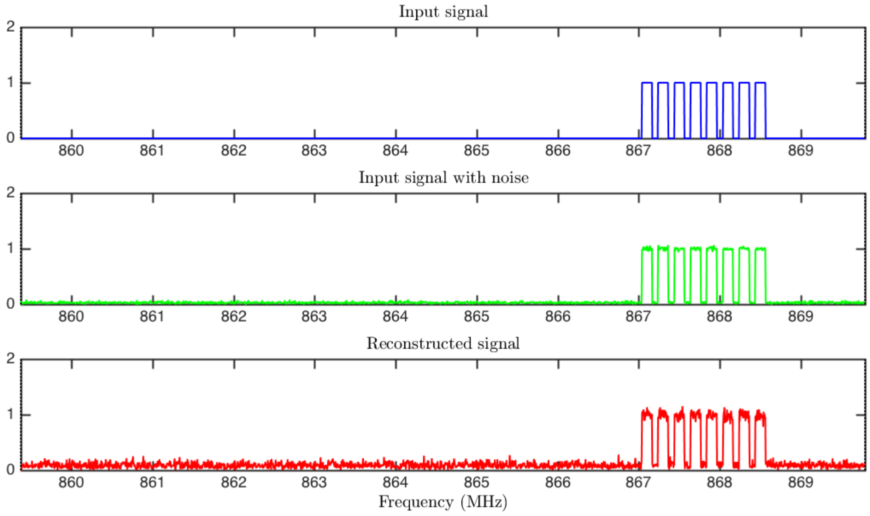

Figure 2.21 – Example of LoRaWAN EU868 blind spectrum reconstruction.

2.3 Hardware implementation in the literature

This section introduces some examples of the MWC analog board. Besides, this section also presents the implementation of each component and points out the device's problems in practice.

2.3.1 Analog boards

Some versions of MWC analog board have been developed by researchers in Technion Israel. Let us introduce these versions by chronological order. A very first version of the MWC has been published in 2009, with the implementation of analog system prototype including a MWC front-end board as in Figure 2.22 [20]. In this board, the system is tested with 2.075 GHz Nyquist rate, the number of symmetric subbands is 3, each subband with bandwidth $B = 19$ MHz. Besides, with extension factor $q = 3$, sign alternating waveform length $L = 108$, sampling rate $F_s = 70$ MHz at each physical channel, the sampling rate is considered as reducing 14% compared to the Nyquist rate. This first version allows to reduce the sampling rate significantly, however, the impacts of analog devices make the reconstruction performance of this first version unimpressive, owing to its complicated architecture [113].

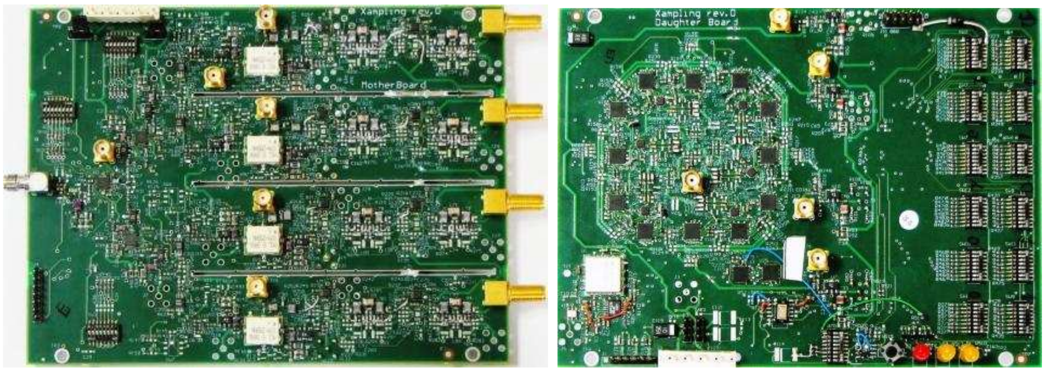

(a) MWC prototype with 4 physical channels.

(b) Four sign-alternating periodic waveforms of length $L = 108$.

Figure 2.22 – The first version of MWC prototype with 4 physical channels [20].

The hardware correction is proposed in 2010, with a method of non-ideal lowpass filter compensation [21]. Then, the system is improved in [6], which can apply for sampling finite rate of innovation signal models at an innovation rate. The generic framework is proposed in 2011 [7], by combining and developing from sampling approaches for signal acquisition in the union of sub-spaces.

The second version analog board of the MWC was introduced in 2014 [22], in this version, the Nyquist rate and subband bandwidth are higher ($F_{Nyq} = 6$ GHz, $B = 18.5$ MHz). Moreover, the sampling rate also increases $F_s = 120$ MHz, modulated waveform repetition length $L = 135$ and extension factor $q = 5$, which can detect 3 symmetric subbands. Figure 2.23 pictures the prototype of the MWC, which is dedicated for cognitive radio.

In this prototype, Gold codes sequences are used in order to modulate the wideband input signal, which is generated by an Arbitrary Wave Generator - Agilent M8190. The MWC card is in the middle composed of multi physical channels analog components. National Instruments PXIe-1065 computer is implemented to reconstruct the signal. By pointing out the imperfection of each analog component, a calibration method [22] is proposed to calculate a correct sensing matrix. The calibration method is briefly presented

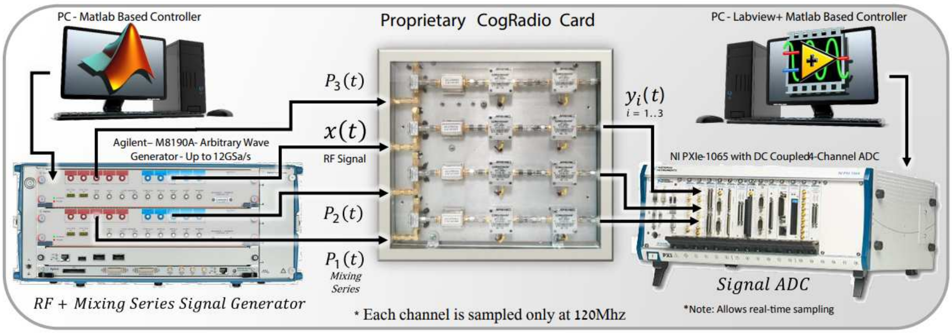

Figure 2.23 – The second version of MWC - CogRadio System [22].

in next sections.

The third version of MWC prototype has firstly been implemented including a MWC front-end board as in Figure 2.24, all of three versions have been developed by Technion - Israel Institute of Technology [23].

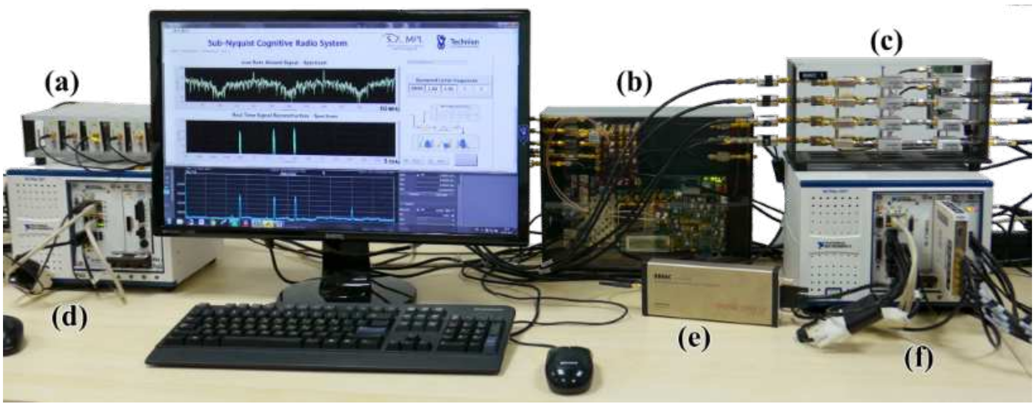

Figure 2.24 – MWC prototype: (a) vector signal generators, (b) FPGA mixing sequences generator, (c) MWC analog front-end board, (d) RF combiner, (e) spectrum analyzer, (f) ADC and DSP [23].

Specifically, this prototype is tested with a 6 GHz Nyquist rate and bandwidth of each subband 200 MHz. The ADC used in this prototype samples at a relative rate 480 MHz, is considered only 8% of the Nyquist rate. In this prototype, the MWC card comprises one high-speed 1-to-4 analog splitter to replicate 4 versions of the wideband input signal and apply to 4 channels of the MWC. The expansion factor (collapsing factor) $q = 5$ is used to achieve 20 virtual channels of the MWC ($M \times q = 20$) (the interest of collapsing factor is explained in Section 2.1.3). The mixed signal is then lowpass filtered, the cutoff of the lowpass filter is chosen at 50 MHz and the 7^{th} order Chebyshev lowpass filter is deployed.

The filtered signal with bandwidth 50 MHz will contain all the useful subbands. At last, four commercial ADCs (National Instrument) can be implemented with sampling rate 120 MHz, which produce a MWC output sampled at $4 \times 120 = 480$ MHz. This prototype is developed and applied to spectrum sensing applications in cognitive radio as well. This system is considered one of the solutions for the sub-Nyquist sampling front-end system, dedicated for spectrum sensing cognitive radios.

Moreover, there are some MWC prototypes which have been developed by other researchers. A MWC with only one channel is proposed in [114] which is deployed to spectrum sensing. The advantage of this prototype is low complexity, however, this prototype is limited in the number of subbands detection. Another approach proposes a 3-channel MWC prototype which deploys the Rocket I/O on Xilinx FPGA to replace a mixing sequence generating digital board [113]. By this way, the hardware of MWC can be simplified. In [115], a prototype of IC mixer integrated in the MWC which helps to provide a targeted mixing sequence, an improved version of random sequence. This integration can reject the blocker harmonic and the noise level. A final version of mixer prototype is demonstrated in [116], which contributes the rejection in blocker band and the delay time between two mixing sequences in two parallel mixing paths.

2.3.2 MWC components imperfections

Theoretically, the sensing matrix which is constructed from the mixing sequence is predetermined. The theoretical MWC assumed ideal components to ensure the reconstruction, it means that the sensing matrix is unaffected by the MWC components. In practice, this assumption cannot be maintained since the non-idealities of analog devices such as mixers, lowpass filter and ADCs [22, 76]. Definitely, these imperfections will impact on the sensing matrix, that makes an undetermined matrix and leads to incorrect reconstructions. Consequently, the imperfections of the MWC components need to be predetermined and a calibration method needs to be proposed. The imperfections are detailed as in following.

Mixer

As explained previously, the mixer is used to shift the input signal into baseband. By applying two signals to the input, a mixer can provide a new signal at a different frequency location. Let us illustrate the function of a mixer by a simple example. The input radio frequency (RF) signal has a simple form $B\cos(2\pi f_{RF} t)$ with amplitude B and frequency f_{RF}, the mixed signal is the output of a Local Oscillator (LO) which has a simple form $A\cos(2\pi f_0 t)$ with amplitude A and frequency f_0. Ideally, the output of the mixer is a mixed signal, denoted $I(t)$, which has an intermediate frequency (IF), such as

$$\begin{aligned} I(t) &= B\cos(2\pi f_{RF} t) \times A\cos(2\pi f_0 t) \\ &= \frac{AB}{2}\cos(2\pi f_0 t - 2\pi f_{RF} t) + \frac{AB}{2}\cos(2\pi f_0 t + 2\pi f_{RF} t). \end{aligned} \tag{2.45}$$

Figure 2.25 illustrates this example with an ideal mixing process from two signals in frequency domain. Then, the expected signal is the signal $I(t) = (AB/2)\cos(2\pi t(f_0 \pm f_{RF}))$ which has one replica in baseband.

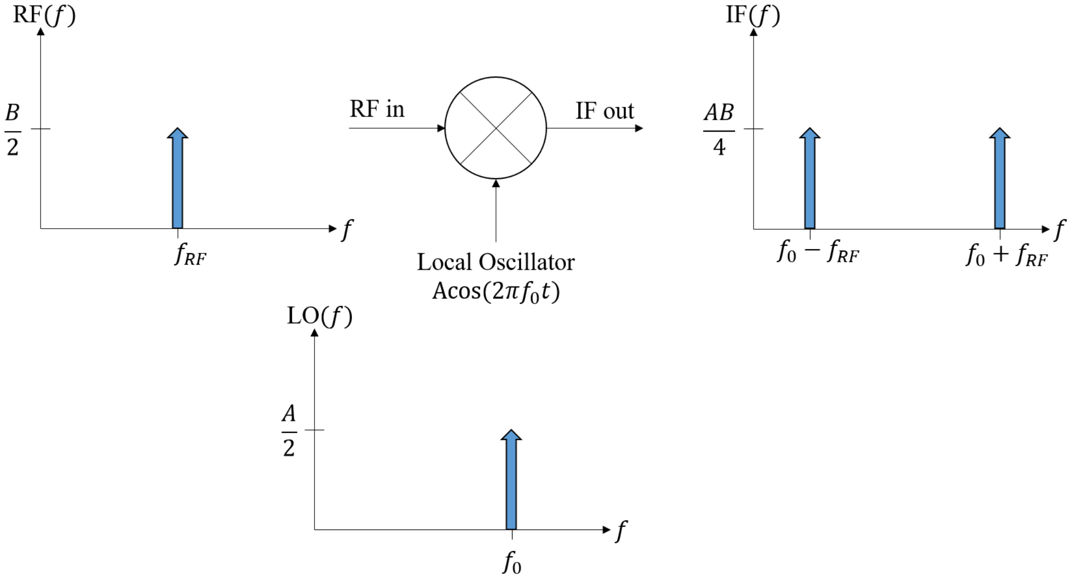

Figure 2.25 – Ideal mixing process.

In practice, the output of a non-linear mixer is presented by a polynomial based on Wiener-Hammerstein [117, 118] model such as

$$I_0(t) = \alpha_0 + \alpha_1 I_i(t) + \alpha_2 I_i^2(t) + \cdots + \alpha_n I_i^n(t). \tag{2.46}$$

in which $I_i(t) = A\cos(2\pi f_0 t) + B\cos(2\pi f_{RF} t)$. The non-linearity presents an intermodulation to the output of the mixer at frequency locations $p2\pi f_0 \pm q2\pi f_{RF}$, with p and q integers and $(p+q)$ is the order of the non-linearity. The expected frequency locations are $(f_0 \pm f_{RF})$, output of an ideal mixer, which is in the case of $p = 1$ and $q = 1$.

Then, $p + q = 2$ the second order of the polynomial non-linearity is the expected output of the mixer. The higher orders are considered as distortion.

Back to the MWC system, the mixer determines a part of the sensing matrix. The CS problem $\mathbf{y} = \mathbf{Pz}$ is a linear model. Based on the non-linearity problem, there will be more than one frequency location which is produced by a real mixer. This problem is also modeled by a polynomial. The CS with non-linear mixer [76, 119] can be modeled as

$$\mathbf{y} = \mathbf{y}_0 + \mathbf{P}_1\mathbf{z} + \cdots + \mathbf{P}_i\mathbf{z}^i + \cdots + \mathbf{P}_n\mathbf{z}^n \tag{2.47}$$

in which $\mathbf{y}_0$ is the output of the MWC itself and $\mathbf{P}_i$ is the polynomial matrix coefficients, which are undetermined in this case. The non-linear imperfections have made a hundred of frequency harmonics at the output of the mixer instead of the desired one. This also makes the sensing matrix to be unknown and difficult to reconstruct the input signal.

The mixer also induces another imperfection that is the jitter error [120]. The mixer is used to mix two signals, the clock jitter is defined as a deviation from the real period of signal. Hence, the clock jitter error and the signal amplitude as well as signal frequency can be considered proportional. The ideal input $x(t) = A\sin(\omega t)$, for example, will have a jitter error such as $x(t + e)$ at an ideal sample of $x(t)$. The jitter variation, as well as the cables and clock, contribute to the unknown and unpredictable time offsets between mixing and sampling processes. Consequently, the jitter error is a non-linear problem and this problem is also significant for the spectrum reconstruction if the jitter error is undetermined.

Low Noise Amplifier

Before mixing with the pseudo-random sequences, the input signal needs to be amplified by Low Noise Amplifier (LNA) to gain signal power and eliminate out-of-band noise. The problem of non-linearity is also provided by the LNA and this problem happened before the mixing step. The non-linearity can be modeled as

$$\mathbf{y} = \mathbf{P}f(\mathbf{z}), \qquad f(\mathbf{z}) = a_0 + a_1\mathbf{z} + \cdots + a_i\mathbf{z}^i + \cdots + \cdot + a_n\mathbf{z}^n. \tag{2.48}$$

with a_i is the coefficient of the polynomial. This non-linearity is considered more tractable than the non-linearity of the mixer, because of the scalar coefficients in $f(\mathbf{z})$ [76]. Nevertheless, this problem also needs a post-processing step to correct the signal. In this study, the problem of LNA is neglected and a focus on mixer and lowpass filter has been made since they are possible to model by Matlab and more important to the MWC output signal.

Lowpass filter

Compared to the ideal filter, practical lowpass filters have non-flat response in the passband and transition band. These problems affect the amplitude of the signal and induce some aliasing effects. Especially, the phase response of analog filters has a dominant impact since it causes an offset to the original location of the input spectrum. The imperfection of some common types of lowpass filter will be detailed in Chapter 3.

Analog-to-digital Converter

There are two steps in the ADC process which are quantizing and converting. The quantizing step introduces quantization errors due to the deviation between quantization levels and signal amplitude. This error plays an important role because it impacts the signal reconstruction. The details of quantizing and converting steps are addressed in Chapter 4.

Mixing sequence

The mixing sequence is a ±1 logic waveform. In practice, generating mixing sequences by the GTX of a FPGA cannot ensure the exact values ±1 of the sequence. As shown in Figure 2.26, compared to the ideal mixing sequence generated by Matlab as in Figure 2.9, the generated sequence by FPGA has a distorted shape. It means that the values of sequence are not exactly ±1, this problem leads to a wrong estimation of the sensing matrix and leads to a bad reconstruction. Another imperfection of the mixing sequence is the desynchronization introduced by GTXs of the FPGA. The desynchronization can be considered as the time delay between multiple mixing sequences. In practice, it is difficult

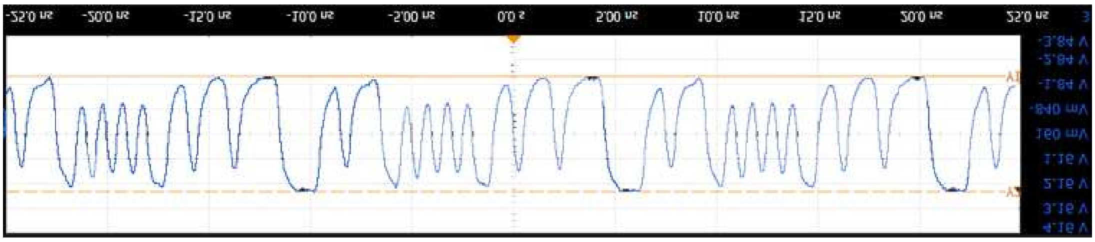

Figure 2.26 – Shape of mixing sequence generated by FPGA GTX.

to have a modulation at the 4 channels of the MWC at the same time. The desynchronization problem is pictured in Figure 2.27. The desynchronization imperfections lead

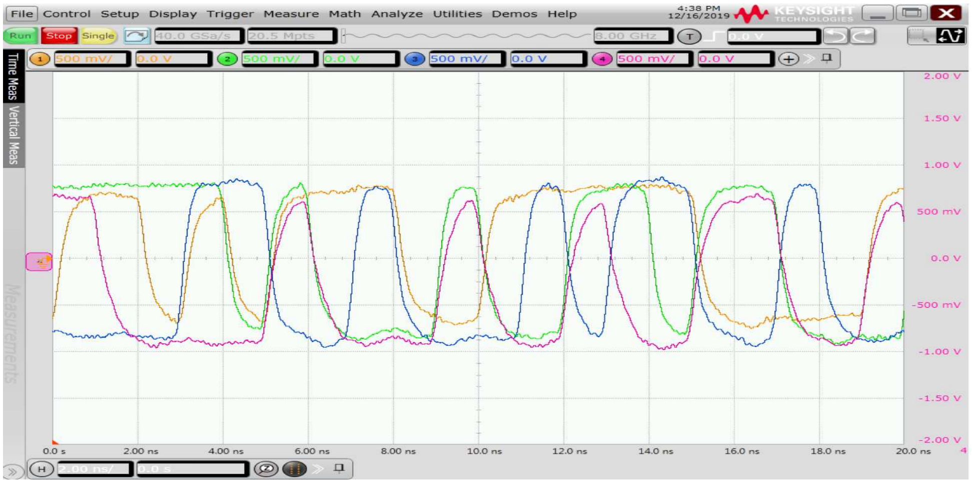

Figure 2.27 – Example of desynchronization between 4 GTXs of FPGA.

to a wrong estimation of the sensing matrix as well. Figure 2.28 shows an example of correct spectrum reconstruction rate and false alarm rate in the MWC with and without desynchronization problem. In this simulation, the MWC parameters are $M = 4$, $q = 7$, $L = 96$ and $F_{Nyq} = 1$ GHz. At the first channel of the MWC, let us consider that there is no delay. The delay in the second channel is 110 ps, the third and the fourth channels are 546 ps and 536 ps, compared to the first channel, respectively. It can be seen that with desynchronization problem, the correct reconstruction rate is reduced for all SNR levels, and the false alarm rate increases also. The mixing sequences are also under the impact of the jitter, this imperfection is produced by the mixer, as explained in the imperfection of the mixer.

2.3.3 Hardware Calibration

For the first version of the MWC developed by Technion [20], a compensation method is proposed to compensate for the imperfection of hardware [6] such as lowpass filter compensation [21]. The lowpass filter compensation is detailed after in Chapter 3 . To avoid desynchronization, a phase shift register is used to generate the sequences set [6].

For the second and the third versions of the MWC, due to many imperfections of analog components above, a calibration method is proposed to deal with such imperfections such as non-linearities, time and phase offsets, etc. The goal of the calibration method

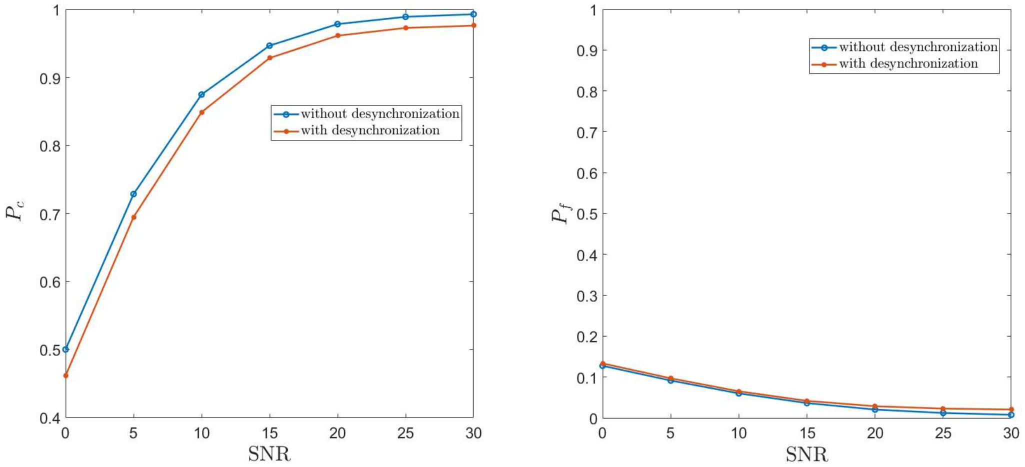

Figure 2.28 – P_c and P_f of the MWC with and without desynchronization.

is to estimate the sensing matrix $\mathbf{P}$ correctly. For the prototype designed by Technion which is presented above, a calibration method is proposed by [22] and provides good reconstruction performance. The method estimates each element of $\mathbf{P}$, with knowledge of only F_p and unknown characteristics of system components. The sensing matrix $\mathbf{P}$ can be viewed as the transfer functions of the MWC system. Then, to search for each element of this matrix, it is necessary to find the coefficient p_{il} which is the Fourier complex coefficient derived from $p_i(t)$, as in Equation 2.9. The impulse response of this system cannot be found since it is neither a linear nor time variant system. At every frequency subband of the spectrum, sinusoidal waves are generated and injected to the input signal, to re-estimate the system response.

Considering Equation 2.15, $\mathbf{y} = \mathbf{Pz}$, with $\mathbf{y}$ consisting of samples $y_i[n]$ and $\mathbf{z}$ denoting the portion of signal $x(t)$ in time domain. At each k iteration of the calibration method ($0 \leq k \leq L_0$), the input signal is inserted by a sinusoidal wave such as [22]

$$x_k(t) = \alpha_0 \sin[2\pi(kF_p + F_0)t + \phi_0], \qquad k \in [0, 1, ..., L_0], \tag{2.49}$$

with α_0 and ϕ_0 arbitrary. The bias frequency F_0 is chosen in $0 \leq F_0 \leq F_p$. In frequency domain, the signal can be seen as

$$X_k(f) = b_0(f - lF_p - F_0) + b_0^*(f - kF_p - F_0), \tag{2.50}$$

with $b_0 = \frac{\alpha_0}{2j} e^{j\phi_0}$. Then, the signal $Z(f)$ ($f \in F_p$) from Equation 2.20 with L subbands and bandwidth F_p becomes

$$(Z_k(f))_l = \begin{cases} b_0\sigma(f - F_0 + kF_p) & l = k \\ b_0^*\sigma(f + F_0 - kF_p) & l = -k \\ 0 \quad l \neq \pm k. \end{cases} \tag{2.51}$$

Then, the system equation 2.15 can be written

$$(\mathbf{Pz})_i(f) = p_{il}^* \cdot b_0^*\sigma(f + F_0) + p_{il} \cdot b_0\sigma(f - F_0), \tag{2.52}$$

which gives the expression in time domain as

$$(\mathbf{Pz})_i[n] = 2\,|b_0 p_{il}|\sin(2\pi F_0 n T_s + \phi_{il}). \tag{2.53}$$

In the system equation $\mathbf{y} = \mathbf{Pz}$, so the equation above is equal to $y[n]$. At the output of the MWC, the coefficient p_{il} can be extracted. This method has been proven by simulating of hardware reconstructing success rate, between $\mathbf{P}_{\text{calibrate}}$ and $\mathbf{P}_{\text{theory}}$. A comparison in terms of success rate between calibrated matrix and theoretical sensing matrix showed that at high SNR (more than 20 dB), the calibrated matrix can achieve more than 90% of success rate while the theoretical matrix always performs bad reconstructions [121].

Nevertheless in practice, for some implementations that have a big length of L, the process of calibration can be repeated iteratively a hundred times. To overcome this drawback, the Lab-STICC/CACS/COM team has proposed a new calibration method without iteration and using only one signal at the MWC input.

2.4 Lab-STICC Prototype and testbed

To do our own experimentation, the Lab-STICC has also developed a MWC prototype depicted in Figure 2.29.

The prototype is firstly deployed to monitor a wideband spectrum with a Nyquist rate $F_{Nyq} = 1$ GHz. The number of physical channels is fixed with $M = 4$ channels. The collapsing factor $q = 7$ is used, then there are 28 virtual channels at the MWC ($M \times q = 28$). Lowpass filters SXLP-36+ are used and each cutoff bandwidth is about 40 MHz. The configuration of this prototype can reduce the sampling rate at 29% of Nyquist rate.

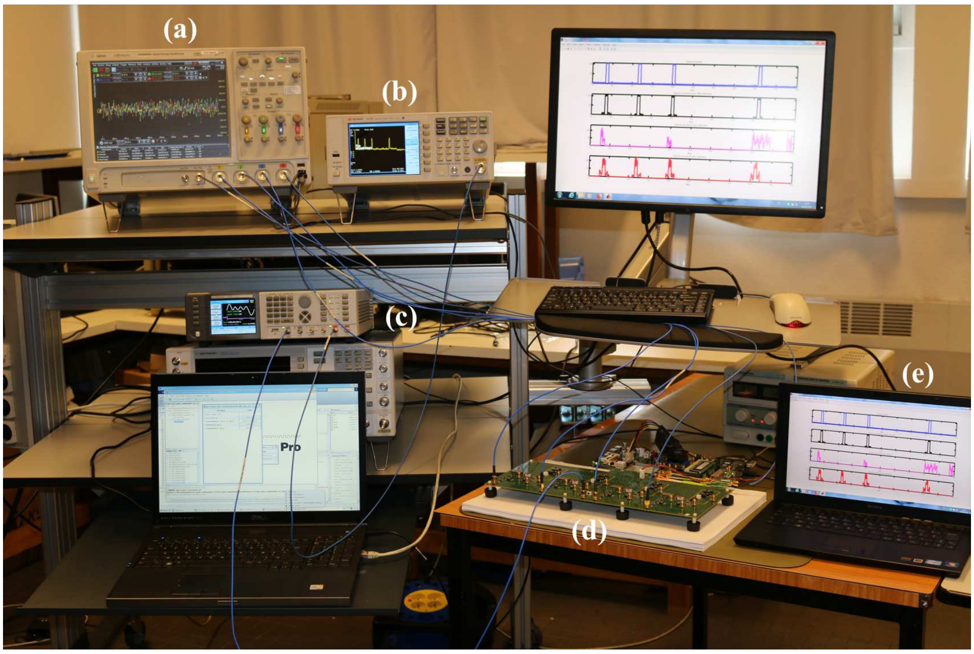

Figure 2.29 – MWC testbed developed by the Lab-STICC: (a) DSO90404A Agilent Infiniium four-channel scope, (b) Spectrum analyzer, (c) Arbitrary waveform generator, (d) MWC prototype board and ML605 board for modulating waveform generation, (e) PC controls.

Figure 2.30 demonstrates in detail the MWC board with 4 physical channels. The MWC board is connected to a Xilinx ML605 board from Avnet Virtex-6 FPGA DSP Kit with AD/DA. The role of ML605 is to generate the pseudo-random modulation waveforms. The Gigabit-Transceiver X (GTX) high-speed SERDES (SERializer-DESrializer) embedded in its Xilinx Virtex-6 model LX240T FPGA and the different debugging cores from Xilinx (Chipscope Pro) of the Virtex-6 FPGA provides the required programmability, speed and development flexibility to output the differential signals implementing the sequence. This allows us to dynamically choose (per channel) the sequence from a compiled list, and fix the size of the mixing sequence. With recompilation, new sequences can be added to the list and changed the bit rate. The clock source can be physically changed to adapt with external generators.

In general, a Keysight 81180A arbitrary waveform generator is used to generate the input signal. A PC controls the generation of the modulating waveforms with the ML605 board and also of the input signal with the arbitrary waveform generator. A MWC analog front-end board, developed in collaboration between the Lab-STICC and Syrlinks company, with four physical channels is designed to acquire and monitor the wideband input

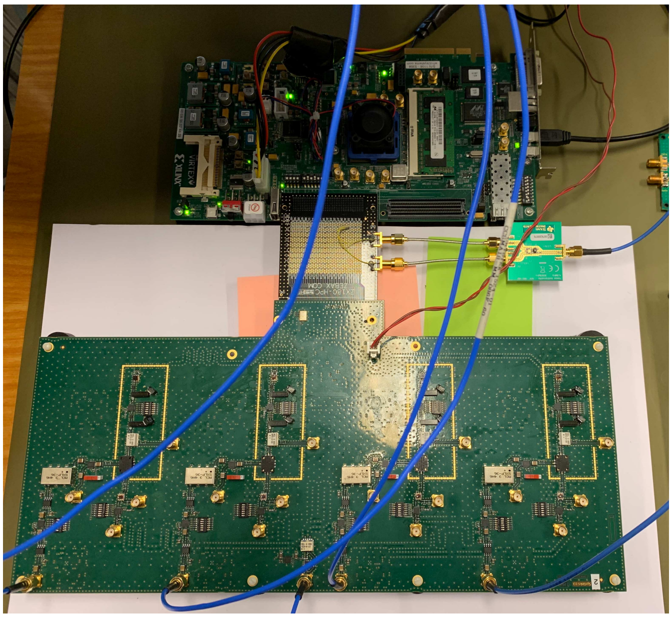

Figure 2.30 – MWC board connected with ML605 board.

signal. A spectrum analyzer is used to verify the input signal.

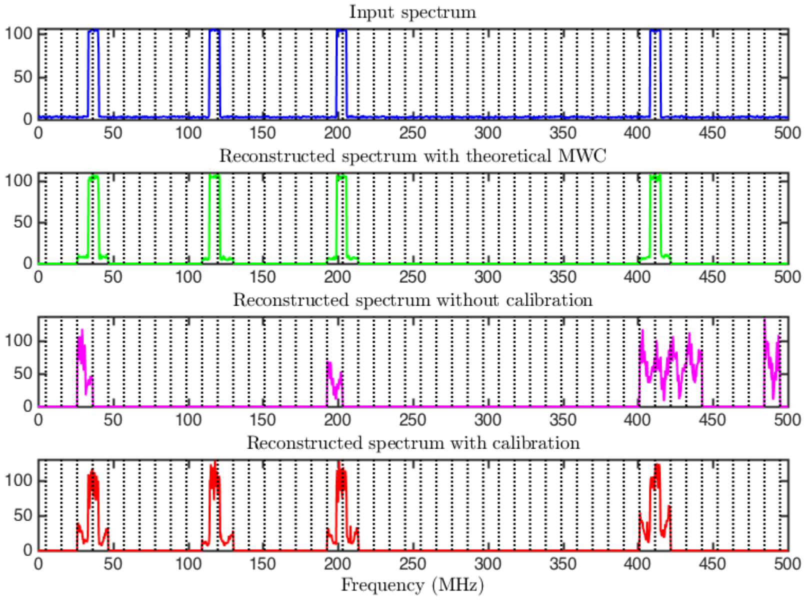

Figure 2.31 – Spectrum reconstruction with and without Lab-STICC's calibration method at SNR = 30 dB.

Another calibration method has also been developed by the Lab-STICC. The advantage of this method compared to [22] is the using of only one calibration signal. Figure 2.31 illustrates a spectrum reconstruction of 4 transmitters (SNR = 30 dB) with $F_{Nyq} = 1$ GHz with and without applying the Lab-STICC's calibration method. With the calibration method, the four signals can be detected and reconstructed correctly with their frequency locations. In the case of no calibration, it appears false alarms and spectrum lost due to the incorrect sensing matrix.

In case of high noise (SNR = 5 dB), Figure 2.32 illustrates a spectrum reconstruction of 4 transmitters with $F_{Nyq} = 1$ GHz with and without applying the Lab-STICC's calibration method. The high noise makes the MWC incapable of detecting the correct input spectrum, even in the theoretical MWC system.

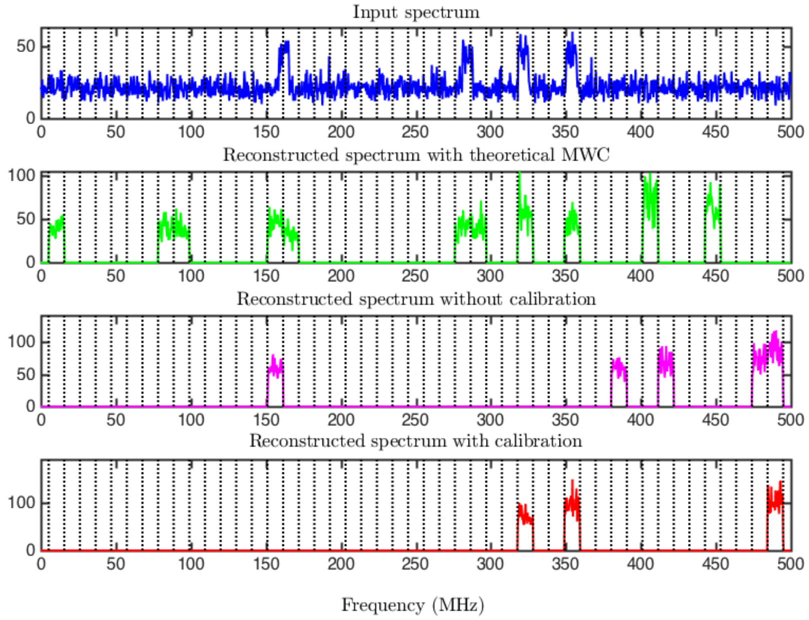

Figure 2.32 – Spectrum reconstruction with and without Lab-STICC's calibration method at SNR = 5 dB.

Figure 2.33 shows the correct reconstruction rate and false alarm rate estimated with and without the calibration method. From Figure 2.33 with the calibration process, the performance of reconstruction is improved significantly. Beside that, at low SNR such as 5 dB, the calibration cannot perform well, due to the high noise level. The calibration process can obtain the correct reconstruction, however, to achieve a reconstruction which is considered as well as ideal reconstruction, each component of the MWC needs to be studied independently.

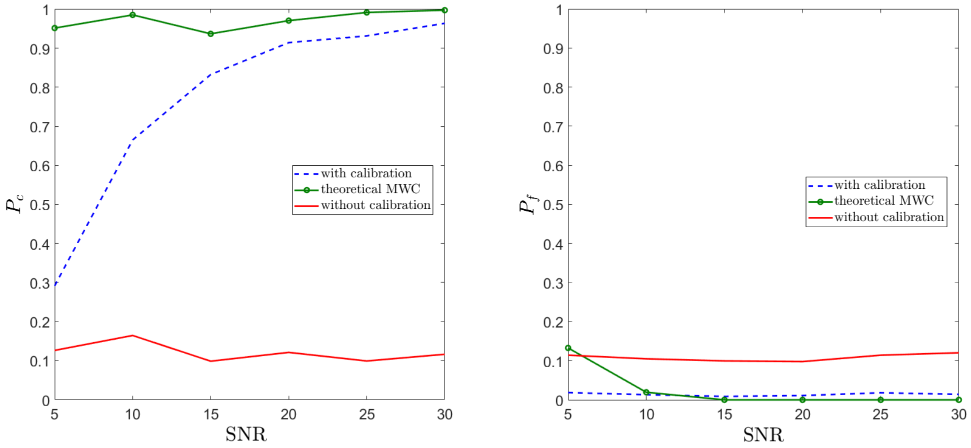

Figure 2.33 – Correct reconstruction rate and false alarm rate with and without calibration method.

2.5 Conclusion

This chapter introduces the principles of the MWC and pre-processing methods applied to the MWC output to estimate the number of active subbands and to reconstruct the input spectrum. To evaluate the performance of correct reconstruction and false alarm, the correct reconstruction rate and false alarm rate are proposed as well. A study of transmitter signal key parameters on the CS spectrum reconstructions is presented in this chapter. Based on this study, a minimum bandwidth and the maximum number of transmitters are pointed out. Besides, the simulation dedicated to the LoRaWAN spectrum detection is conducted to evaluate the performance of spectrum reconstruction. Finally, a comparison between the MWC prototype and testbed between our approach and the literature is described. In the next chapter, the imperfections of lowpass filter are detailed and the method to approach the performance of the ideal lowpass filter is proposed.

Chapter 3

Implementation of non-ideal lowpass filter on the MWC

This chapter focuses on non-ideal filters in the MWC scheme. As explained before, the MWC output of the ideal components will ensure a perfect reconstruction. In practice, the reconstruction should be based on the output of non-ideal components, especially filters. Consequently, non-ideal filters will trigger a bad reconstruction since it cannot produce an ideal output. In this chapter, a detailed study on non-ideal lowpass filters imperfections used in MWC CS scheme is synthesized. A digital post-processing scheme with amplitude and phase compensation is proposed. This post-processing scheme is applied after the non-ideal analog lowpass filtering step to obtain the filtered output as close as the ideal one. The spectrum reconstructions obtained from different simulated lowpass filters are compared, with different parameters of MWC. Finally, the correct reconstruction rate and false alarm rate are come up with to evaluate the output obtained from the MWC. To study the impacts of real lowpass filters, all other MWC components are assumed to be ideal.

3.1 Non-ideal lowpass filter in the MWC

3.1.1 Introduction

The problems of lowpass filter in the MWC have been addressed in [21, 122] and a processing methods based on Finite Impulse Response (FIR) filters have been proposed as well. The authors in [21] applied a moderate oversampling method to the signal after filtering step. This method is applied in frequency domain, assuming that $H(f)$ the real filter and $G(f)$ the FIR filter. The FIR coefficients are obtained by minimizing the function $H(f) \times G(f)$ such that $H(f) \times G(f)$ respects the characteristics of an ideal filter. This method is applied to the prototype of the MWC analog board first version, to compensate imperfections of the elliptic filter in digital domain [6]. In [23], the third version prototype of the MWC deploys a Chebyshev filter. This chapter proposes a method, which can be considered simple to implement in practice, because there is no optimization method needed as [21, 122]. It only requires the characterization of filter from spectrum analyzer and low computational cost.

This chapter investigates in detail the imperfections of lowpass filters which impact on the spectrum reconstruction. To solve this problem of the lowpass filter imperfections, a different post-processing method is proposed after filtering; to provide the output which is considered as close as an ideal filter. Moreover, the performances of the MWC reconstructions with this post-processing method will be evaluated, based on the correct reconstruction and false alarm rates. A comparison between the MWC with the post-processing method and the traditional MWC is demonstrated in order to prove the efficiency of this post-processing method.

3.1.2 Analog filters

Position of the problems

In theory, all components of the MWC scheme are assumed to be ideal to guarantee a perfect reconstruction. In the first approach, considering only the magnitude response for the filtering step, a lowpass filter can be considered as ideal if its magnitude response verifies three main properties [21] (Figure 3.1). Firstly, the magnitude response in the passband must be totally flat to avoid the problem of attenuation and thus the loss of signal. After that, the lowpass filter must have a sharp cutoff to avoid the problem of aliasing during the sampling step. Finally, the magnitude response in the stopband must be equal to zero, not to be disturbed by high frequency signal components. In practice, however, these characteristics can not be perfectly achieved by real filters. Consequently, the impact of real filters on reconstruction needs to be evaluated and solutions must be proposed to correct these imperfections in case of significant decrease in performance of the system.

In order to deploy a realistic testbed of the MWC, the set of parameters of the MWC is chosen such as $M = 4$, $q = 5$, $L = 96$ and $F_{Nyq} = 1$ GHz. Then, non-ideal lowpass filters are simulated and integrated with this set of parameters. By following the expression of the equivalent model of MWC system $F_p = F_{Nyq}/L = 10^9/96 = 10.4$ MHz, and $F_s = qF_p = 52$ MHz. (The magnitude response of the ideal filter belongs to the bandwidth $[\frac{-F_s}{2}; \frac{F_s}{2}]$, thus the cutoff of the ideal filter is fixed at $F_c = F_s/2 = 26$ MHz).

It is also necessary to choose the selectivity by fixing an order to the filter. For our future prototype of a CS system based on the MWC, several real filters have been considered and one of them could be the filter SXLP-36+ [24] designed by Mini-Circuits. Indeed, the filter SXLP-36+ has the advantages for our application, which provides a flat passband and a sharp cutoff. To match the selectivity of the filter SXLP-36+ with the Butterworth filter, the order of Butterworth filter (in simulation) is chosen as 12 and the cutoff frequency as 26 MHz. To have the same elements of comparison, the order of Chebyshev type I and II and Bessel filters (in simulation as well) are also fixed to 12 and cutoff 26 MHz.

In the following part, different classical lowpass filters, such as Butterworth, Chebyshev type I and II, and Bessel, are firstly compared. Then, these lowpass filters are simulated in the MWC scheme and reconstruction results obtained by each filter are examined.

Comparison of the different filters

Butterworth Filter: The differences between an ideal filter and an order 12 Butterworth filter are shown in Figure 3.1.

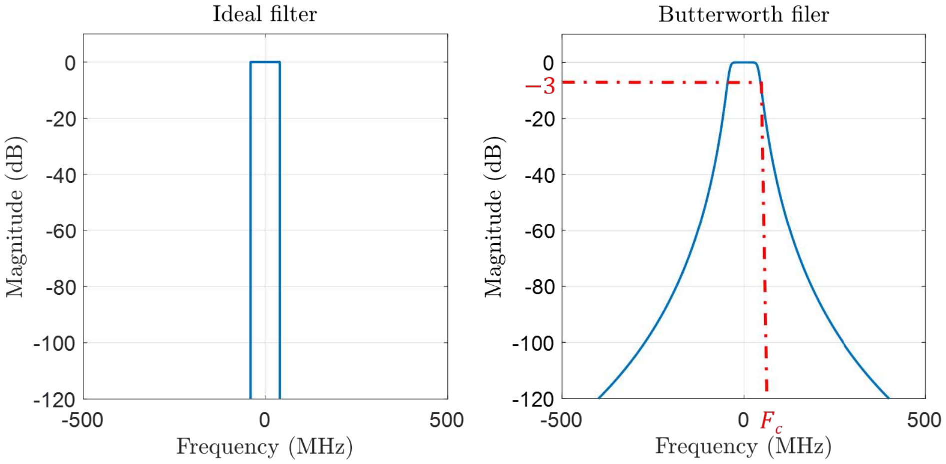

Figure 3.1 – Comparison of magnitude responses between ideal and Butterworth filters.

The magnitude response of Butterworth filter is not absolutely flat in passband and decreases to reach a value of −3 dB at the cutoff frequency; but the decrease is regular and quite smooth without ripples. Beyond the cutoff frequency, the attenuation is a multiple of −20 dB/decade depending on the order of the filter [123]. The advantages of Butterworth filter are relative flatness in the passband and non-ripple in stopband. However, it requires a very high order to quickly reach sufficient attenuation in stopband, which is essential in the MWC scheme to not have aliasing information, compared to other filters [124]

Chebyshev Filter: The magnitude responses of order 12 Chebyshev filters type I and type II filter are shown in Figure 3.2. The advantages of Chebyshev type I are the sharp cutoff and non-ripple in stopband. The advantage of Chebyshev type II filter is also the flatness in passband better than the Butterworth and its sharper cutoff in transition band. Moreover, Chebyshev type II filter may reach the same transition attenuation with a lower order than Butterworth filter. However, the drawback of Chebyshev type I is the ripple in passband and Chebyshev type II is the ripple in stopband [125] which may lead to unattended aliasing information if the attenuation is not sufficient.

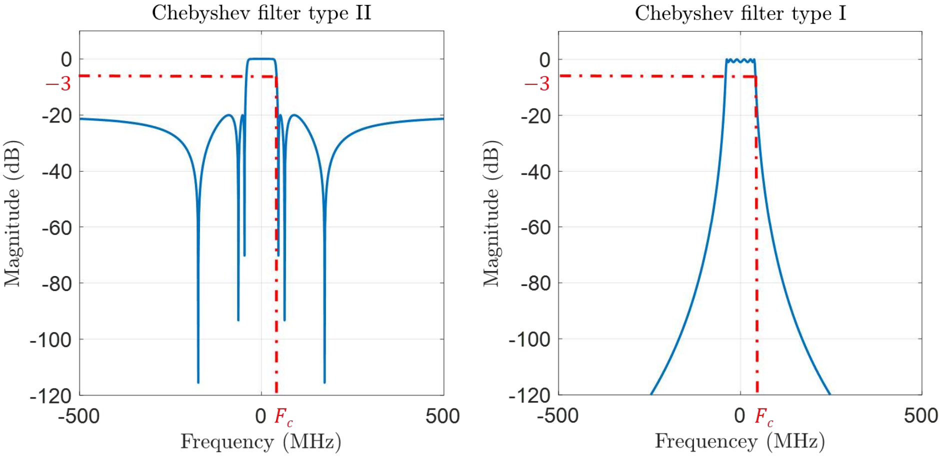

Figure 3.2 – Magnitude response of two types of Chebyshev filter.

Bessel Filter: Figure 3.3 shows the magnitude response of order 12 Bessel filter, which is not flat in the passband, not sharp in the transition band but there is no ripple in the stopband. It should have a higher order than the Butterworth to have the same specifications. Bessel filter is only suitable for those applications where the phase shift is very important. While two types of Chebyshev and Butterworth filters have a big fluctuated group delay [126], Bessel filter has a constant group delay. It is also considered as a maximal flat group/phase delay filter. In contrast with these two types of filter, Bessel filter has the advantage of delay when the order of filter is high, it means the filter delay is unchanged when the order is increased or decreased.

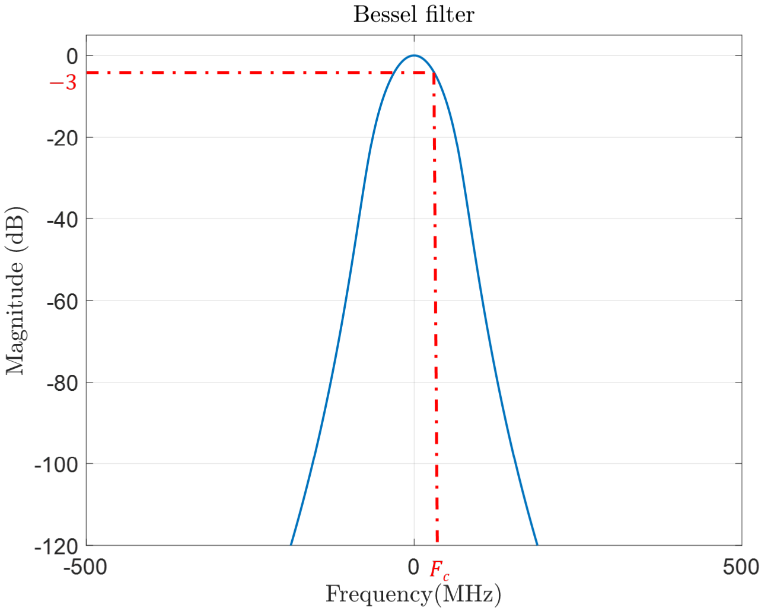

Figure 3.3 – Magnitude response of Bessel filter.

Table 3.1 summarizes the characteristics of all parameters of four filters. Figure 3.4 shows a visual comparison between the frequency responses of them. In this figure, it can be easy to observe that the Chebyshev type II filter has the sharpest cutoff compared with these three practical filters. In the next part, these lowpass filters are simulated in the MWC scheme and reconstruction results are examined.

	Buterworth	**Chebyshev**		**Bessel**
		Type I	Type II	
Passband	*flat*	*ripple*	*flat*	*not flat*
Width of transition band	*medium*	*shortest*	*medium*	*largerst*
stopband	*flat (not exactly 0)*	*flat (not exactly 0)*	*ripple*	*flat (not exactly 0)*
Phase/Group Delay	*not constant*	*not constant*	*not constant*	*constant*

Table 3.1 – The comparison table of parameters of Butterworth, Chebyshev type II and Bessel filters.

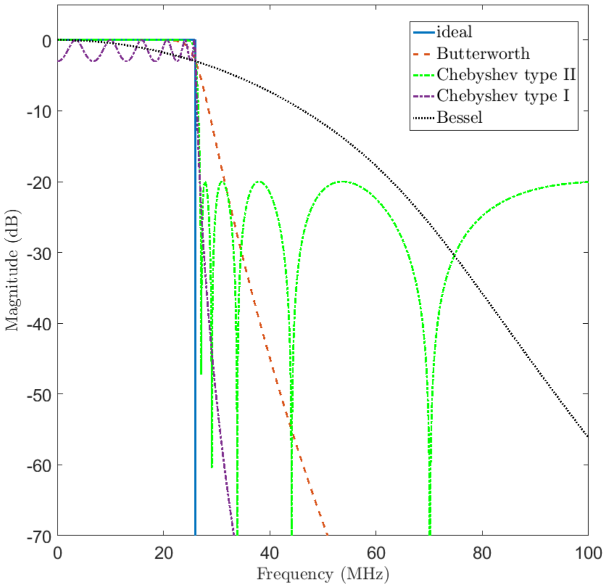

Figure 3.4 – The comparison of filter frequency responses.

Lowpass filter simulations

The set of parameters of the MWC is chosen such as $M = 4, q = 5$ and $L = 96$ (notice case 1 as in Table 3.2) as mentioned in subsection 3.1.2. We also consider the set of parameters $M = 16, q = 1$ and $L = 32$ (notice case 2 in Table 3.2) which is expensive to design due to the high number of physical channels M. Thus, mentioning that case 2 with $q = 1$ is a particular case because $F_s = F_p$. The other parameters of the system can be derived in Table 3.3.

	Case 1	**Case 2**
M	4	16
q	5	1
L	96	32
F_{Nyq} (GHz)	1	1

Table 3.2 – Table of MWC parameters.

For example in case 1 the number of transmitters N_t in Nyquist bandwidth has been fixed to 4 with a transmitted bandwidth $B = 7$ MHz for each transmitter. The condition sparsity $s < Mq$ must be subjected to, where s number of active subbands. The number of s is also related to the number of transmitters that the MWC can detect. Consequently,

	Case 1	**Case 2**
B (MHz)	7	20
N_t	4	3
SNR (dB)	20	20
F_p (MHz)	10.4	31.25
F_s (MHz)	52	31.25

Table 3.3 – Deduced parameters of the MWC.

$B < F_p$ is fixed to position the band of each transmitter inside one MWC subband or astride two MWC subbands. In the simulation, with respect to the sparsity condition, the number of active subbands is strictly set $s < Mq - 1$ and to take into account the worst case that one transmitter can be astride two active subbands, then $s = (Mq - 1)/2$. Since the transmitters are symmetric in real case (double side spectra), thus the maximum number of transmitters $N_t = s/2 = (Mq - 1)/4$ is finally set with the nearest lower integer of N_t. It is important to note that in this case, we consider only one sideband, because the two sidebands are symmetric (in the case double sideband, $N_t = 8$ with case 1 and $N_t = 6$ with case 2). It is also denoted that the SNR is the Signal-to-Noise Ratio in each active subband of the original spectrum, it is possible to give an idea of the overall SNR in Nyquist bandwidth SNR_{Nyq} by

$$\text{SNR} = \text{SNR}_{Nyq} + 10 \log \left(\frac{F_{Nyq}}{N_t \times B} \right), \tag{3.1}$$

with the given SNR $= 20$ dB, corresponding to $\text{SNR}_{Nyq} = 7.45$ dB (case 1), a value with a significant noise. For further simulation, the SNR is pre-determined and has values SNR $= [5 : 5 : 30]$ dB. Hence, to generate the RF signal with the given SNR in simulation, the power of noise is calculated by overall SNR $= P_{signal}/P_{noise}$, with P_{signal} and P_{noise} the powers of signal and noise respectively.

The frequency responses of simulated filters are shown in Figure 3.5. Figure 3.6 illustrates the spectrum of input signals at 4 physical channels of MWC and its filtered spectra. Non negligible information can be observed for frequency beyond the cutoff frequency $F_s/2 = 26$ MHz compared to an ideal filter. Consequently, the aliasing effect appears during the sampling step (Figure 3.7).

In this case, these non-ideal filters are deployed into the MWC system with cutoff frequency $F_c = F_s/2$ and then analog-to-digital converted at F_s, according to the principles of the MWC scheme [5]. The spectrum reconstruction is done by the OMP algorithm. Note

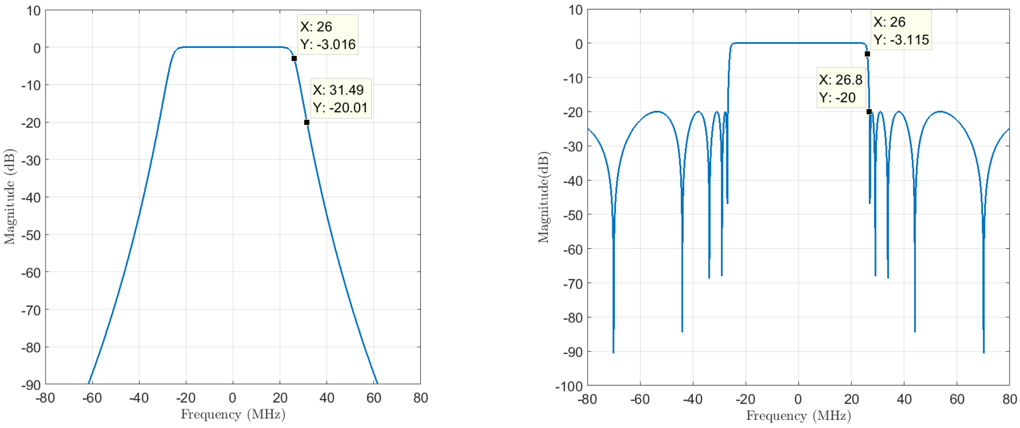

(a) Magnitude response of Butterworth filter

(b) Magnitude response of Chebyshev type II filter

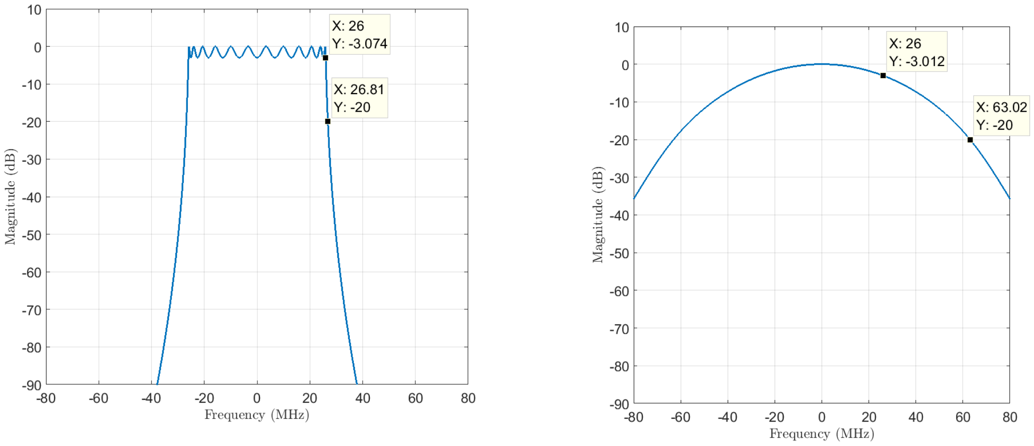

(c) Magnitude response of Chebyshev type I filter

(d) Magnitude response of Bessel filter

Figure 3.5 – Magnitude response of simulated filters.

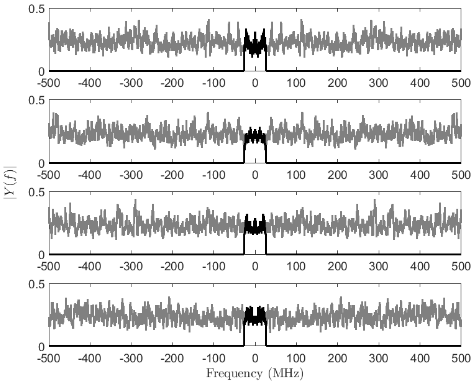

(a) Spectrum before and after ideal filter

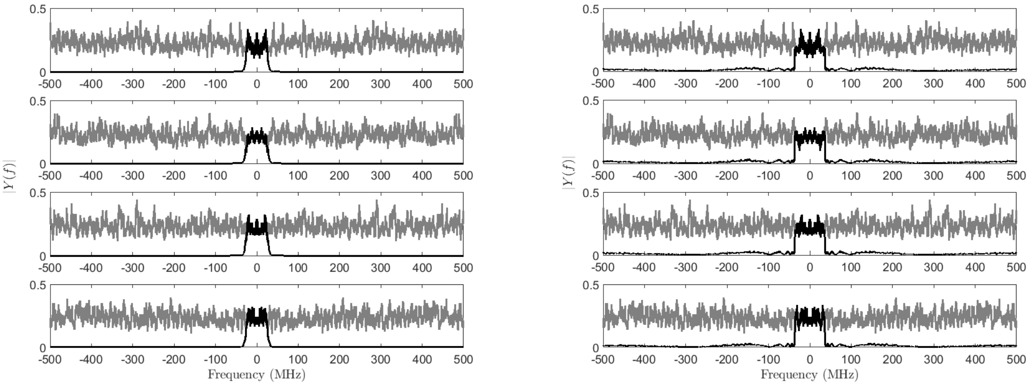

(b) Spectrum before and after Butterworth filter

(c) Spectrum before and after Chebyshev type II filter

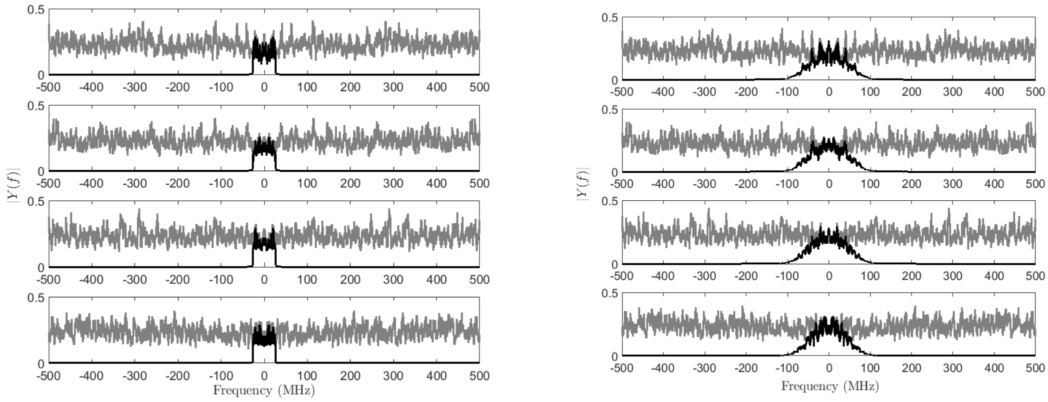

(d) Spectrum before and after Chebyshev type I filter

(e) Spectrum before and after Bessel filter

Figure 3.6 – Spectrum of input signals (grey) and filtered signals (black) at 4 physical channels of MWC when $M = 4$, $q = 5$, $L = 96$, $B = 7$ MHz, SNR = 20 dB and $F_{Nyq} = 1$ GHz.

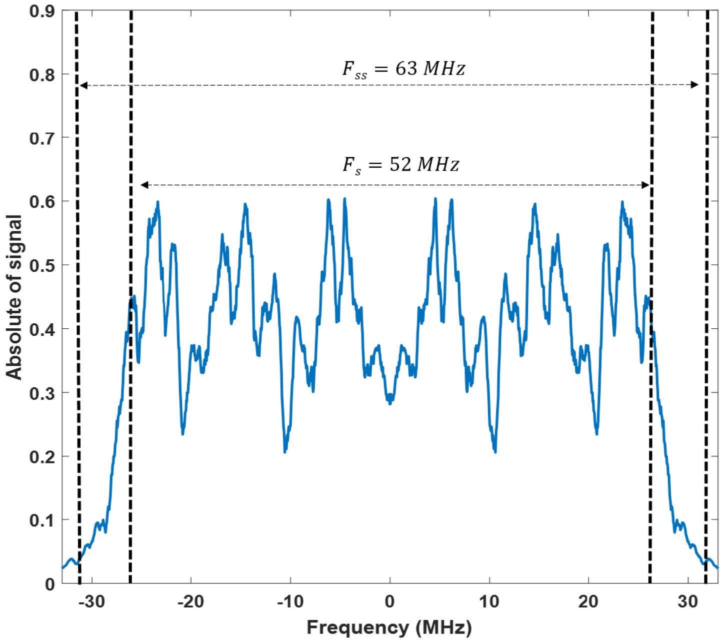

Figure 3.7 – Example of zoom of spectrum after Butterworth filter at one channel when $M = 4$, $q = 5$, $L = 96$, $B = 7$ MHz, SNR $= 20$ dB and $F_{Nyq} = 1$ GHz.

that the MWC system is based on the detection of the aliasing of the wideband input spectrum (transmitters and noise). That is the reason why in Figure 3.8 and Figure 3.9, noisy side lobes appear in the reconstructed spectrum even in ideal filter and real filter compared to the input spectrum. After that, a threshold based procedure may retain only transmitter signal contributions and eliminate the noise.

The results of reconstruction are displayed in Figure 3.8 with four different types of lowpass filter. Regarding Figure 3.8, it can be predicted that the spectrum reconstructions from the real filters are not correct due to the requirement of ideal filtered output of the MWC. The reconstruction algorithm cannot detect the frequency supports and the number of active subbands for Butterworth, Chebyshev type I and II and Bessel filters, owing to the aliasing effect.

In case 2, the number of transmitters N_t in Nyquist bandwidth has been fixed to 3 with a transmitting bandwidth $B = 20$ MHz. The given SNR is 20 dB which gives an overall SNR$_{Nyq}$ in Nyquist bandwidth a quite low value 10.97 dB. For the case $q = 1$, $M = 16$, and $L = 32$, the spectrum reconstruction is shown in Figure 3.9 in which the MWC system can detect three transmitters. Depending on the characteristics of each

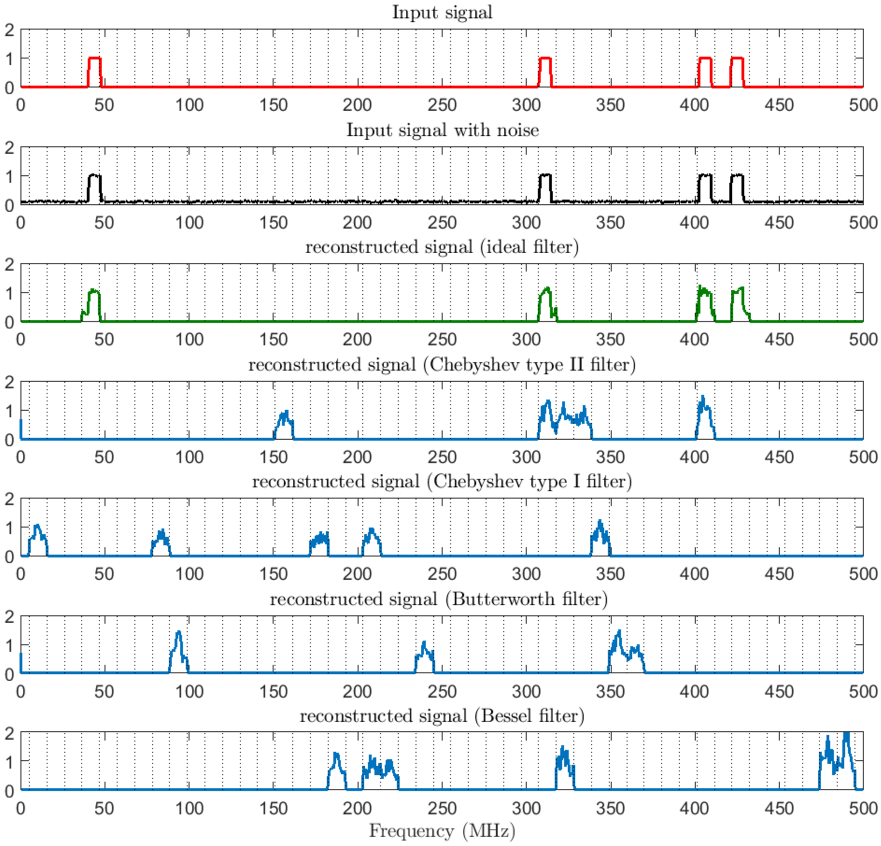

Figure 3.8 – Reconstructed spectrum without compensation with four types of non-ideal filters when $M = 4$, $q = 5$, $L = 96$, $B = 7$ MHz, SNR $= 20$ dB and $F_{Nyq} = 1$ GHz.

analog filter, however, the reconstructed spectrum consists of more noise due to the ripple (such as Chebyshev type II filter), and the losing width of spectrum due to the quick attenuation (such as Bessel filter). It could be inferred that owing to the aliasing effect and the attenuation of the analog filter amplitude, bad reconstructions are obtained. Because of the imperfections of filters, a post-processing method on the filter output will be proposed to solve the problems of magnitude and phase of the lowpass filter.

Figure 3.10 shows average values of P_c and P_f after running the simulation 2000 times. In Figure 3.10, the spectrum reconstruction is done with MWC output sampled at F_s and lowpass filter cutoff frequency $F_s/2$ (with configuration $M = 4$, $q = 5$, $L = 96$, $B = 7$ MHz, SNR $= 20$ dB and $F_{Nyq} = 1$ GHz).

It can be observed that the correct reconstruction rate P_c of all non-ideal filters is low.

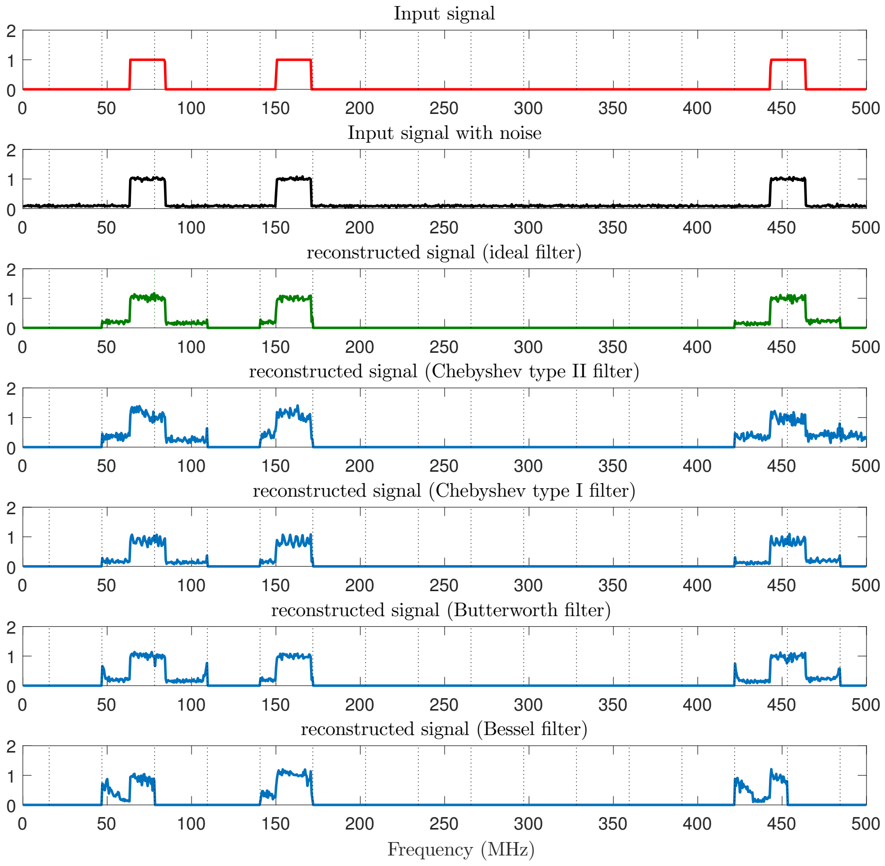

Figure 3.9 – Reconstructed spectrum without compensation in a particular case of the MWC when $M = 16$, $q = 1$, $L = 32$, $B = 20$ MHz, SNR $= 20$ dB and $F_{Nyq} = 1$ GHz.

Moreover, the false alarm rate P_f of these filters are high compared to the ideal filter since there are no correctly detected subbands at the reconstruction. In summary, due to the requirement of an ideal filter in the MWC system, it is impossible to directly reconstruct the signal after deploying a non-ideal lowpass filter and sampling at ideal frequency F_s. The next section will propose a post-processing method to solve the problems of analog filters.

3.1.3 Post-processing method and Simulation results

This section develops a post-processing method for non-ideal filters in the MWC scheme.

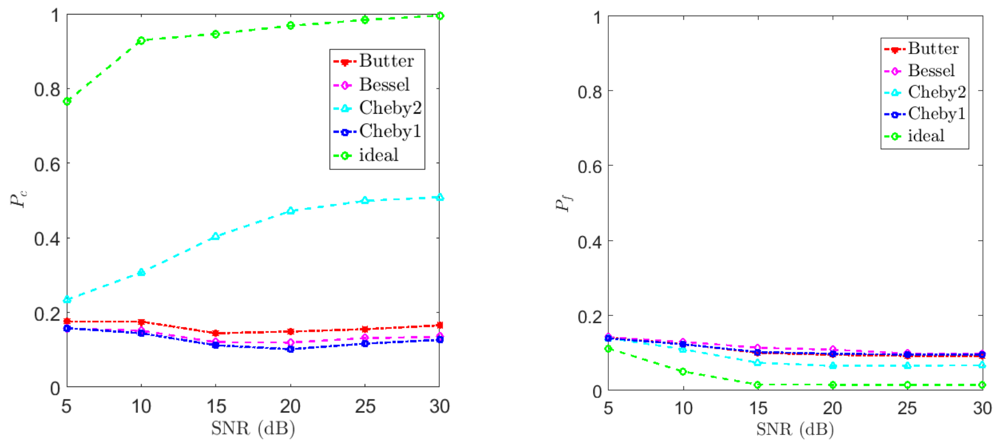

(a) The correct reconstruction rate P_c. (b) The false alarm rate P_f.

Figure 3.10 – The P_c and P_f for different SNRs without compensation when $M = 4$, $q = 5$, $L = 96$, $B = 7$ MHz and $F_{nyq} = 1$ GHz.

Amplitude compensation

As explained in Section 3.1.2, a non-ideal lowpass filter will introduce a non-sharp transition band. It means that the relevant information of the signal will be kept until the first decade of the filters (until -20 dB) owing to the property of them [123] and this relevant information cannot be neglected. This constraint defines the practical sampling frequency F_{ss} of the ADC in the real MWC scheme. For example, the frequency at -20 dB for Butterworth filter is equal to $F_{ss}/2 = 31.5$ MHz. For Chebyshev filter type I, $F_{ss}/2 = 26.8$ MHz, and type II, $F_{ss}/2 = 26.8$ MHz. For Bessel filter $F_{ss}/2 = 63$ MHz, there is more unexpected information for Bessel filter than the others (as mentioned in the previous section). The transition band of Bessel filter gives a bad effect since it attenuates very fast. Note also that the real sampling frequency F_{ss} (for example 63 MHz for Butterworth filter) is different to the ideal sampling frequency F_s (52 MHz for Butterworth filter).

In order to solve the problem of the contribution of unexpected information outside the cutoff range owing to the analog filter effects and to find the conditions as close as the ideal filter, some post-processing steps must be processed. We propose a method of post-processing shown in Figure 3.11. It should be noticed that this post-processing scheme is applied for each physical channel of the MWC. The ADC will first sample the signal at F_{ss}. The expected information, however, is only in the band $[\frac{-F_s}{2}, \frac{F_s}{2}]$ instead of $[\frac{-F_{ss}}{2}, \frac{F_{ss}}{2}]$. Hence, there will remain a part of the signal with the frequency beyond $[\frac{-F_s}{2}, \frac{F_s}{2}]$ due to the analog filter. It is therefore necessary to apply a digital (ideal) filter with cutoff frequency $\frac{F_s}{2}$ which eliminates the information between $\frac{F_s}{2}$ and $\frac{F_{ss}}{2}$, then the filtered signal remains with the band of interest $[\frac{-F_s}{2}, \frac{F_s}{2}]$. Finally, it needs to be re-sampled at the frequency F_s to achieve the conditions which are closed to an ideal analog filter $[\frac{-F_s}{2}, \frac{F_s}{2}]$ and the sampling frequency at F_s. Besides, the attenuation of analog filter from 0 dB to -3 dB is estimated with the corresponding frequency locations. It means that the gain value, which is used to make the compensation, is determined by $20\log_{10}|H| + 20\log_{10}|A| = 0$ (dB). This condition allows a flat filter amplitude in the passband. In frequency domain, the amplitude compensation step will add a value of $-20\log_{10}|A|$ (dB) to the spectrum of signal in order to compensate for the signal loss by the filter amplitude.

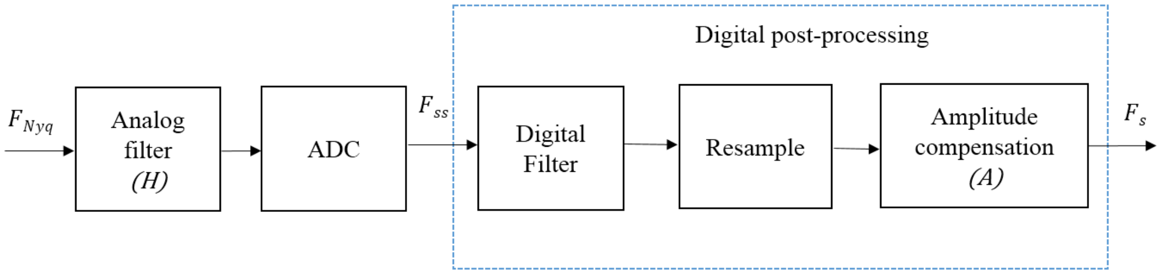

Figure 3.11 – Amplitude compensation scheme.

Figure 3.12 shows the spectrum of signal in one channel of the MWC obtained by Butterworth filter after each step of the amplitude compensation scheme. After this scheme, the expected information belongs to the bandwidth of $[\frac{-F_s}{2}, \frac{F_s}{2}]$ as well as the ideal condition of the MWC scheme.

The spectrum reconstruction in case 1 is shown in Figure 3.13. Nevertheless, there are still bad reconstructions and no correct detection subband. The problem will be figured out in the next subsection.

In case 2 with $q = 1$, the performance comparison of Chebyshev type II and Bessel is shown in Table 3.4. Moreover, the spectrum reconstruction for these filters is shown in Figure 3.14 with SNR = 20 dB. Regarding Table 3.4 and Figure 3.14, the amplitude compensation scheme can improve, in this particular case, the low performance of reconstruction (in red color) and provide higher performance (in blue color) for Chebyshev type II and Bessel filters, especially in the low SNRs. Moreover, the other filters can have an improvement in the bandwidth of each subband.

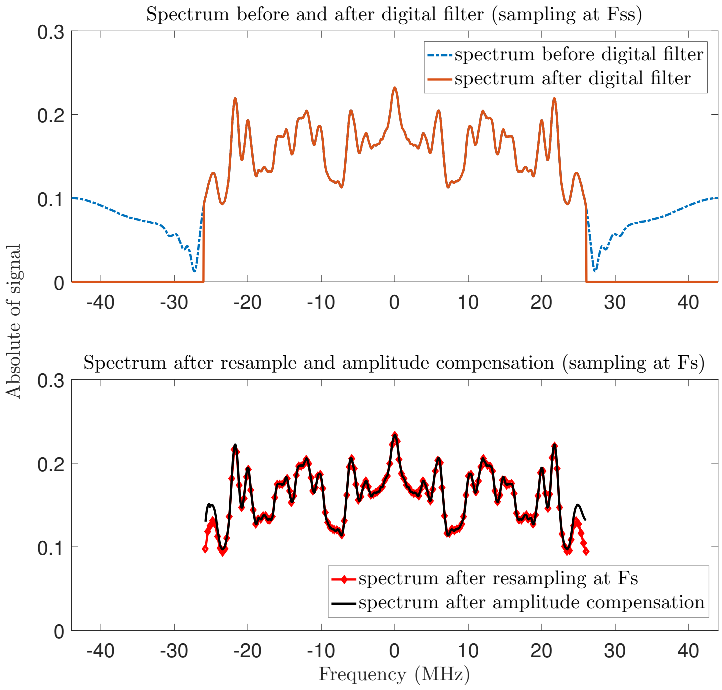

Figure 3.12 – Spectrum in one channel of the MWC (obtained by Butterworth filter) before and after applying digital filter at cutoff $F_s/2 = 26$ MHz and after resampling and amplitude compensation steps when $M = 4$, $q = 5$, $L = 96$, $B = 7$ MHz, SNR $= 20$ dB and $F_{Nyq} = 1$ GHz.

SNR (dB)	No compensation				Amplitude compensation				ideal filter	
	Cheby2		Bessel		Cheby2		Bessel			
	P_c	P_f	P_c	P_f	P_c	P_f	P_c	P_f	P_c	P_f
5	0.89	0.20	0.83	0.25	0.92	0.13	0.90	0.15	0.93	0.12
10	0.92	0.15	0.86	0.18	0.93	0.06	0.92	0.08	0.94	0.06
15	0.93	0.12	0.87	0.09	0.95	0.06	0.93	0.07	0.97	0.06
20	0.97	0.08	0.87	0.09	0.98	0.05	0.96	0.06	0.98	0.05
25	0.99	0.08	0.93	0.07	0.99	0.05	0.94	0.06	0.99	0.05
30	0.99	0.07	0.95	0.05	0.99	0.04	0.99	0.05	0.99	0.04

Table 3.4 – Average values of reconstruction rates P_c and P_f of Chebyshev type II and Bessel filters before and after applying amplitude compensation for all SNRs with configuration $q = 1$, $M = 16$, $L = 32$, $B = 20$ MHz and $F_{Nyq} = 1$ GHz.

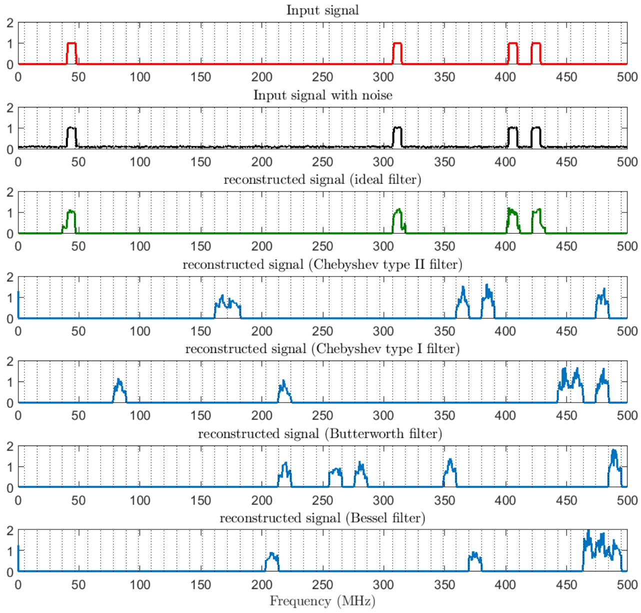

Figure 3.13 – Spectrum reconstruction with amplitude compensation scheme when $M = 4$, $q = 5$, $L = 96$, $B = 7$ MHz, SNR $= 20$ dB and $F_{Nyq} = 1$ GHz.

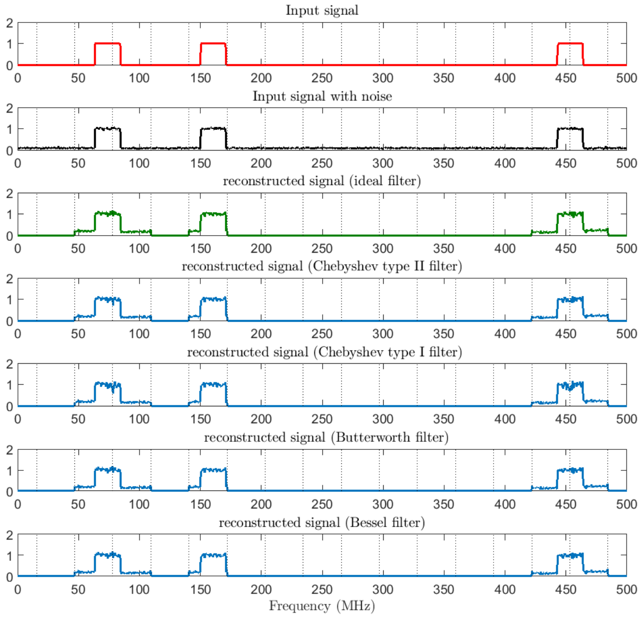

Figure 3.14 – Reconstructed spectrum in a particular case of the MWC with amplitude compensation scheme when $q = 1$, $M = 16$, $L = 32$, $B = 20$ MHz, SNR $= 20$ dB and $F_{nyq} = 1$ GHz.

For the case $q > 1$, Figure 3.15 shows the P_c and P_f rates of signal reconstruction after applying the post-processing scheme of amplitude compensation. Compared to Figure 3.10, the performances of all non-ideal filters do not improve. The amplitude default seems to be not predominant. Consequently, another filter impact must be pointed out: the phase response of filters.

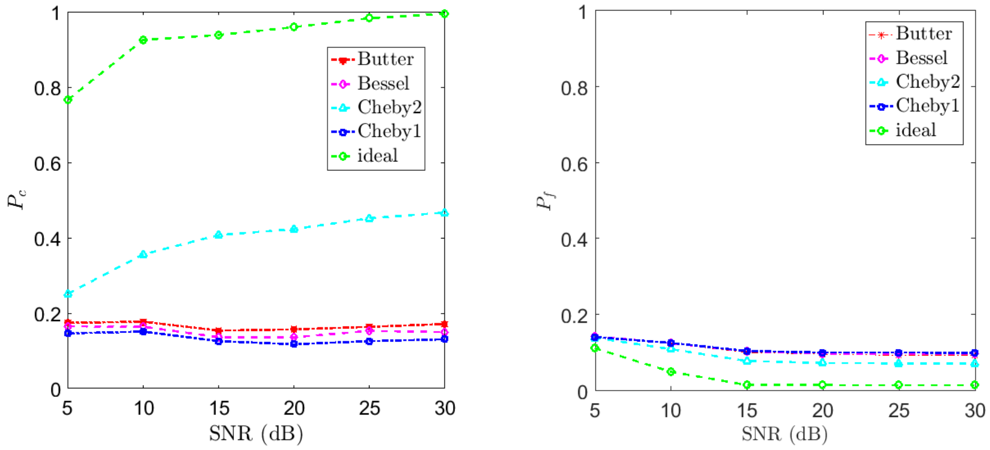

(a) The correct detection rate P_c.

(b) The false alarm rate P_f.

Figure 3.15 – The rates P_c and P_f for different SNRs after applying amplitude compensation when $M = 4$ $q = 5$, $L = 96$, $B = 7$ MHz and $F_{Nyq} = 1$ GHz.

Phase compensation

An ideal filter must verify the fourth property: the phase shift must be equal to zero. For a non-ideal filter, the problem is based on the property of filter phase delay. Indeed, the output signal is shifted during the convolution step of input signal and filter response. In real devices, the phase of filters would never be equal to 0. In a Linear Time Invariant (LTI) system, the frequency response of a filter is computed by

$$H(j\omega) = |H(j\omega)|\, e^{j\theta(\omega)}, \tag{3.2}$$

where $\theta(\omega) = arg(H(j\omega))$ the phase shift of the filter. Consequently, the sensing matrix $\mathbf{P}$ is not correct, this is the reason why the performances of reconstructions have deteriorated.

Hence, in order to have a correct output, a phase compensation step must be applied to the simulation environment. With the phase compensation method by multiplying with $e^{-j\theta(\omega)}$, the output signal will be shifted to its correct location. In practice, the signal sampled at F_s is obtained from each channel and the compensation is also applied to the signal in the frequency domain. The value of the phase compensation is determined such that $phase(H) + phase(T) = 0$ (since an ideal filter has no phase shift). In the phase compensation step, the output is simply added $phase(T) = -phase(H)$ by pre-determining the phase of real filter H in the frequency domain.

This approach assumes that the phase has been beforehand determined. Figure 3.16 shows the scheme of phase compensation with the traditional MWC. Let us mention the particular case $q = 1$ ($F_s = F_p$), there is no shift in the sensing matrix $\mathbf{P}$ (in the case of using collapsing factor q). When $q = 1$, the sensing matrix $\mathbf{P}$ is correct. Consequently, it does not need to compensate for the phase shift when $q = 1$. This observation explains the results obtained in Figure 3.14. As displayed in Figure 3.17, the phase response of Bessel filter is constant since it is illustrated by a linear line while Butterworth filter and Chebyshev type I and II have a significant variation phase response.

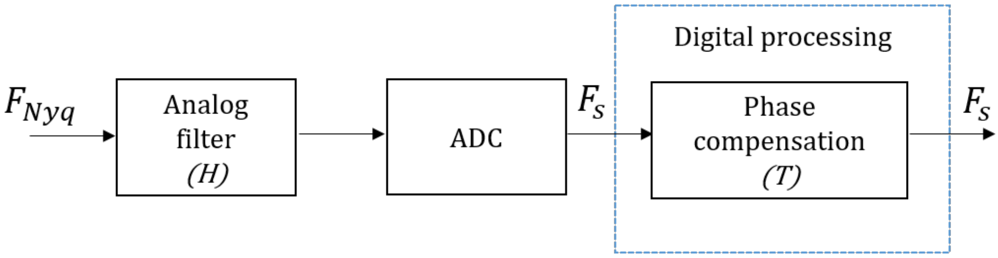

Figure 3.16 – Traditional MWC scheme with filter phase compensation.

After phase compensating, although the output signal is in its correct location (Figure 3.19), there exist some false alarms at the spectrum reconstruction. It is logical to see that without the aliasing correction, the analog filter of the traditional MWC will contribute more unexpected information, then lead to more unexpected spectra compared to the input signal. It could be inferred that without amplitude and phase compensation, these filters will not ensure a correct reconstruction. Moreover, Figure 3.18 illustrates the P_c and P_f rates of the traditional MWC with phase compensation.

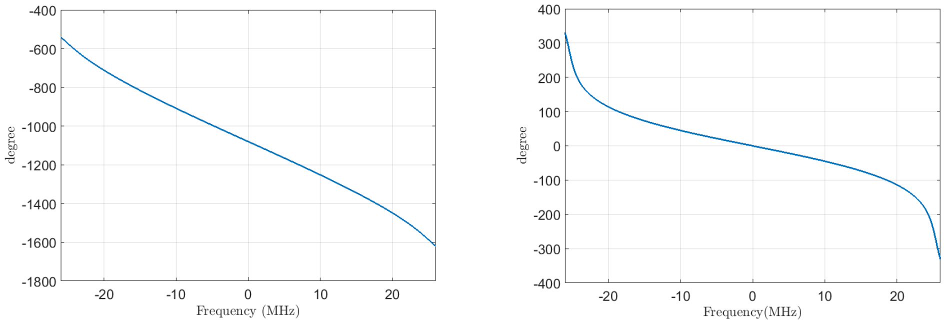

(a) Butterworth filter phase response.

(b) Chebyshev type II filter phase response.

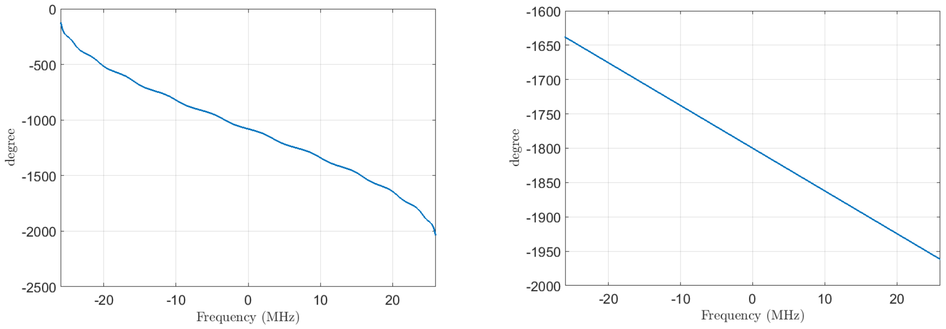

(c) Chebyshev type I filter phase response.

(d) Bessel filter phase response.

Figure 3.17 – Smooth plots of phase response of the filters.

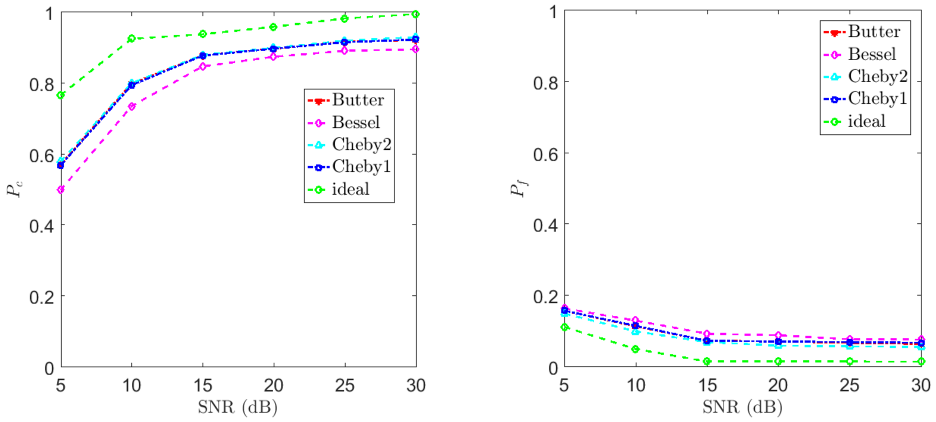

(a) The correct reconstruction rate P_c.

(b) The false alarm rate P_f.

Figure 3.18 – The rates P_c and P_f for all SNRs (sampling F_s + phase compensation) $M = 4$, $q = 5$, $L = 96$, $B = 7$ MHz and $F_{Nyq} = 1$ GHz.

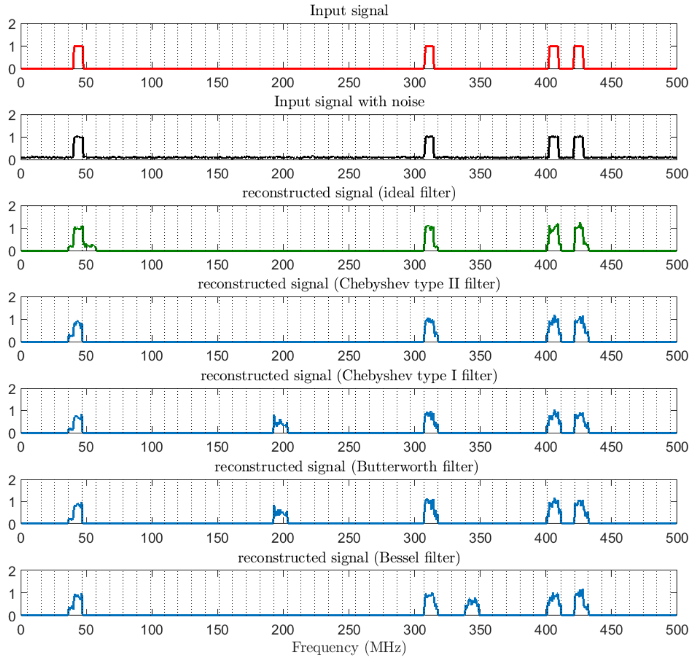

Figure 3.19 – Reconstructed spectrum of traditional MWC system (sampling F_s + phase compensation) $M = 4$, $q = 5$, $L = 96$, $B = 7$ MHz, SNR $= 20$ dB and $F_{Nyq} = 1$ GHz.

Although the correct reconstruction rate of the filters in the traditional MWC with this phase compensation is better at high SNRs with a clear improvement compared to the case of without compensation. Nevertheless, there exists a degradation of performance at low SNR due to the non-amplitude compensation (aliasing effect). It indicates that there are more false alarms at the output of the traditional MWC. The MWC is a blind detection system, so it is very difficult to distinguish the expected signal and false alarms. Consequently, the post-processing scheme is proposed in the next part with a combination of amplitude and phase compensation: global compensation.

Global compensation

It is important to consider where the compensation process should be applied to have the best performance and cost for the real system. Theoretically, there are three possible points which can apply the compensation process as after the analog filter, after ADC at F_{ss} or after resampling at F_s.

The first point is just after the analog filter. The compensation needs to be made with the coefficients which are estimated on F_{Nyq} bandwidth. Moreover, the signal at this point is still analog, so it is not practical to do digital processing on an analog signal. In contrast, the digital processing can be implemented at the second point after ADC at F_{ss} and the third point after resampling at F_s. The second point is after ADC at F_{ss}. In practice, the digital processing can be applied and the number of compensating coefficients needs to be estimated on F_{ss} bandwidth. The last point is after resampling step at F_s. The digital processing can be applied and the number of compensating coefficients needs to be estimated on F_s bandwidth. This point is more efficient than the previous two points since it needs less coefficients than compensating at F_{ss} and F_{Nyq}.

Consequently, one example of Butterworth filter with the P_c and P_f rates estimated by average of 2000 achievements are shown in Table 3.5, to indicate which point will provide the best performance.

Performance / SNR (dB)	P_c			P_f		
	F_{Nyq}	F_{ss}	F_s	F_{Nyq}	F_{ss}	F_s
5	0.756	0.753	0.755	0.109	0.109	0.109
10	0.918	0.915	0.918	0.043	0.043	0.043
15	0.935	0.934	0.935	0.004	0.004	0.003
20	0.955	0.955	0.955	0.003	0.003	0.003
25	0.982	0.982	0.982	0.003	0.003	0.003
30	0.992	0.992	0.992	0.003	0.003	0.003

Table 3.5 – Comparison table of Butterworth filter with correct reconstruction rate P_c and false alarm rate P_f when compensating at 3 possible points.

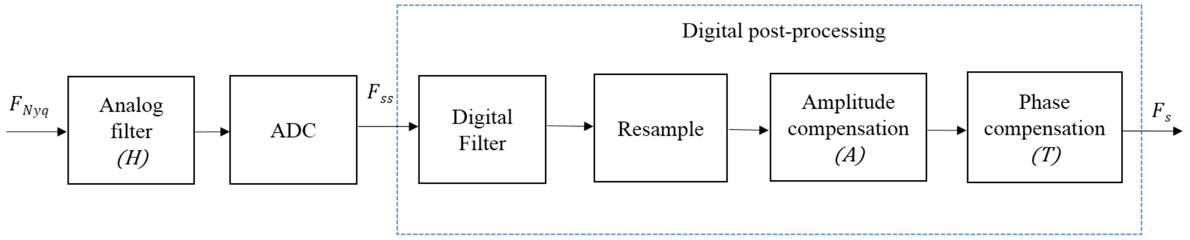

Figure 3.20 – Global compensation scheme.

Regarding Table 3.5, there are no significant differences between the performances when compensating at these 3 points. In practice, the compensation can be done at F_{ss}

or F_s. The compensation at F_s, however, will reduce the complexity compared to F_{ss} due to the low number of samples to estimate. Consequently, the phase compensation should be made after resampling at F_s. Figure 3.20 shows the post-processing scheme with the combination of amplitude and phase compensations, called global compensation.

After global compensation, the spectrum reconstruction is in its correct location and the false alarms have been drastically reduced and coincide with what obtained by the ideal filter as in Figure 3.21.

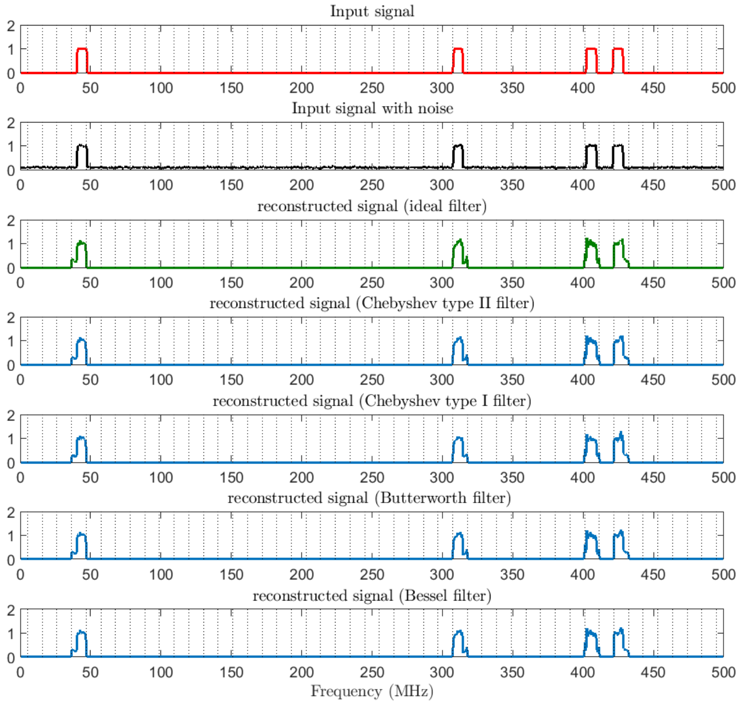

Figure 3.21 – Reconstructed spectrum of the MWC system with global compensation post-processing scheme when $M = 4$, $q = 5$, $L = 96$, $B = 7$ MHz, SNR $= 20$ dB and $F_{Nyq} = 1$ GHz.

Performances of reconstruction after applying a post-processing scheme with global compensation are illustrated in Figure 3.22. It is easy to see that, after the correct spectrum reconstruction with the post-processing scheme, the performances of reconstruction are high when the noise levels are low and their correct reconstruction rates are higher than 0.7 in the case of very high noise SNR $= 5$ dB. The false alarm rates P_f are reduced and their values are approximately 10% in the case of high noise (5 dB). In the cases of high SNR, the false alarm rates are low (approximately 1%). In general, this performance can prove that the post-processing scheme is efficient and it can be well-applied to any practical lowpass filters. Moreover, the most important approach is that the reconstruction results are very close, even identical to those obtained from an ideal filter.

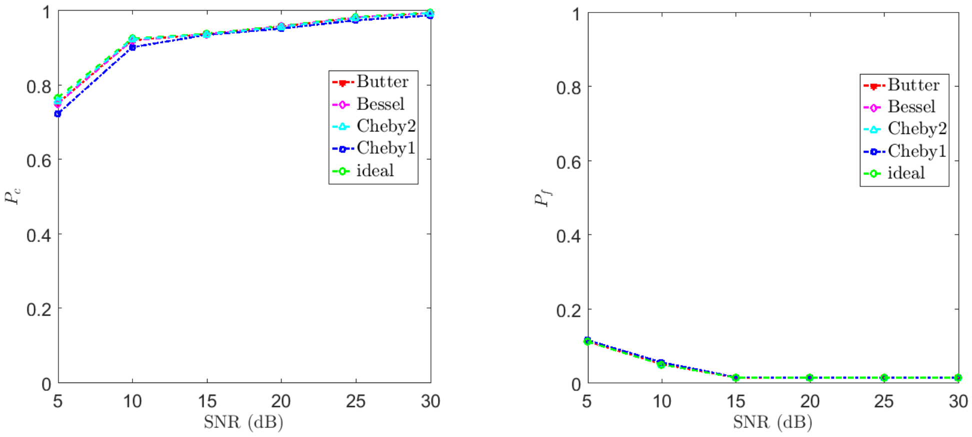

(a) The correct reconstruction rate P_c. (b) The false alarm rate P_f.

Figure 3.22 – The rates P_c and P_f for different SNRs after applying post-processing scheme with global compensation when $M = 4$, $q = 5$, $L = 96$, $B = 7$ MHz and $F_{Nyq} = 1$ GHz.

3.1.4 Different parameters simulations

In this section, the post-processing scheme is applied to a set of MWC physical parameters in the general case ($q > 1$), and the impact of noise on spectrum reconstruction is also evaluated.

For instance, in the configuration of $M = 4, q = 3, L = 32, B = 41.7$ MHz and $F_{Nyq} = 2$ GHz. Figure 3.23 shows the reconstruction of four types of filter in the case of SNR = 20 dB. Moreover, Figure 3.24 shows the performance of reconstruction in terms of average values P_c and P_f. It is observed that the differences of P_c between these practical filters and the ideal filter are small. Moreover, the average values of false alarm rate P_f are low in all SNRs. This result confirms that the post-processing method is efficient based on the high correct reconstruction rates and low false alarm rates.

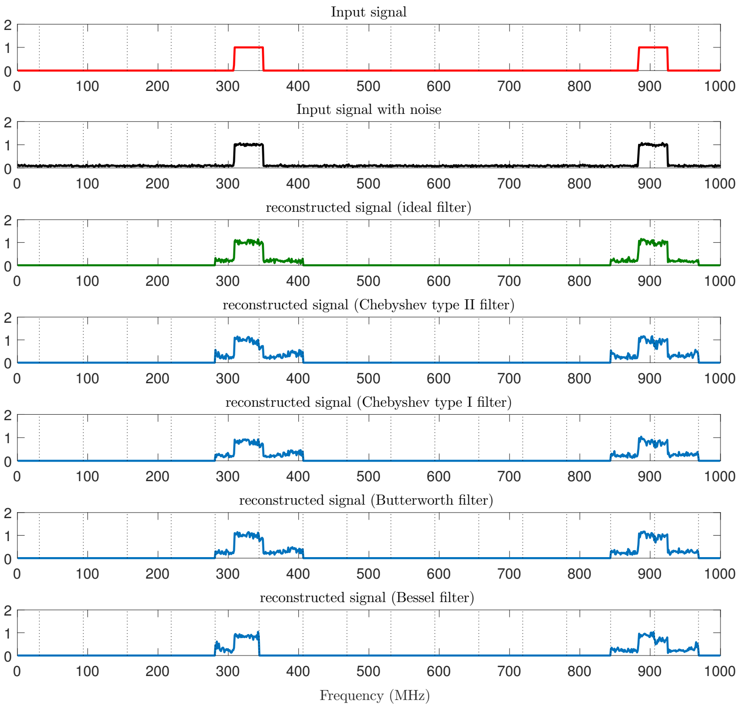

Figure 3.23 – Reconstructed spectrum of the MWC with global compensation when $M = 4$, $q = 3$, $L = 32$, $B = 41.7$ MHz, SNR $= 20$ dB and $F_{Nyq} = 2$ GHz.

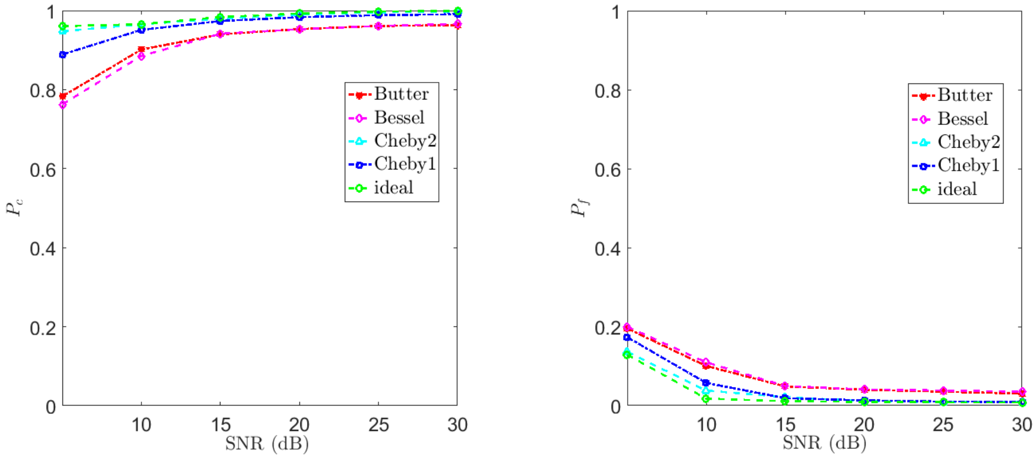

(a) The correct reconstruction rate P_c.

(b) The false alarm rate P_f.

Figure 3.24 – The rates of P_c and P_f for different SNRs after applying post-processing scheme with global compensation when $M = 4$, $q = 3$, $L = 32$, $B = 41.7$ MHz and $F_{Nyq} = 2$ GHz.

In the configuration of $M = 4$, $q = 5$, $L = 64$, $B = 20.8$ MHz and $F_{Nyq} = 2$ GHz, the spectrum reconstruction is shown in Figure 3.25 with SNR = 20 dB and Figure 3.26 shows the performances of reconstruction in terms of average values P_c and P_f. Based on this figure, the correct reconstruction rates of these practical filters are high (more than 80%) even if SNR = 5 dB. Moreover, the false alarm rates P_f of these practical filters are low for all values of SNRs, approximately 20% in the case of SNR = 5 dB.

In the configuration of $M = 4$, $q = 7$, $L = 64$, $B = 52$ MHz and a very large $F_{Nyq} = 5$ GHz, Figure 3.27 presents the reconstruction in the case of SNR = 10 dB. Figure 3.28 shows performances of reconstruction in terms of average values P_c and P_f. The correct reconstruction rates P_c of these practical filters are high in all cases of SNRs. Besides, the rates P_f of these filters are low for all cases of SNRs as well.

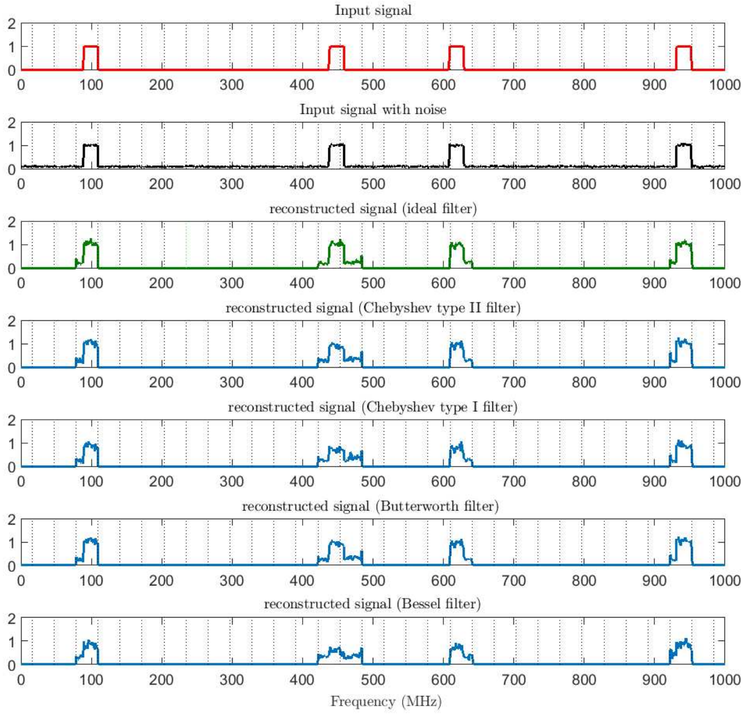

Figure 3.25 – Reconstructed spectrum of the MWC with global compensation when $M = 4$, $q = 5$, $L = 64$, $B = 20.8$ MHz, SNR = 20 dB and $F_{Nyq} = 2$ GHz.

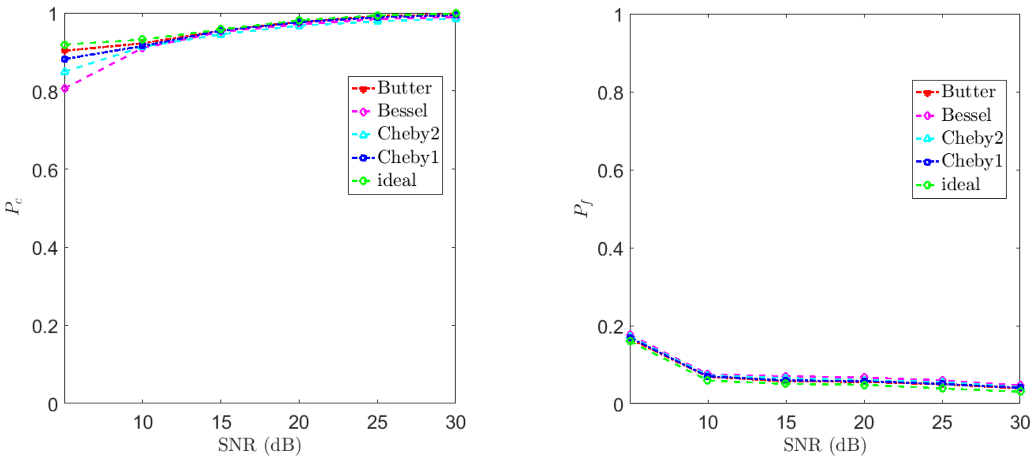

(a) The correct reconstruction rate P_c.

(b) The false alarm rate P_f.

Figure 3.26 – The rates of P_c and P_f for different SNRs after applying post-processing scheme with global compensation when $M = 4$, $q = 5$, $L = 64$, $B = 20.8$ MHz and $F_{Nyq} = 2$ GHz.

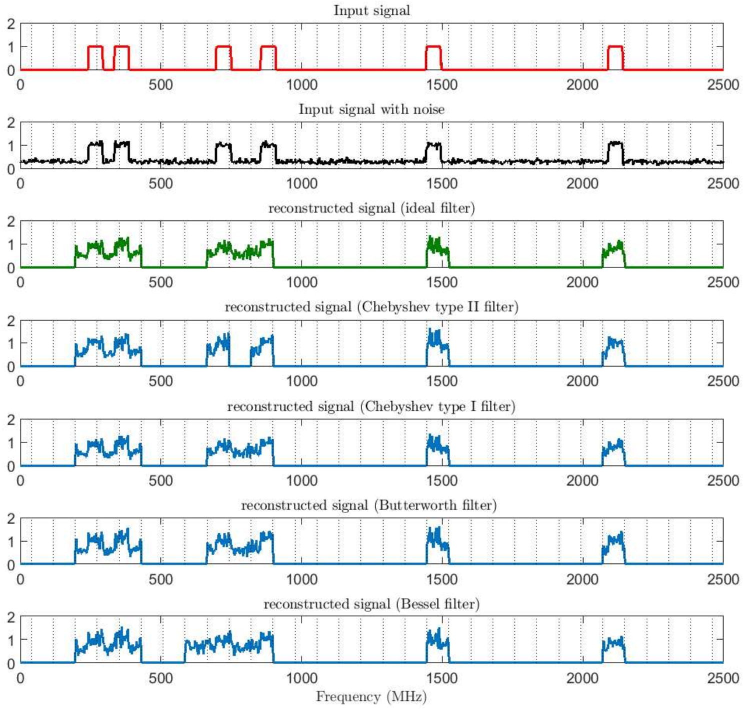

Figure 3.27 – Reconstructed spectrum of the MWC with global compensation when $M = 4$, $q = 7$, $L = 64$, $B = 52$ MHz, SNR = 10 dB and $F_{Nyq} = 5$ GHz.

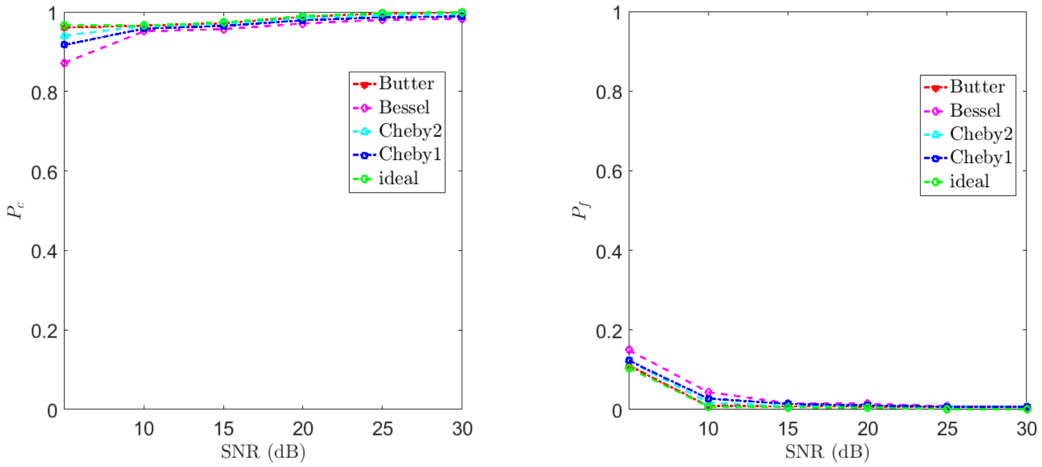

(a) The correct good reconstruction rate P_c.

(b) The false alarm rate P_f.

Figure 3.28 – The rates of P_c and P_f for different SNRs after applying post-processing scheme with global compensation when $M = 4$, $q = 7$, $L = 64$, $B = 52$ MHz and $F_{Nyq} = 5$ GHz.

3.2 COTS lowpass filter with global compensation for the MWC

This section presents an implementation of the MWC CS scheme using Commercial Off-The-Shelf (COTS) lowpass filter (SXLP-36+ from Mini-Circuits®, which has been selected for Lab-STICC's MWC prototype configuration). In this section, the SXLP-36+ lowpass filter is characterized to implement amplitude and phase compensation methods without any optimization algorithms. With the goal to achieve an output as close as possible to the ideal MWC output, the results of spectrum reconstruction are evaluated with respect to correct reconstruction and false alarm rates.

3.2.1 Implementation and characterization of SXLP-36+ real filter

Based on a preliminary study on different popular types of filter (Butterworth, Chebyshev type I and II, Bessel) and different sets of MWC parameter in simulation environment, which deployed the proposed post-processing scheme as well, the obtained results from simulated filters can approach the results of ideal filter. This section extends the problem to a COTS lowpass filter with the goal of producing a prototype based on the MWC CS scheme.

In order to reproduce a prototype of CS system based on the MWC, the MWC configuration has been chosen as $M = 4$, $F_{Nyq} = 1$ GHz, $L = 96$, and $q = 7$ (as addressed in Chapter 2). Thus, the sampling rate is theoretically $F_s = q \times F_p = q \times F_{Nyq}/L = 72.9$ MHz, the cutoff of filter in MWC system is estimated by $F_c = F_s/2 = 36.45$ MHz, and the range of filtered bandwidth is $[\frac{-F_s}{2}; \frac{F_s}{2}]$. In practice, several COTS real lowpass filters have been analyzed and the filter SXLP-36+ [24] designed by Mini-Circuits® is selected for our project as in Figure 3.29, because it has the cutoff approximately 40 MHz (suitable for this configuration) and advantages of flat passband and sharp cutoff, which benefit to our application.

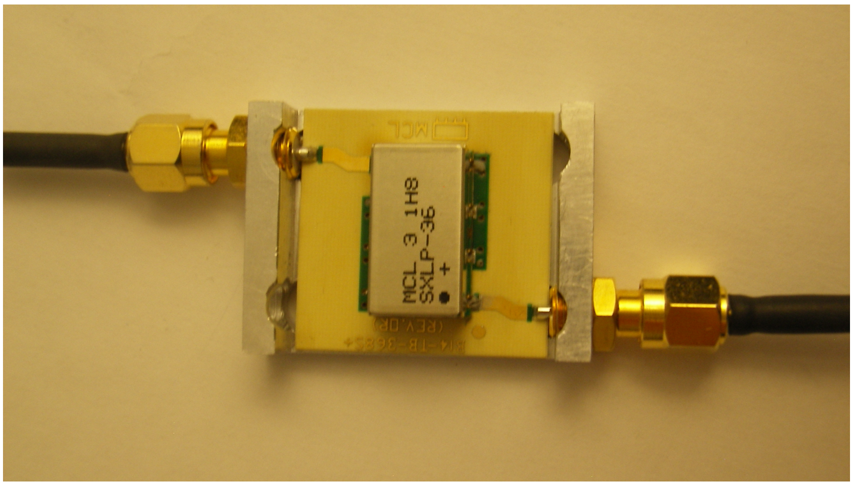

Figure 3.29 – Photo of COTS filter SXLP-36+.

By using a Vector Network Analyser (VNA), the amplitude and phase response of this filter are firstly measured. After that, a linear interpolation method is used to compute the least squares polynomial coefficients for the data of amplitude and phase. Then, these coefficients are used to model the amplitude and phase responses, as in Figure 3.30. Note that the cutoff of the real filter is approximately 40 MHz at -3 dB as in Figure 3.30a.

3.2.2 Simulation results

In the MWC hypothesis, the input bandwidth is divided into L subbands. Hence, the bandwidth of each transmitter is put $B < F_p$ (since $L = F_{Nyq}/F_p$), to position the

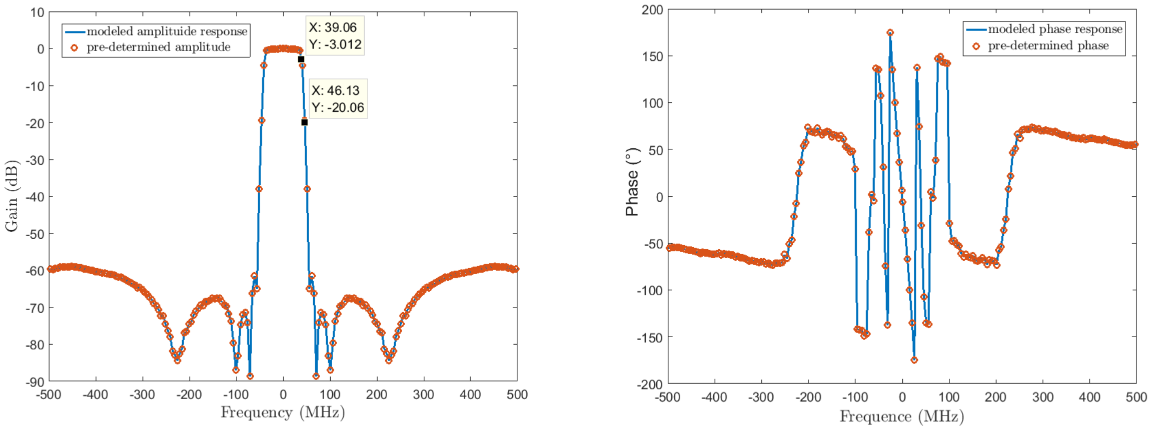

(a) Modeled amplitude response.

(b) Modeled phase response.

Figure 3.30 – Modeled amplitude and phase responses of SXLP-36+ filter.

transmitter inside one subband of the MWC or it can be astride two subbands maximally. Moreover, the condition of sparse active subbands must be respected, denoted that $s < Mq$ where s is the maximum number of active channels of the equivalent model and it can be considered as the number of transmitters that the MWC can detect.

As mentioned in Section 3.1.2, the real filter will introduce an aliasing effect owing to the ripple in stopband and non-sharp in transition band. To have a correct spectrum reconstruction, the post-processing scheme is applied into the MWC scheme with this real filter. First of all, the frequency $F_{ss} = 46.1 \times 2 = 92.2$ MHz is determined at -20 dB and then the ADC samples the filtered signal at F_{ss}. After that, a digital filter is applied with cutoff $F_s/2$. After this step, the digital filtered signal is re-sampled at F_s rate and compensates the phase and amplitude with the known responses. The real output of the MWC system in this step is considered equivalently the ideal output of the MWC system. Figure 3.31 illustrates the spectrum reconstruction at 20 dB SNR, which applied the modeled real lowpass filter SXLP-36+ in the simulation environment with and without applying the post-processing method. In this case the reconstruction algorithm OMP [11], which reconstructs signal only in detected active subbands, is used.

In the simulation environment, the correct reconstruction and false alarm rates are estimated by 2000 trials for each SNR level. The mean value of P_c and P_f are shown in Figure 3.32. According to this figure, it should be noted that the reconstruction of SXLP-36+ filter without compensation are not correct and have a high false alarm rate. For the SXLP-36+ filter with global compensation, the correct reconstruction rate is high in cases

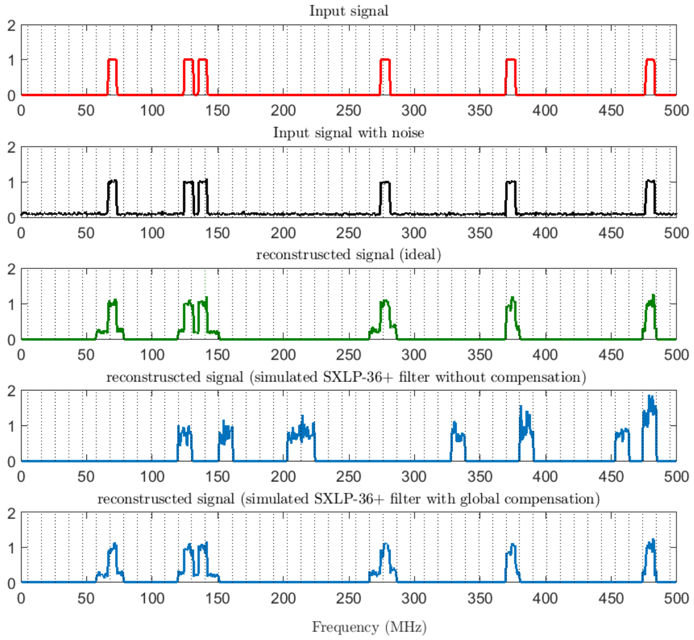

Figure 3.31 – Example of spectrum reconstruction of the MWC system with SXLP-36+ lowpass filter in simulation environment with and without global compensation (SNR = 20 dB) when $M = 4$, $L = 96$, $q = 7$ and $F_{Nyq} = 1$ GHz.

of low noise level (more than 90% when SNR from 10 to 30 dB) and it is still acceptable in case of high noise level (approximately 85% when SNR = 5 dB). The false alarm rate is approximately 8% in this SNR and it is extremely reduced in cases of higher SNR. The correct reconstruction and false alarm rates of the real filter with compensation are very close to the ideal filter. This performance proves the efficiency of the post-processing scheme and the implementation possibility of a real lowpass filter into the MWC system.

3.3 Practical results with testbed

In this part, the experiments with SXLP-36+ lowpass filter with real generated signal are measured. After that, the performances of correct reconstruction and false alarm are estimated.

The configuration of the MWC in this experiment is the same as in the simulation, which is $M = 4$, $q = 7$, $L = 96$, and $F_{Nyq} = 1$ GHz. Firstly, an automatized measurement platform including a controlling computer running Matlab, a Keysight DSO90404A

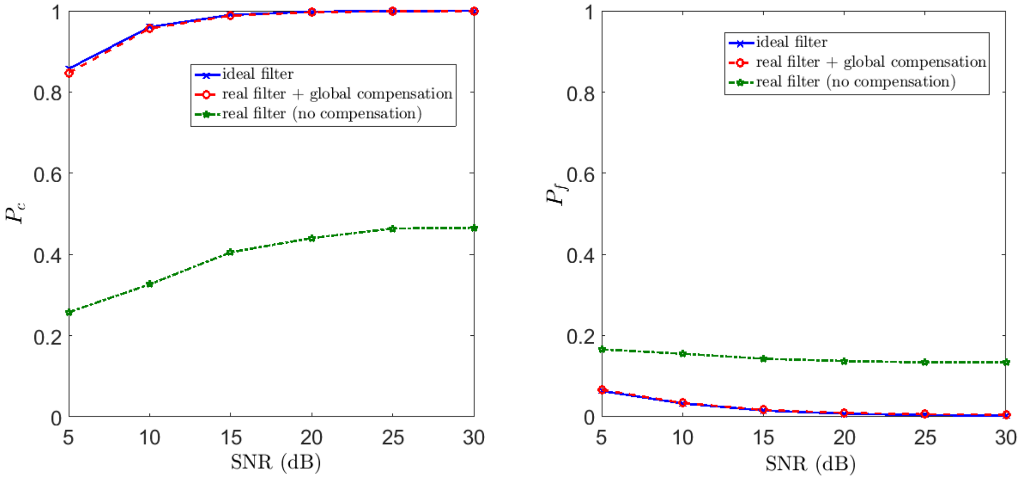

Figure 3.32 – The correct reconstruction and false alarm rates for all SNRs with applying SXLP-36+ in simulation when $M = 4$, $L = 96$, $q = 7$ and $F_{Nyq} = 1$ GHz.

Infinium oscilloscope and a Keysight 81180A arbitrary waveform generator are set up by Transmission Control Protocol/Internet Protocol (TCP/IP) local networking. For each channel of the MWC, the modulated signal $x_i(t)$ ($i \in [1, M]$) is firstly simulated and saved with 4 GSample/s rate, to be compatible with the arbitrary waveform generator. Next, each signal $x_i(t)$ is generated by this generator and then passed through the low-pass filter SXLP-36+. Output signal $y_i(t)$ is acquired by DSO90404 Infiniium scope at 40 GSample/s. This output signal is recorded for post-processing. Figure 3.33 presents the photo of our testbed. On the left is the arbitrary waveform generator. In the middle, the real filter is connected to the DSO90404A Infinium oscilloscope. On the right hand side, a PC controls the arbitrary generator.

Figure 3.34 shows an example of acquisition of visualized signals on the oscilloscope. The yellow signal corresponds to the signal generated by the arbitrary generator. The green signal represents the signal obtained at the output of the filter. The blue signal is the synchronization peak. The beige signal shows the Fast Fourier transform of the green signal and the turquoise signal shows the Fast Fourier transform of the yellow signal.

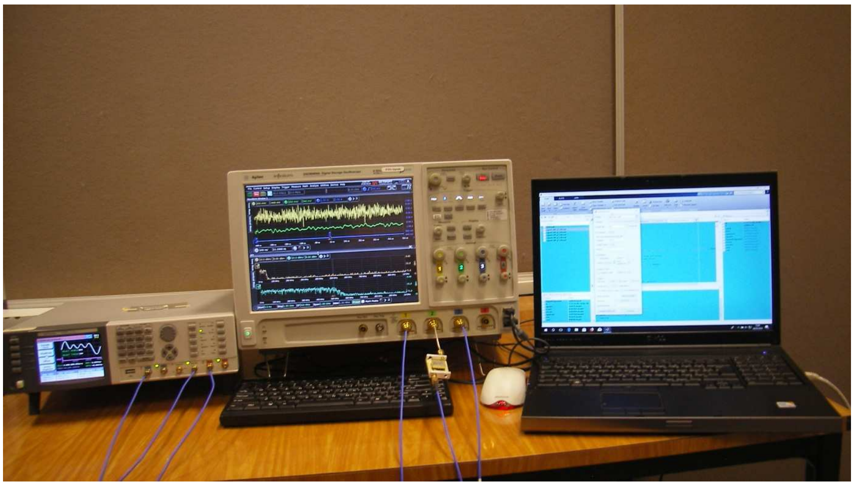

Figure 3.33 – Photo of the testbed.

Figure 3.34 – Example of signals acquisition during the filtering step.

The spectra of real input signal and reconstruction are shown in Figure 3.35. After applying the post-processing scheme, the real signal is well-reconstructed with the real lowpass filter at 30 dB of SNR and it is as good as the reconstruction with the ideal filter, which cannot be obtained in the case without post-processing.

Moreover, the correct reconstruction and false alarm rates, which are measured by 100 real experiments for each SNR level, are shown in Figure 3.36. For the real filter without compensation, the correct reconstruction and false alarm are not satisfactory. For the real filter with global compensation, compared to Figure 3.32, it is easy to see that at low

SNR level, the real filter has a lower rate of correct reconstruction and a higher rate of false alarm than the ideal filter. The performance loss, however, is not significant and the experimental results fit well with the simulated ones. The proposed post-processing method is thus proven to be effective for compensating the real filter in the MWC scheme.

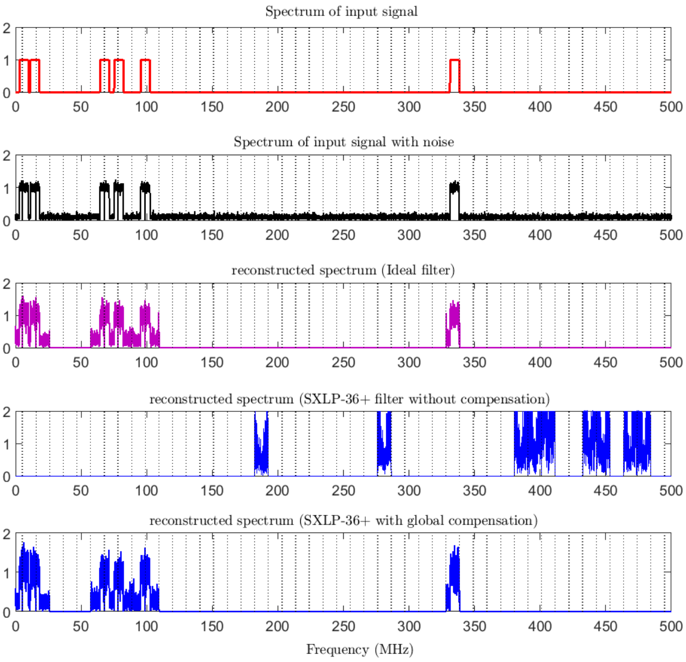

Figure 3.35 – Example of reconstructed spectrum (at 30 dB SNR) with ideal filter and real filter SXLP-36+ (with and without post-processing).

3.4 Conclusion

This chapter examines in detail the properties of four types of classical filter, by this way, the problems of non-ideal filters in the MWC system have been pointed out. To solve the problems of analog filters and to find the same condition as the ideal analog filter, a method of post-processing has been proposed. Firstly, the analog processing will consist of filtered signal with a real lowpass filter at cutoff frequency $F_{ss}/2$ and sampled at F_{ss} frequency. After that, a digital post-processing is applied with an ideal filter at cutoff $F_s/2$ and then resamples at F_s accompanied by amplitude compensation and phase compensation to obtain the correct reconstruction of the input signal spectrum. This

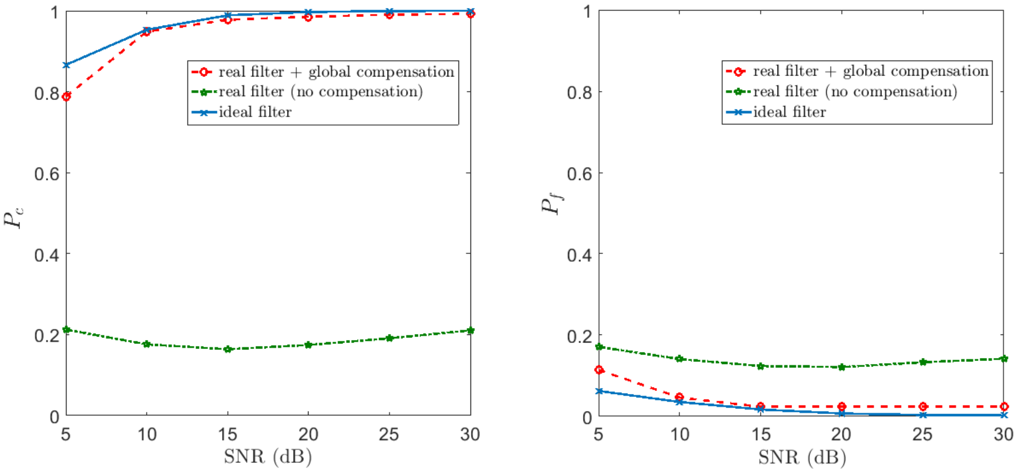

Figure 3.36 – The correct reconstruction and false alarm rates estimated by experiments for all SNRs.

approach assumes the knowledge of amplitude and phase response of the using real filter, which is usually the case in practice. The proposed method proves that the reconstruction with non-ideal filters is almost identical to that obtained by using ideal filter. Moreover, the simulation results with many experiments have been investigated with significant noise levels and different physical parameters of the MWC system. This method of compensation is especially simple to implement and it has a very low additional calculation cost.

This chapter also presents an implementation of real lowpass filter SXLP-36+ into the MWC system. By applying the proposed post-processing scheme, the correct reconstruction and false alarm rates are experimentally measured to demonstrate the effectiveness of our approaches. The next chapter is to study the implementation of low bit quantizer in the MWC

Chapter 4

LOW-BIT QUANTIZATION METHODS FOR THE MWC CS

4.1 Introduction

As mentioned before, there are two conditions of the MWC to ensure the correct reconstruction. First, the wideband input signal must consist of sparse active subbands. Secondly, all analog devices in the MWC scheme are assumed to produce ideal output. For example, the MWC output can be reconstructed when it is obtained from an ideal lowpass filter (flat passband, non-existence phase shift, transition band and stopband) and high resolution ADCs without any distortion. In [23], it has been demonstrated that MWC can be implemented with non-ideal hardware (mixers, lowpass filters) with proposed hardware calibration method to the analog and physical distortion or imperfections. In addition, to implement the analog compressed acquisition chain of the MWC, the impacts of each non-ideal component need to be evaluated independently. By assuming the other components ideally, in previous chapters, it has been demonstrated that MWC can be implemented with non-ideal and COTS SXLP-36+ lowpass filter with little performance loss. This chapter focuses on the implementation MWC system with non-ideal low-bit ADCs.

The impacts of low-bit quantization to wideband signal reconstruction with the MWC are studied. Several real types of ADCs are firstly simulated for the MWC and their results on wideband signal reconstruction are compared based on the low-bit criterion of the ADCs. Assessing the wideband reconstruction performances, this study proposes a trade-off between the oversampling factor, the number of bits and the type of quantizer, which can achieve the performances of reconstruction as close as possible to the ideal reconstruction.

The state-of-art ADCs have been analysed in [127, 128]. As discussed previously, the growth of wireless technology such as wideband applications or cognitive radios that go beyond the capability of ADC devices. The sampling methods which are dedicated to reduce sampling rate under the Nyquist rate have been presented in [47]. Generally, the problems of a conventional ADC are considered as the bandwidth of input signal and the sampling rate. Depending on each application the ADC architecture can be chosen, as displayed in Figure 4.1 [129].

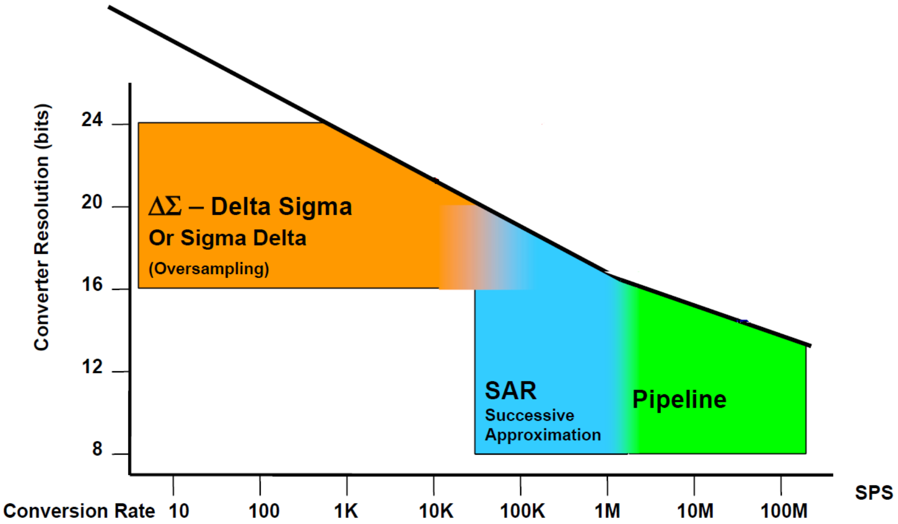

Figure 4.1 – Types of ADC and its resolutions depending on applications conversion rate requirement (sample per second) [129].

There are some main architectures of ADC such as Successive Approximation (SAR) [130], ΣΔ [131] and Pipeline [132]. In comparison, the ΣΔ has advantages of low cost and low power consumption, the SAR has low latency time while the Pipeline can accept high bandwidth of input signal and operates at higher sampling rate compared to the others [133]. In CS field, the ADC AD9057 type Pipeline [134] has been deployed in the very first MWC prototype [135]. In another approach, the 16-bit resolution ADC such as AD9460 [136], and ADS5562 [137] which also have pipeline architecture, are deployed in the other versions of the MWC prototype as well [6, 20]. It can be seen that, with the large bandwidth of converter and high sampling rate, the Pipeline ADC is quite suitable for wideband applications. Nevertheless, its drawbacks include high cost and high power consumption [129]. Besides, the ΣΔ is widely used in wireless applications as well because of its cheap hardware and simple implementation, it can be deployed in the MWC depending on the requirement of applications [138]. For example, the spectrum sensing for the IoT or cognitive radio which do not need a high sampling rate and a very large bandwidth, is sufficient to implement ΣΔ ADC, such as AD9361 receiver including a 12-bit $\Sigma\Delta$ ADC [139]. With the goal of studying spectrum sensing for low cost and low power consumption applications, this chapter deploys the $\Sigma\Delta$ ADC to the MWC due to its benefits above. There is also drawback of $\Sigma\Delta$ ADC due to its sampling bandwidth constraint. It will become useless if the sampling rate exceeds a hundred MHz, because the oversampling process for a wideband sensing signal needs to be carefully applied in order to not go backward the sub-Nyquist hypothesis [51].

The benefits of low-bit ADCs are low cost, low power consumption in case of green communications and simple hardware. Furthermore, low-bit ADCs have not been thoroughly investigated in the context of the MWC. The main constraint of a low-bit ADC, however, is the significant quantization error between input and quantized output. The advantage of a low-bit memoryless ADC is that it can be deployed in the MWC easily, and a common way to reduce the quantization error is to implement oversampling [140]. Nevertheless, in the context of wideband sampling, the MWC scheme aims to reduce sampling rate into sub-Nyqusit rate. Thus, we take an alternative approach by increasing the sub-Nyquist sampling rate by only a few times. In addition, 1-bit $\Sigma\Delta$ ADC is studied in the MWC due to its noise shaping capability of the quantization error at baseband. We then show that the $\Sigma\Delta$ ADC can reduce the quantization error better than a memoryless ADC applied with an optimal quantization technique at moderate oversampling values. Consequently, based on our simulation results, a trade-off is proposed between oversampling rate and number of bits of an ADC which can be reasonable for a sub-Nyquist sampling system under the condition of low-bit, low consumption and hardware complexity. The next section presents a low-bit memoryless ADC.

4.2 Low-bit memoryless ADC and Oversampling method

4.2.1 Low-bit memoryless ADC

To quantize an analog signal, the easiest way is the peak-to-peak quantization. This method, however, is not an optimal way because in the high noise environment, the sampled signal always has high amplitude. Assuming that there are a few samples with high amplitude (considered as noise), while the rest of samples which contain useful information present at low amplitude. The peak-to-peak quantizing method will waste bits to quantize the noise. A better method is to quantize the signal based on its distribution, for example in case of 2-bit quantization, the useful samples will be distributed on two lower regions. Absolutely, it wastes two upper regions to quantize the noise, while only 1-bit quantizer is needed. Consequently, an optimal quantization scheme must take into account input signal distribution. To study the impact of low-bit ADC, we consider that the mixers and lowpass filters of the MWC are ideal.

Let us assume that the signal after lowpass filter of the MWC has Gaussian distribution. The optimal uniform quantizer for a Gaussian source has been shown in [141], by minimizing the distortion function D of a uniform quantizer $\mathcal{Q}(y)$

$$D = \int_{-\infty}^{a_1} (y - \tilde{y_1})^2 \mathcal{Q}(y)dy + \sum_{i=1}^{N-2} \int_{a_1+(i-1)\Delta}^{a_1+i\Delta} (y - \tilde{y}_{i+1}) \mathcal{Q}(y)dy + \int_{a+(N-2)\Delta}^{\infty} (y - \tilde{y}_N)^2 \mathcal{Q}(y)dy, \tag{4.1}$$

where y the value of non-quantizing sampled signal while $\tilde{y}$ the quantized value of sampled signal. The range of quantizer is divided into N regions, the length of each region is defined by Δ step-size. Hence, minimizing D with respect to these variables will provide an optimal quantization level by numerical results based on the input with standard deviation unity (unit variance Gaussian) and a zero-mean.

In order to apply a low-cost hardware quantizer for the MWC scheme, only few-bit quantizers are deployed in this case (1-bit and 2-bit quantizers for example). Especially, for 2-bit mid-rise quantizer, N is even and in this case $N = 4$, then the optimal quantized level Δ is 0.9957 with mean squared error $D = 0.118$ from [141]. For 1-bit mid-rise quantizer, the quantization step-size $\Delta = 1.596$. In the first simulation, the MWC filtered signal is first sampled and then quantized with uniform mid-rise quantizer with and without applying optimal Gaussian source quantized technique.

For a normal mid-rise quantizer, the step size Δ is calculated by $\Delta = \frac{2 \times |y_{i_{max}}|}{2^n}$ with n the number of bits and $y_{i_{max}}$ the biggest value of the sampled signal. Hence, the quantized level of a normal mid-rise depends on the maximum amplitude of the sampled signal. Figure 4.2 illustrates the performances of correct reconstruction and false alarm with respect to the SNR from 5 to 30 dB with the MWC configuration as $M = 4$, $q = 7$, $L = 96$ and $F_{Nyq} = 1$ GHz. Assuming that in $[0, F_{Nyq}/2]$, there are six transmitters which can be reconstructed ($N_t = 6$). The bandwidth of each subband is $B = 7$ MHz with identical power levels. The method for estimating these correct reconstruction and false alarm rates was explained in previous chapters.

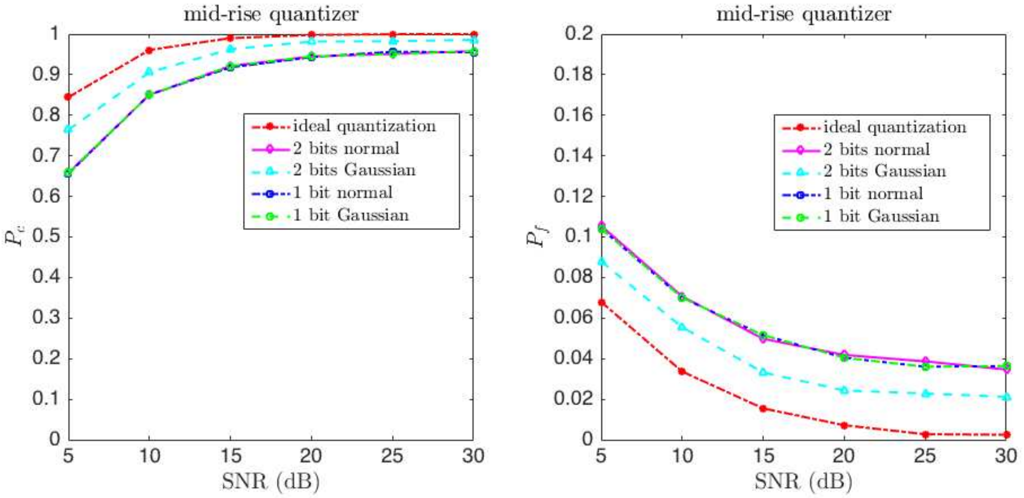

Figure 4.2 – Correct reconstruction and false alarm rates in the MWC when using 1 and 2 bits mid-rise quantizer with and without applying optimal Gaussian source quantized technique.

It is interesting to notice that the 2-bit mid-rise with optimal Gaussian source quantized technique has a considerable improvement compared to the normal mid-rise quantizer. As explained above, the 1-bit mid-rise quantizer can achieve the performance of a 2-bit quantizer approximately due to the high amplitude of noise. Another interesting thing is that for 1-bit quantizer, these two techniques are nearly equal, since all amplitudes are mapped to the same levels (only 2 up and down levels in this case), hence the performances of correct reconstruction and false alarm of these 2 techniques are nearly the same. Nevertheless, the gap between non-quantized and quantized signal reconstructions cannot be ignored. This gap may lead to a problem at the post processing of the MWC output.

The memoryless 1 to 4-bit mid-rise ADCs applying an optimal Gaussian source quantizing technique are firstly simulated in the MWC scheme (Figure 2.1) with assumptions that the mixers and the lowpass filters are ideal. The MWC configuration is the same with the last simulation. The performances of these real ADCs based on correct reconstruction and false alarm are compared to the ideal ADC as in Figure 4.3. The correct reconstruction and false alarm rates are in function of SNR changing from 0 to 30 dB. It can be observed that high-bit ADCs need to be deployed (3 and 4-bit) to approach the ideal quantization. The main problem of low-bit quantization is the quantization error. To reduce the quantization error, an oversampling technique will be presented to the MWC in the following section.

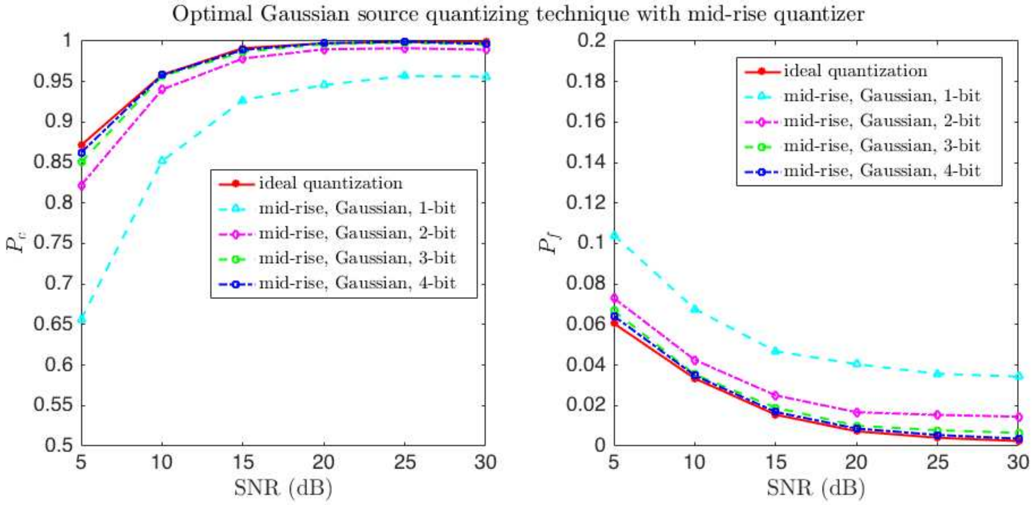

Figure 4.3 – Correct reconstruction and false alarm rates in function of SNRs (dB) obtained by the MWC with 1 to 4 bits common mid-rise quantizers applying optimal Gaussian source quantizing technique.

4.2.2 Oversampling

The quantization error is produced during the quantized process, and usually called quantization noise. The quantized sample is given by

$$\tilde{y}_i[n] = y_i[n] + e_i[n], \tag{4.2}$$

with e_i the quantization noise (quantization error). Indeed, when $\tilde{y}_i$ is chosen at midpoint of quantization regions, the random additive noise e_i has amplitude distribution in $-\Delta/2 \leq e_i \leq \Delta/2$ (with Δ is quantization interval). For the MWC system, the input signal is filtered at $F_c = F_s/2$ and then sampled at F_s giving a root mean square of quantization noise $E(f) = \frac{\Delta}{\sqrt{12}}$ [142]. Thus, the distribution of quantization noise is uniform in F_s bandwidth. The quantization noise spectral density in F_s bandwidth is

$$N_e(f) = \frac{|E(f)^2|}{F_s} = \frac{\Delta^2}{12F_s}. \tag{4.3}$$

At this time, the MWC filtered signal is bounded in $[-F_c, F_c]$ at baseband. Finally, this baseband quantization noise spectral density is

$$S_B = \int_{-F_c}^{F_c} N_e(f)df = \frac{\Delta^2}{12}\left(\frac{2F_c}{F_s}\right) = \frac{\Delta^2}{12}. \tag{4.4}$$

Let us denote m the oversampling factor with $F_s' = mF_s$, when F_s' a sampling frequency m times greater than F_s. Hence,

$$S_{Bm} = \frac{\Delta^2}{12}\;\frac{2F_c}{F_s'}\Bigg) = \frac{\Delta^2}{12}\left(\frac{2F_c}{mF_s}\right) = \frac{S_B}{m}. \tag{4.5}$$

From Equation 4.5, it can be seen that oversampling helps reduce the noise power spectral density. Thus, the lowpass filter and downsampling process would keep only the filtered noise power, which is low. The hypothesis of the MWC system is to sample under the Nyquist rate, $F_s \ll F_{Nyq}$. Hence, a moderate value of m needs to be chosen carefully to meet this condition of sub-Nyquist sampling, $mF_s \ll F_{Nyq}$. Figure 4.4 shows a conventional MWC system and its oversampling counterpart. The decimator in an oversampling scheme plays a role as a digital filter, to suppress the samples outside filtered bandwidth F_c.

(a) MWC conventional sampling scheme.

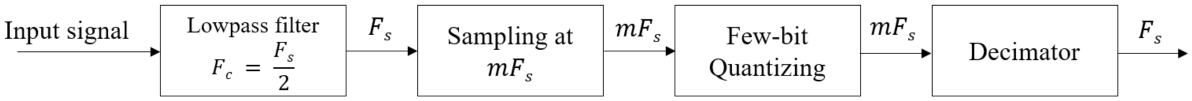

(b) MWC oversampling scheme.

Figure 4.4 – MWC conventional sampling and oversampling schemes.

Overall, the memoryless quantizer is easy to implement into the MWC and it can improve 3 dB in Signal-to-Quantization-Noise Ratio (SNR$_Q$) per doubling sampling rate [140]. Nevertheless, due to the hypothesis of sub-Nyquist sampling rate, the following section presents the ΣΔ ADC which can shape quantization noise at baseband significantly lower than a memoryless ADC (such as mid-rise ADC) with a moderate oversampling value.

Figure 4.5 shows the spectra of quantization noise when sampling at F_s and mF_s respectively. The quantization noise spectrum is spread over the bandwidth F_s when sampling at F_s. Moreover, when sampling at mF_s, the quantization noise is spread over the bandwidth mF_s, while the input spectrum is unchanged. The quantization noise which falls outside the band interest will be eliminated by the lowpass filter (Decimator).

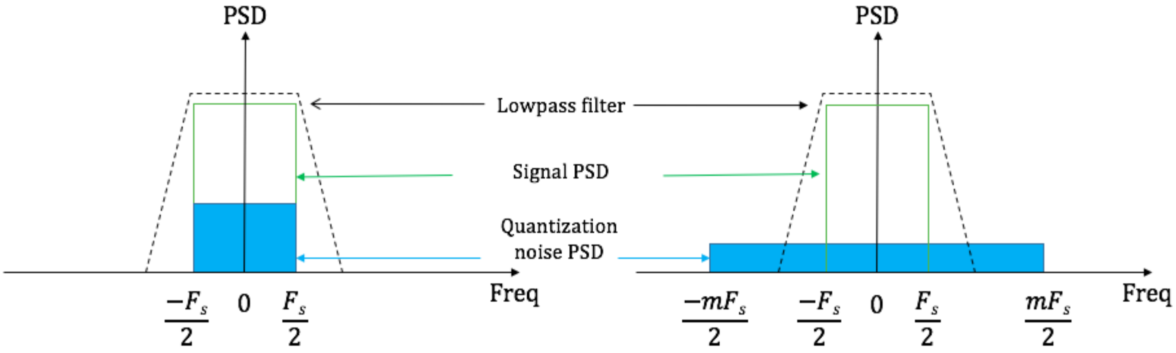

Figure 4.5 – Input spectrum and quantization noise spectrum at Fs and mFs sampling rate.

4.3 ΣΔ Analog-to-Digital Converter

The 1-bit ΣΔ ADC is a low power consumption and simple hardware [143]. The ΣΔ ADC is a combination of noise shaping, oversampling and decimation stages as shown in Figure 4.6. The functions of noise shaping and oversampling are performed by the ΣΔ modulator. The first order of ΣΔ modulator is illustrated in Figure 4.7. The 1-bit digital output of the ΣΔ modulator is then passed through the digital decimation filter. The output of the decimation filter provides a digital representation of the quantized input signal at sampling rate F_s.

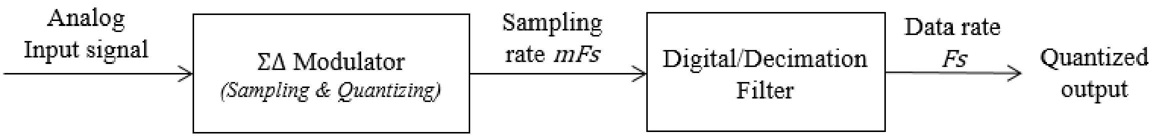

Figure 4.6 – ΣΔ ADC block diagram.

The ΣΔ modulator includes an analog difference node, an integrator, a 1-bit quantizer and a 1-bit digital-to-analog converter (DAC) in the feedback loop. The signal which is applied to the integrator is the difference between the analog input y_i and the predicted analog input from the quantized output $\tilde{y}_i$ by the DAC. This difference is considered as the quantization error. This quantization error is accumulated by the integrator and then quantized by a 1-bit quantizer. The quantization error of the 1-bit quantizer is large, however, the decimation filter can provide an accurate output by averaging the sampled input over several sample periods [144].

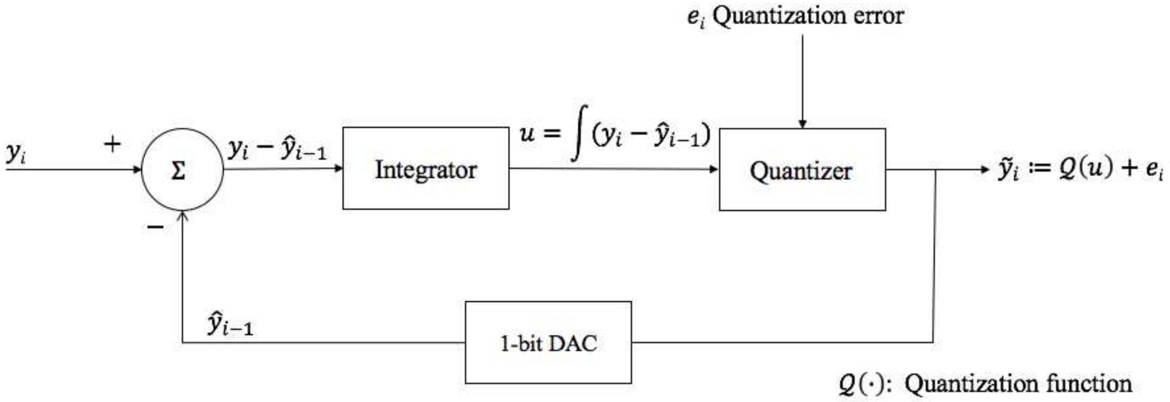

Figure 4.7 – First-order ΣΔ modulator.

In z-domain, let us denote the transfer function of the integrator which is $I(z)$, the ΣΔ modulator equation in z-domain gives [144]

$$\begin{aligned}\tilde{Y}_i(z) &= E_i(z) + I(z)(Y_i(z) - z^{-1}\tilde{Y}_i(z)) \\ &= E_i(z)\frac{1}{1+I(z)z^{-1}} + Y_i(z)\frac{I(z)}{1+I(z)z^{-1}},\end{aligned} \tag{4.6}$$

the ideal integrator is considered as $I(z) = \frac{1}{1-z^1}$, the output of ΣΔ modulator in (4.6) can be simplified

$$\tilde{Y}_i(z) = Y(z) + (1 - z^{-1})E(z). \tag{4.7}$$

In time domain, the output of the ΣΔ modulator is $\tilde{y}_{i\Sigma\Delta}[n] = y_i[n] + e_i[n] - e_i[n-1]$ due to the integrator (accumulating quantization error from the last stage). Let us denote that $n_{e\Sigma\Delta}[n] = e_i[n] - e_i[n-1]$ is the noise at output of ΣΔ modulator. Thus, in frequency domain $n_{e\Sigma\Delta}$ becomes

$$\begin{aligned} N_{e\Sigma\Delta}(f) &= E(f) - E(f)e^{-j\omega T'_s} \\ &= E(f)(1 - e^{-j\omega T'_s}) \\ &= E(f)2e^{-j\omega\frac{T'_s}{2}}(\frac{e^{j\omega\frac{T'_s}{2}} - e^{-j\omega\frac{T'_s}{2}}}{2}) \\ &= E(f)2e^{-j\omega\frac{T'_s}{2}}j\sin(\omega\frac{T'_s}{2}) \\ &= E(f)2e^{-j\omega\frac{T'_s}{2}}e^{\frac{-j\pi}{2}}sin(\omega\frac{T'_s}{2}) \\ &= 2E(f)\sin(\frac{\omega T'_s}{2})e^{-j(\omega T'_s-\pi)/2}, \end{aligned} \tag{4.8}$$

where $E(f)$ is $e_i[n]$ in the frequency domain and $F'_s = 1/T'_s = mF_s$ is the oversampling frequency of the MWC. Hence, the noise spectral density in F'_s bandwidth (oversampling of F_s) is $N_{e\Sigma\Delta} = \frac{|N_{e\Sigma\Delta}(f)|^2}{F'_s}$. Assuming that the $\Sigma\Delta$ has the same quantization level Δ as mid-rise quantizer in previous section, $E(f) = \Delta/\sqrt{12}$ from equation (4.3), then $N_{e\Sigma\Delta} = \frac{4\Delta^2(\sin(\frac{\pi f}{F'_s}))^2}{12F'_s}$. The baseband quantization noise spectral density is:

$$\begin{aligned} S_{B\Sigma\Delta} &= \int_{-F_c}^{F_c} N_{e\Sigma\Delta}(f)df \\ &= \int_{-F_c}^{F_c} \frac{\Delta^2}{12F'_s} \left. \quad 2sin\frac{\pi f}{F'_s}\right)^2 df \\ &\approx \frac{\pi^2}{3} \left. \quad \frac{2F_c}{F'_s}\right)^3 \frac{\Delta^2}{12} \\ &\approx \frac{\pi^2}{3}\frac{S_B}{m^3}, \end{aligned} \tag{4.9}$$

with S_B is the baseband quantization noise spectral density with normal sampling rate F_s as in equation (4.4). It is easy to see from equation (4.9) that the quantization noise in $\Sigma\Delta$ quantizer is reduced much more than these types of memoryless quantizers as in equation (2.11) when m is high. Indeed, [140] has shown that by doubling the sampling frequency F_s, the quantization noise will decrease by $3(2m'+1)$ dB in the band of interest, with m' is a doubling factor.

Figure 4.8 shows the spectra of input signal and quantization noise at normal mid-rise quantizer and $\Sigma\Delta$ quantizer respectively. It can be obtained that the $\Sigma\Delta$ quantizer can shape the quantization noise spectrum at low frequency band, and push it into high frequency band. The filtered spectra at baseband contains the quantization noise spectrum which is reduced more than a uniform memoryless quantizer such as mid-rise quantizer.

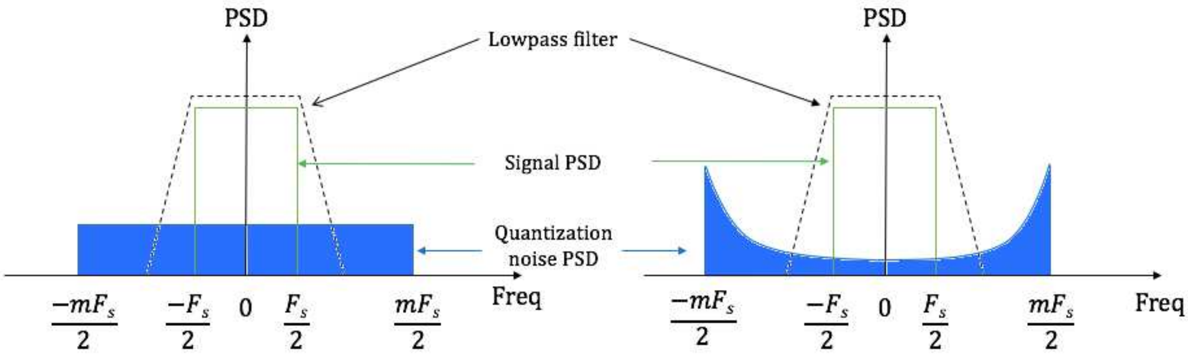

Figure 4.8 – Input signal spectrum and quantization noise spectrum of mid-rise quantizer (left) and $\Sigma\Delta$ quantizer (right) at mF_s sampling rate.

4.4 Simulation Results

In the MWC, the output of the lowpass filter is firstly sampled and then quantized. Then, the SNR_Q is computed by comparing the power of the quantization input to the power of the quantization noise:

$$\text{SNR}_Q = 10\log_{10} \left. \frac{\tilde{Y}_i^2(f)}{E^2(f)} \right), \tag{4.10}$$

where $E^2(f) = \frac{\Delta^2}{12}$ and $\Delta = \frac{X_m}{2^n}$ with X_m the quantization range and n number of bits for a memoryless uniform quantizer. Hence, equation (4.10) becomes

$$\begin{aligned} \text{SNR}_Q &= 10\log_{10}\left(\frac{12\tilde{Y}_i^2(f)}{\frac{X_m^2}{2^{2n}}}\right) \\ &= n20\log_{10}2 + 10\log_{10}12 + 20\log_{10} \left. \frac{\tilde{Y}_i(f)}{X_m} \right) \\ &\approx n6.02 + 10.79 + 20\log_{10} \left. \frac{\tilde{Y}_i(f)}{X_m} \right) (\text{dB}). \end{aligned} \tag{4.11}$$

It is easy to see that for the peak-to-peak uniform quantizer, increasing 1 bit can improve 6 dB in SNR_Q. Then, for m times oversampling, the SNR_{Qm} can improve $10\log_{10}$ m

(dB). In case of $\Sigma\Delta$ quantizer, the $\mathrm{SNR}_{Q\Sigma\Delta}$ will be

$$\begin{aligned}\mathrm{SNR}_{Q\Sigma\Delta} &= 10\log_{10}\left.\frac{\tilde{Y}_i^2(f)}{\frac{\Delta^2}{12m^3}\times\frac{\pi^2}{3}}\right) \\ &= 30\log_{10} m + n20\log_{10} 2 + 10\log_{10} 12 \\ &+ 10\log_{10} 3 - 20\log_{10}\pi + 20\log_{10}\left.\frac{\tilde{Y}_i(f)}{X_m}\right)(\mathrm{dB}).\end{aligned} \tag{4.12}$$

Hence, when $m = 2$, the $\Sigma\Delta$ quantizer can improve $30\log_{10} m = 9$ dB while the memoryless peak-to-peak quantizer can improve only $10\log_{10} m = 3$ dB in the SNR_Q. In case of optimal quantization technique for Gaussian source, let us assume that 1-bit quantizer is used, the quantization level will be 1.59 [141], then the quantization range is $X_m = 2 \times 1.59 = 3.18$. Consequently, the quantization noise spectrum will be $E_G^2(f) = \frac{\Delta^2}{12} = \frac{3.18^2}{12\times 2n}$. Hence

$$\begin{aligned}\mathrm{SNR}_{QG} &= 10\log_{10}\left(\frac{\tilde{Y}_i^2(f)}{\frac{3.18^2}{12m\times 2^{2n}}}\right) \\ &= 10\log_{10} 12 - 20\log_{10} 3.18 + 10\log_{10} m \\ &+ n20\log_{10} 2 + 20\log_{10}(\tilde{Y}_i(f))\ (\mathrm{dB}).\end{aligned} \tag{4.13}$$

In practice, the quantization range in $\Sigma\Delta$ quantizer is usually set at $X_m = 4$, it corresponds to the input voltage of the device 2V [145]. At oversampling factor $m = 2$, number of bits $n = 1$, the $\mathrm{SNR}_{Q\Sigma\Delta} = 8.6 + 20\log_{10}(\tilde{Y}_i)$ (dB) while $\mathrm{SNR}_{QG} = 9.8 + 20\log_{10}(\tilde{Y}_i)$ (dB). It can be seen that at double sampling rate ($m = 2$), the optimal Gaussian quantizing technique can improve the SNR_Q better than the $\Sigma\Delta$ quantizer. In case $m = 4$, however, the $\Sigma\Delta$ quantizer can perform better than the optimal Gaussian quantizer, since $\mathrm{SNR}_{Q\Sigma\Delta} = 17.7 + 20\log_{10}(\tilde{Y}_i)$ (dB) and $\mathrm{SNR}_{QG} = 12.8 + 20\log_{10}(\tilde{Y}_i)$ (dB) at $m = 4$ and $n = 1$. Figure 4.9 shows the performances of correct reconstruction and false alarm with the same MWC parameters as in Figure 4.3 ($M = 4$, $q = 7$, $L = 96$ and $F_{Nyq} = 1$ GHz).

Figure 4.9 verified that the improvement in SNR_Q of $\Sigma\Delta$ and Gaussian source mid-rise quantizers are proved by calculating in equations (4.12) and (4.13). It should be noted that the SNR in these figures is different to SNR_Q since SNR is the ratio between wideband input signal and the noise in the communications environment, while SNR_Q is

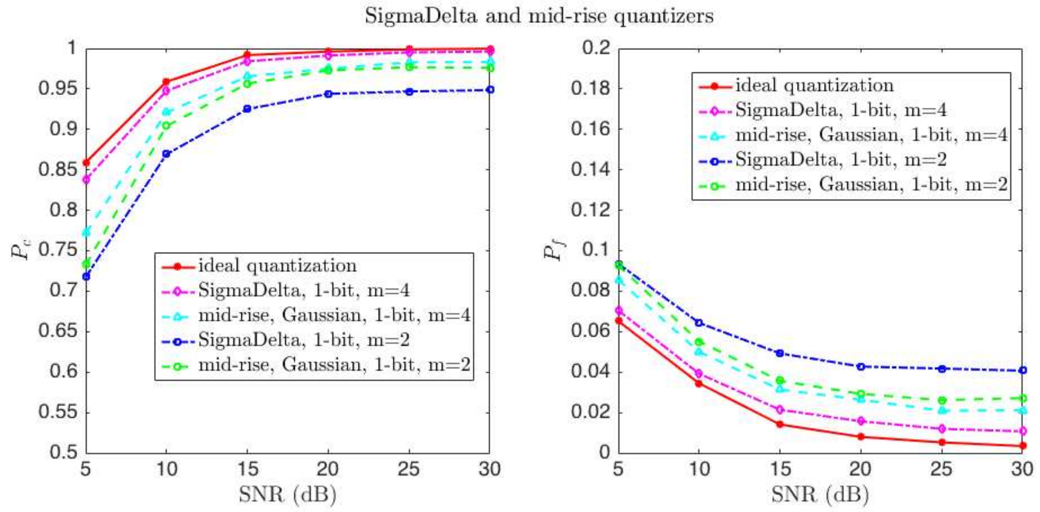

Figure 4.9 – Correct reconstruction and false alarm rates in function of SNRs (dB) obtained by the MWC with oversampling factor 2 to 4, 1-bit ΣΔ and Gaussian source mid-rise quantizers.

the ratio between filtered signal and the quantization noise, which is produced during the quantization process. Moreover, Figure 4.10 shows an example of spectrum reconstructions at 20 dB SNR with the ideal ADC and 1-bit ΣΔ ADC versus 1-bit Gaussian source mid-rise ADC at oversampling factors changing from 2 to 4. It can be observed that at $m = 2$, although the locations of the input spectrum are reconstructed correctly, there are more errors in spectrum reconstructions than at $m = 4$.

In case of 2-bit quantizers, Figure 4.11 illustrates the performances obtained by the MWC with 2-bit ΣΔ and Gaussian source mid-rise quantizers and oversampling factors are changed from 2 to 4. From the Figures 4.9 and 4.11, with oversampling factor $m = 2$, the Gaussian source quantizer can perform better than the ΣΔ quantizer even in cases 1-bit and 2-bit. At $m = 4$, however, the ΣΔ quantizer can have better performance because equation (4.9) has shown that the bigger of m, the better performance can be archived in ΣΔ quantizer. From these results, they will lead to the trade-off that at 1-bit quantizers, the ΣΔ quantizer with oversampling factor $m = 4$ can approach the performance of the ideal quantizer as in Figure 4.9, because with four times oversampling, the sampling rate F_s' is still under the Nyquist sampling rate F_{nyq} ($F_s' = 4F_s \ll F_{nyq}$), while increasing one bit, the complexity and power consumption of the hardware will increase also [143].

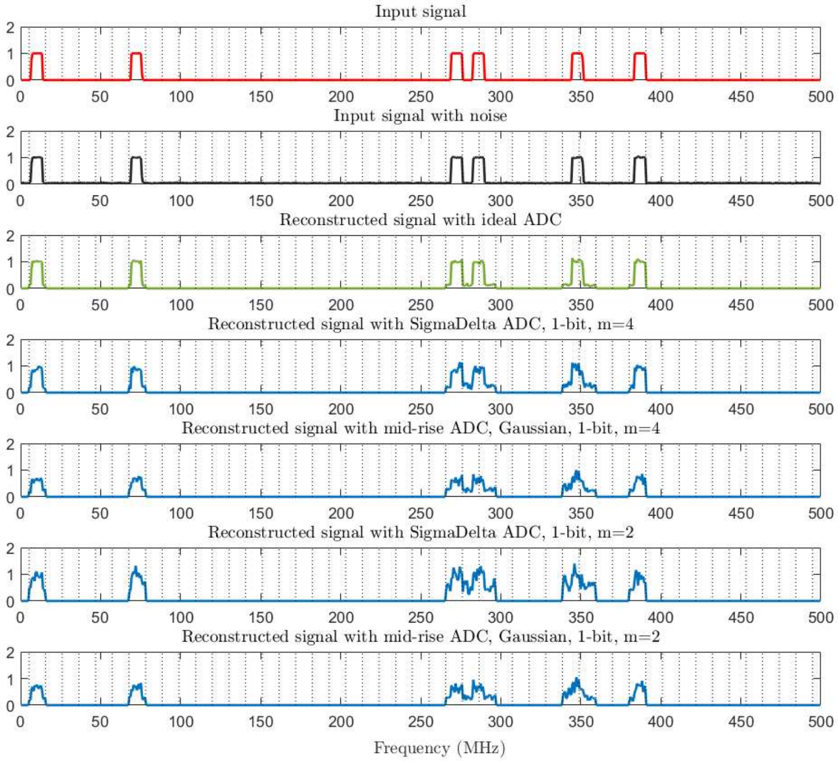

Figure 4.10 – Example of reconstructed spectra (at 20 dB SNR) with ideal ADC and 1-bit $\Sigma\Delta$ ADC versus 1-bit Gaussian source mid-rise ADC at oversampling $m = 2$ and $m = 4$.

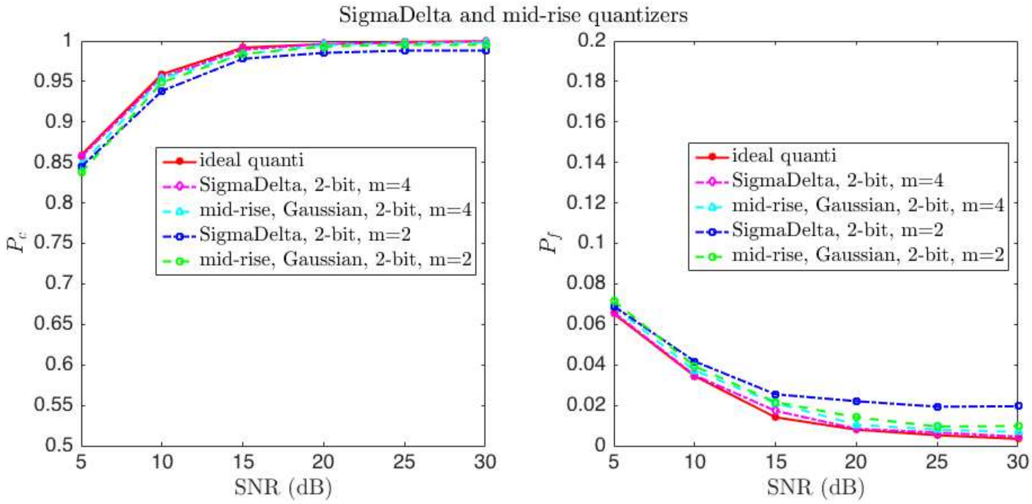

Figure 4.11 – Correct reconstruction and false alarm rates in function of SNRs (dB) obtained by the MWC with oversampling factor 2 to 4, 2-bit $\Sigma\Delta$ and Gaussian source mid-rise quantizers.

Overall, the simulations in the previous section show that a 4-bit common mid-rise ADC applying optimal Gaussian source quantizing technique (mid-rise, Gaussian, $n = 4$, $m = 1$) can provide the performance as well as the ideal ADC. Alternatively, 1-bit $\Sigma\Delta$ ADC at four times oversampling ($\Sigma\Delta$, $n = 1$, $m = 4$) can perform nearly the same as the ideal ADC performance. While at the same oversampling factor, a common ADC applying optimal Gaussian source quantizing technique needs 2 bits to approach the same ideal ADC performance (mid-rise, Gaussian, $n = 2$, $m = 4$).

4.5 Conclusion

This chapter presents low-bit quantizers which can be deployed into the MWC under the hypothesis of CS. From the simulation results, a trade-off between oversampling factor, the number of bits and type of quantizers have been proposed. In the future, the integration of a possible real ADC which exists on the market will be investigated and evaluated, such as implementations on the AD9361 [139] transceiver with receiver operating from 70 MHz to 6.0 GHz and which can be useful for IoT spectrum sensing applications.

CONCLUSION AND FUTURE WORKS

Conclusion

This thesis has demonstrated the needs in wideband monitoring. By studying the state-of-art technologies, the MWC system based on CS hypothesis is explored and improved, to solve the issue of blind spectrum sensing and detection, dedicated to cognitive radio and IoT applications.

The CS technology is decomposed in two main processes: sampling and reconstruction. In the sampling process, some methods have been introduced such as uniform interleaved sampling and non-uniform interleaved sampling. Although these methods are not considered as a complete compressed sampling, they are premises which allowed the proposal of a practical and accurate compressed sampling system called the MWC. For the reconstruction process, an efficient method of reconstruction which can be deployed for a sparse and wideband signal with blind spectrum, the OMP, is simulated. Furthermore, actual evidence of CS technology has been analyzed by the implementation of MWC prototype. Beside that, this thesis has brought a different way of explanation on mathematical view and theory, it is a useful tool to study the functions and impacts of each MWC component by assuming the others to be ideal. This thesis also studied the role of each physical MWC parameter and the output signal of MWC. In addition, the result of simulation makes a specific vision of how the system works and its outputs.

With the objective to produce a wideband monitoring prototype, the first contribution of this thesis is a study on the MWC analog components: method to correct the component imperfection and practical implementation. In particular, the imperfections of different common types of analog filter have been highlighted. Consequently, a post-processing method with a global compensation scheme is proposed to deal with the imperfections of the lowpass filters and can provide an output close to the ideal one. After that, the method to evaluate the correct reconstruction rate and false alarm rate is also proposed. The comparisons and evaluations between the non-ideal filters and an ideal filter are made based on these rates. This result shows an efficient implementation with non-ideal lowpass filter on the MWC and a possibility to produce a relevant prototype of this scheme. A

COTS SXLP-36+ lowpass filter has been deployed to the Lab-STICC's MWC prototype. With the experiments, the wideband signal reconstruction is made based on the output of the MWC testbed. In the same manner, the correct reconstruction and false alarm rates are evaluated and compared to the ideal filter with good and conclusive results.

The second contribution of this thesis is a study of low-bit quantizer applied to the MWC scheme. Besides, to choose the most suitable ADC, some quantizing methods are compared and investigated such as peak-to-peak quantization, optimal Gaussian source quantization and $\Sigma\Delta$ quantization. The mathematical calculations regarding the SNR_Q have shown that under a moderate oversampling rate, the 1-bit $\Sigma\Delta$ quantizer can perform better than the others and provide better performance when integrated into the MWC. This thesis also proposed a trade-off between oversampling factor, number of bits and type of quantizers.

Moreover, this study also contributes to the field of IoT spectrum detection. By analysing the key parameters of a wideband signal, their impacts on the spectrum reconstruction of the MWC are evaluated. This research also focused on one of the common IoT standards, LoRaWAN 868EU and the detection of transmitter spectrum with respect to this standard.

At last, this thesis has shown the MWC prototype of the Lab-STICC CACS/COM team, based on the studies of this thesis, and an introduction of the Lab-STICC's MWC calibration method as well.

Future Works

There are many interesting factors that still remain in MWC that should be examined further. A lot of reconstruction algorithms have been studied in the case of a sparse signal, and of course they have their own advantages and disadvantages. The goal of this research is also to improve these algorithms which can adapt efficiently to the MWC output signal. Moreover, with an extension of algorithms to frequency hopping, the sparse signal can be treated well in time and frequency domain.

During the performance tests, it appeared that the choice of pseudo-random sequences has a significant impact on the spectrum reconstructions. The criterion for ensuring good reconstruction is to have the lowest possible coherence degree of the coherence matrix. It is possible to have such an optimal sequence; however, there are non-optimal reconstructions according to the spectral content. One of the objectives is to propose a new method in choosing an optimal sequence according to specific spectral content. Therefore, an optimum set of sequences will bring a benefit to the reconstruction. The practical problem of synchronization time needs to be taken into account and the solution for this problem should be proposed. All the problems here have all impacts on the correctness of the sensing matrix. Generally, a calibration method is proposed and deployed to obtain a correct sensing matrix.

In the future, a real ADC which exists on the market will be integrated and evaluated. Besides, the power of each subband will be randomly generated to examine the impacts of multi-level spectrum input signals and real ADC on the correct spectrum reconstruction rate in the context of wide spectrum sensing.

In another objective, a study on the ability of discrimination between adjacent transmitters will be improved to evaluate the limits and a particular interest must be focused, according to the difference of transmitted power levels. This will also allow us to parameterize a real system by being able to do a compromise between an improvement of performance and an extra computing cost (therefore an extra power consumption). The research can be extended to reconstruct the signal in the time domain.

PUBLICATIONS

Journal

1. Lap Luat Nguyen, Roland Gautier, Anthony Fiche, Gilles Burel and Emanuel Radoi. "Digital compensation of lowpass filters imperfection in the Modulated Wideband Converter compressed sensing scheme for radio frequency monitoring". Elsevier, *Signal Processing*, 152(2018): 292-310.

International Conferences

1. Lap Luat Nguyen, Duy H.N. Nguyen, Anthony Fiche, Thang Huynh and Roland Gautier. "Low-Bit Quantization Methods for Modulated Wideband Converter Compressed Sensing". *IEEE Global Communications Conference*, Hawaii, US, 2019.
2. Lap Luat Nguyen, Anthony Fiche, Roland Gautier and Emanuel Radoi. "Impacts of the transmitter signal key parameters on the Compressed Sensing spectrum reconstruction for IoT Cognitive Radio applications". *Asia-Pacific Conference on Communications*, pp. 461–466, Hochiminh, Vietnam, 2019.
3. Lap Luat Nguyen, Anthony Fiche, Roland Gautier, Charles Canaff, Emanuel Radoi, and Gilles Burel. "Implementation of Modulated Wideband Converter Compressed Sensing scheme based on COTS lowpass filter with amplitude and phase compensation for spectrum monitoring". *IEEE International Conference on Advanced Video and Signal Based Surveillance*, pp. 1–6, Auckland, New Zealand, 2018.

BIBLIOGRAPHY

[1] S. Ashley, “Cognitive radio,” *Scientific American*, vol. 294, no. 3, pp. 66–73, 2006.

[2] H. Nyquist, “Certain topics in telegraph transmission theory,” *Trans. of the American Inst. of Electric. Eng.*, vol. 47, no. 2, pp. 617–644, 1928.

[3] C. E. Shannon, “Communication in the presence of noise,” *Proc. of the IRE*, vol. 37, no. 1, pp. 10–21, 1949.

[4] E. J. Candès, J. Romberg, and T. Tao, “Robust uncertainty principles: Exact signal reconstruction from highly incomplete frequency information,” *IEEE Trans. Inform. Theo.*, vol. 52, no. 2, pp. 489–509, 2006.

[5] M. Mishali and Y. C. Eldar, “From theory to practice: Sub-nyquist sampling of sparse wideband analog signals,” *IEEE J. Sel. Top. Sig. Process.*, vol. 4, no. 2, pp. 375–391, 2010.

[6] M. Mishali, Y. C. Eldar, O. Dounaevsky, and E. Shoshan, “Xampling: Analog to digital at sub-Nyquist rates,” *IET Cir., Devices and Syst.*, vol. 5, pp. 8–20, Jan. 2011.

[7] M. Mishali, Y. C. Eldar, and A. J. Elron, “Xampling: Signal acquisition and processing in union of subspaces,” *IEEE Trans. Sig. Process.*, vol. 59, no. 10, pp. 4719–4734, 2011.

[8] Y.-P. Lin and P. Vaidyanathan, “Periodically nonuniform sampling of bandpass signals,” *IEEE Trans. Cir. and Sys. II: Analog and Digit. Sig. Process.*, vol. 45, no. 3, pp. 340–351, 1998.

[9] J. N. Laska, S. Kirolos, M. F. Duarte, T. S. Ragheb, R. G. Baraniuk, and Y. Massoud, “Theory and implementation of an analog-to-information converter using random demodulation,” in *IEEE Int. Symp. on Circuits and Syst.*, pp. 1959–1962, IEEE, 2007.

[10] J. A. Tropp, J. N. Laska, M. F. Duarte, J. K. Romberg, and R. G. Baraniuk, “Beyond nyquist: Efficient sampling of sparse bandlimited signals,” *IEEE Trans. Inf. Theo.*, vol. 56, no. 1, pp. 520–544, 2010.

[11] T. T. Cai and L. Wang, "Orthogonal Matching Pursuit for sparse signal recovery with noise," *IEEE Trans. on Inf. Theory*, vol. 57, no. 7, pp. 4680–4688, 2011.

[12] D. L. Donoho, "Compressed Sensing," *IEEE Trans. Inform. Theo.*, vol. 52, no. 4, pp. 1289–1306, 2006.

[13] E. J. Candes, J. K. Romberg, and T. Tao, "Stable signal recovery from incomplete and inaccurate measurements," *Commun. Pure Appl. Math.*, vol. 59, no. 8, pp. 1207–1223, 2006.

[14] S. Mendelson, A. Pajor, and N. Tomczak-Jaegermann, "Uniform uncertainty principle for Bernoulli and subgaussian ensembles," *Constr. Approx.*, vol. 28, no. 3, pp. 277–289, 2008.

[15] R. Baraniuk, M. Davenport, R. DeVore, and M. Wakin, "A simple proof of the Restricted Isometry Property for random matrices," *Constr. Approx.*, vol. 28, no. 3, pp. 253–263, 2008.

[16] Y. C. Eldar and G. Kutyniok, *Compressed sensing: theory and applications.* Cambridge University Press, 2012.

[17] R. Gold, "Optimal binary sequences for spread spectrum multiplexing (corresp.)," *IEEE Trans. Inf. Theory*, vol. 13, no. 4, pp. 619–621, 1967.

[18] T. Kasami, "Weight distribution formula for some class of cyclic codes," *Coordinated Science Laboratory Report no. R-285*, 1966.

[19] J. Hadamard, "Resolution d'une question relative aux determinants," *Bull. des sciences math.*, vol. 2, pp. 240–246, 1893.

[20] M. Mishali, Y. C. Eldar, O. Dounaevsky, and E. Shoshan, "Sub-Nyquist acquisition hardware for wideband communication," in *IEEE Workshop on Sig. Process. Sys.*, pp. 156–161, IEEE, 2010.

[21] Y. Chen, M. Mishali, Y. C. Eldar, and A. O. Hero, "Modulated wideband converter with non-ideal lowpass filters," in *Acoustics Speech and Signal Processing (ICASSP), 2010 IEEE International Conference on*, pp. 3630–3633, IEEE, 2010.

[22] E. Israeli, S. Tsiper, D. Cohen, E. Shoshan, R. Hilgendorf, A. Reysenson, and Y. C. Eldar, "Hardware calibration of the modulated wideband converter," in *IEEE Glob, Commun. Conf.*, pp. 948–953, IEEE, 2014.

[23] D. Cohen, S. Tsiper, and Y. C. Eldar, "Analog to Digital Cognitive Radio: Sampling, Detection, and Hardware," *IEEE Sig. Process. Mag.*, vol. 35, no. 1, pp. 137–166, 2018.

[24] Mini-Circuits, *Surface Mount: Low Pass Filter SXLP -36+.* Mini-Circuits.

[25] J. Nuechterlein and P. Weiser, "Digital crossroads," *American Telecommunications Policy in the Internet Age, Cambridge (MA)*, 2005.

[26] N. Kaabouch, *Handbook of Research on Software-Defined and Cognitive Radio Technologies for Dynamic Spectrum Management.* IGI Glob. J., 2014.

[27] L. Lu, X. Zhou, U. Onunkwo, and G. Y. Li, "Ten years of research in spectrum sensing and sharing in cognitive radio," *EURASIP J. Wirel. Commu. and Network.*, vol. 2012, no. 1, p. 28, 2012.

[28] T. Yucek and H. Arslan, "A Survey of Spectrum Sensing Algorithms for Cognitive Radio Applications," *IEEE Commun. Surv. Tutorials*, vol. 11, no. 1, pp. 116–130, 2009.

[29] A. Ghasemi and E. S. Sousa, "Spectrum sensing in cognitive radio networks: requirements, challenges and design trade-offs," *IEEE Commun. Mag.*, vol. 46, no. 4, pp. 32–39, 2008.

[30] Ž. Tabaković, "A survey of cognitive radio systems," *Post Electron. Commun. Agency*, vol. 13, 2011.

[31] J. Mitola, "Software radios: Survey, critical evaluation and future directions," *IEEE Aerospace and Electron. Syst. Mag.*, vol. 8, no. 4, pp. 25–36, 1993.

[32] J. Mitola, "Cognitive radio architecture evolution," *Proc. IEEE*, vol. 97, no. 4, pp. 626–641, 2009.

[33] I. F. Akyildiz, W.-Y. Lee, and K. R. Chowdhury, "CRAHNs: Cognitive radio ad hoc networks," *AD hoc netw.*, vol. 7, no. 5, pp. 810–836, 2009.

[34] M. Marnat, *Radio frequency receivers based on compressive sampling for feature extraction in cognitive radio applications.* PhD thesis, 2018.

[35] N. Alliance, "Backhaul provisioning for LTE-advanced & Small Cells," 2014.

[36] X. Zhang, *Compressive Spectrum Sensing in Cognitive IoT.* PhD thesis, Queen Mary University of London, 2018.

[37] G. Hattab and D. Cabric, "Unlicensed Spectrum Sharing for Massive Internet-of-Things Communications," *ArXiv*, vol. abs/1903.01504, 2019.

[38] U. Raza, P. Kulkarni, and M. Sooriyabandara, "Low power wide area networks: An overview," *IEEE Commu. Surv. Tutorials*, vol. 19, no. 2, pp. 855–873, 2017.

[39] SIGFOX. `http://www.sigfox.com`, 2019.

[40] N. Sornin, M. Luis, T. Eirich, T. Kramp, and O. Hersent, "LoRaWAN Specification," *LoRa Alliance*, 2015.

[41] S. Grant, "3GPP Low Power Wide Area Technologies-GSMA White Paper," *gsma.com*, 2016.

[42] "Internet-of-Things (IoT)." `https://www.keysight.com/us/en/assets/7018-05035/posters/5992-1217.pdf`. KEYSIGHT Technologies, 2016.

[43] J. A. Ansere, G. Han, H. Wang, C. Choi, and C. Wu, "A Reliable Energy Efficient Dynamic Spectrum Sensing for Cognitive radio IoT Networks," *IEEE Internet of Things J.*, 2019.

[44] L. L. Nguyen, A. Fiche, R. Gautier, and E. Radoi, "Impacts of the transmitter signal key parameters on the Compressed Sensing spectrum reconstruction for IoT Cognitive Radio applications," *Asia-Pacific Conf. Commu.*, pp. 461–466, 2019.

[45] C. Herley and P. W. Wong, "Minimum rate sampling and reconstruction of signals with arbitrary frequency support," *IEEE Trans. Inform. Theory*, vol. 45, no. 5, pp. 1555–1564, 1999.

[46] R. Venkataramani and Y. Bresler, "Perfect reconstruction formulas and bounds on aliasing error in sub-Nyquist nonuniform sampling of multiband signals," *IEEE Trans. Inf. Theory*, vol. 46, pp. 2173–2183, Sept, 2000.

[47] M. Mishali and Y. C. Eldar, "Sub-Nyquist sampling: Bridging theory and practice," *IEEE Signal Process. Mag.*, vol. 28, no. 6, pp. 98–124, Nov,2011.

[48] M. Mishali and Y. C. Eldar, "Blind multiband signal reconstruction: Compressed sensing for analog signals," *IEEE Trans. on Sig. Process.*, vol. 57, no. 3, pp. 993–1009, 2009.

[49] L. L. Nguyen, R. Gautier, A. Fiche, G. Burel, and E. Radoi, "Digital compensation of lowpass filters imperfection in the Modulated Wideband Converter Compressed Sensing scheme for radio frequency monitoring," *Sig. Process.*, vol. 152, pp. 292–310, 2018.

[50] L. L. Nguyen, A. Fiche, R. Gautier, C. Canaff, E. Radoi, and G. Burel, "Implementation of Modulated Wideband Converter Compressed Sensing scheme based on COTS lowpass filter with amplitude and phase compensation for spectrum monitoring," in *IEEE Int. Conf. Advanced Video and Sig. Based Surveil.*, pp. 1–6, 2018.

[51] L. L. Nguyen, D. H. Nguyen, A. Fiche, T. Huynh, and R. Gautier, “Low-Bit Quantization Methods for Modulated Wideband Converter Compressed Sensing,” *IEEE Glob. Commu. Conf.*, 2019.

[52] M. Lustig, D. L. Donoho, J. M. Santos, and J. M. Pauly, “Compressed Sensing MRI,” *IEEE Sig. Process. Mag.*, vol. 25, no. 2, p. 72, 2008.

[53] Y.-S. Yoon and M. G. Amin, “Compressed Sensing technique for high-resolution radar imaging,” in *Sig. Process., Sensor Fusion, and Target Recog. XVII*, vol. 6968, p. 69681A, International Society for Optics and Photonics, 2008.

[54] Z. Tian and G. B. Giannakis, “Compressed sensing for wideband cognitive radios,” in *IEEE Int. Conf. Acoustics, Speech and Sig. Process.*, vol. 4, pp. IV–1357, IEEE, 2007.

[55] “Federal Communications Commission.” `https://www.fcc.gov`. Federal Communications Commission 445 12th Street SW, Washington, DC 20554.

[56] “The Directorate for Spectrum Control.” `https://www.anfr.fr/en/anfr/organisation/the-directorates/the-directorate-for-spectrum-control/`. The National Frequency Agency (ANFR).

[57] “CORRIDOR Project.” `https://corridor.ifsttar.fr/final_workshop.php`. IFSTTAR, 2012.

[58] B. Wang and K. R. Liu, “Advances in cognitive radio networks: A survey,” *IEEE J. Sel. Top. in Sig. Process.*, vol. 5, no. 1, pp. 5–23, 2010.

[59] E. Axell, G. Leus, E. G. Larsson, and H. V. Poor, “Spectrum sensing for cognitive radio: State-of-the-art and recent advances,” *IEEE Sig. Process. Mag.*, vol. 29, no. 3, pp. 101–116, 2012.

[60] F. Salahdine, N. Kaabouch, and H. El Ghazi, “Techniques for dealing with uncertainty in cognitive radio networks,” in *IEEE Ann. Comput. Commun. Works. Conf.*, pp. 1–6, IEEE, 2017.

[61] J. Wang, S. Feng, Q. Wu, X. Zheng, and Y. Xu, “Hierarchical cognition cycle for cognitive radio networks,” *China Commun.*, vol. 12, no. 1, pp. 108–121, 2015.

[62] F. Salahdine, “Compressive Spectrum Sensing for Cognitive Radio Networks,” *PhD Dissertation, National Institute of Posts and Telecommunications, Morocco*, 2018.

[63] A. Papoulis, “Generalized sampling expansion,” *IEEE Trans. Cir. and Sys.*, vol. 24, no. 11, pp. 652–654, 1977.

[64] M. A. Herman and T. Strohmer, "High-resolution radar via compressed sensing," *IEEE Trans. Sig. Process.*, vol. 57, no. 6, pp. 2275–2284, 2009.

[65] M. S. O. O. Alink, E. A. Klumperink, M. C. Soer, A. B. Kokkeler, and B. Nauta, "A 50mhz-to-1.5 ghz cross-correlation cmos spectrum analyzer for cognitive radio with 89dB sfdr in 1mhz rbw," in *IEEE Sympo. New Frontiers Dyna. Spec.*, pp. 1–6, IEEE, 2010.

[66] M. S. O. Alink, E. A. Klumperink, A. B. Kokkeler, M. C. Soer, G. J. Smit, and B. Nauta, "A cmos-compatible spectrum analyzer for cognitive radio exploiting crosscorrelation to improve linearity and noise performance," *IEEE Trans. Cir. Sys. I: Regular Papers*, vol. 59, no. 3, pp. 479–492, 2012.

[67] M. S. O. Alink, E. A. Klumperink, A. B. Kokkeler, Z. Ru, W. Cheng, and B. Nauta, "Using crosscorrelation to mitigate analog/rf impairments for integrated spectrum analyzers," *IEEE Trans. Microw. Theo. and Techni.*, vol. 61, no. 3, pp. 1327–1337, 2013.

[68] M. S. O. Alink, A. B. Kokkeler, E. A. Klumperink, G. J. Smit, and B. Nauta, "Spectrum sensing with high sensitivity and interferer robustness using cross-correlation energy detection," *IEEE J. Emerg. Sel. Top. Cir. and Sys.*, vol. 3, no. 4, pp. 566–575, 2013.

[69] A. Goel, B. Analui, and H. Hashemi, "A 130-nm cmos 100-hz–6-ghz reconfigurable vector signal analyzer and software-defined receiver," *IEEE Trans. Microw. Theo. and Techni.*, vol. 60, no. 5, pp. 1375–1389, 2012.

[70] J. Park, T. Song, J. Hur, S. M. Lee, J. Choi, K. Kim, K. Lim, C.-H. Lee, H. Kim, and J. Laskar, "A fully integrated uhf-band cmos receiver with multi-resolution spectrum sensing (mrss) functionality for ieee 802.22 cognitive radio applications," *IEEE J. of Solid-State Cir.*, vol. 44, no. 1, pp. 258–268, 2009.

[71] R. T. Yazicigil, T. Haque, M. R. Whalen, J. Yuan, J. Wright, and P. R. Kinget, "Wideband rapid interferer detector exploiting compressed sampling with a quadrature analog-to-information converter," *IEEE J. of Solid-State Cir.*, vol. 50, no. 12, pp. 3047–3064, 2015.

[72] D. Schneider, "New camera chip captures only what it needs," *IEEE Spectrum*, vol. 50, no. 3, pp. 13–14, 2013.

[73] M. F. Duarte, M. A. Davenport, D. Takhar, J. N. Laska, T. Sun, K. F. Kelly, and R. G. Baraniuk, "Single-pixel Imaging via Compressive Sampling," *IEEE Sig. Process. Mag.*, vol. 25, no. 2, pp. 83–91, 2008.

[74] G. Huang, H. Jiang, K. Matthews, and P. Wilford, "Lensless imaging by Compressive Sensing," in *IEEE Int. Conf. Image Process.*, pp. 2101–2105, IEEE, 2013.

[75] J. Wright, A. Y. Yang, A. Ganesh, S. S. Sastry, and Y. Ma, "Robust face recognition via sparse representation," *IEEE Trans. Pattern Analysis and Machine Intell.*, vol. 31, no. 2, pp. 210–227, 2008.

[76] S. R. Becker, *Practical Compressed Sensing: modern data acquisition and signal processing.* PhD thesis, California Institute of Technology, 2011.

[77] D. Chu, "Polyphase codes with good periodic correlation properties (corresp.)," *IEEE Trans. on Inf. theory*, vol. 18, no. 4, pp. 531–532, 1972.

[78] S. Kirolos, J. Laska, M. Wakin, M. Duarte, D. Baron, T. Ragheb, Y. Massoud, and R. Baraniuk, "Analog-to-information conversion via random demodulation," in *IEEE Dallas/CAS Works. Design, Appl., Integr. and Soft.*, pp. 71–74, 2006.

[79] P. Feng and Y. Bresler, "Spectrum-blind minimum-rate sampling and reconstruction of multiband signals," in *IEEE Int. Conf. Acoustics, Speech, and Sig. Process.*, vol. 3, pp. 1688–1691, 1996.

[80] R. Grigoryan, *Acquisition of Multi-Band Signals via Compressed Sensing.* PhD thesis, Ph. D. Thesis, Aalborg University, Aalborg, Denmark, 2015.

[81] Z. Yang, C. Zhang, J. Deng, and W. Lu, "Orthonormal expansion ℓ_1-minimization algorithms for compressed sensing," *IEEE Trans. Sig. Process.*, vol. 59, no. 12, pp. 6285–6290, 2011.

[82] Y. Zhang, "Theory of compressive sensing via ℓ_1-minimization: a non-rip analysis and extensions," *J. of the Operations Research Society of China*, vol. 1, no. 1, pp. 79–105, 2013.

[83] T. Blumensath, M. E. Davies, G. Rilling, Y. Eldar, and G. Kutyniok, "Greedy algorithms for compressed sensing," in *Compressed sensing: Theory and applications*, pp. 348–393, Cambridge Univ. Press, 2012.

[84] S. S. Chen, D. L. Donoho, and M. A. Saunders, "Atomic decomposition by basis pursuit," *SIAM review*, vol. 43, no. 1, pp. 129–159, 2001.

[85] S. Becker, J. Bobin, and E. J. Candès, "Nesta: A fast and accurate first-order method for sparse recovery," *SIAM J. on Imaging Sciences*, vol. 4, no. 1, pp. 1–39, 2011.

[86] S. R. Becker, E. J. Candès, and M. C. Grant, "Templates for convex cone problems with applications to sparse signal recovery," *Mathematical programming computation*, vol. 3, no. 3, p. 165, 2011.

[87] E. Van Den Berg and M. P. Friedlander, "Probing the pareto frontier for basis pursuit solutions," *SIAM Journal on Scientific Computing*, vol. 31, no. 2, pp. 890–912, 2008.

[88] J. A. Tropp and S. J. Wright, "Computational methods for sparse solution of linear inverse problems," *Proceed. of the IEEE*, vol. 98, no. 6, pp. 948–958, 2010.

[89] J. Tropp, A. C. Gilbert, *et al.*, "Signal recovery from partial information via orthogonal matching pursuit," *IEEE Trans. Inf. Theo.*, vol. 53, no. 12, pp. 4655–4666, 2007.

[90] J. A. Tropp, A. C. Gilbert, and M. J. Strauss, "Algorithms for simultaneous sparse approximation. part i: Greedy pursuit," *Sig. Process.*, vol. 86, no. 3, pp. 572–588, 2006.

[91] D. Needell and J. A. Tropp, "Cosamp: iterative signal recovery from incomplete and inaccurate samples," *Commun. of the ACM*, vol. 53, no. 12, pp. 93–100, 2010.

[92] T. Blumensath and M. E. Davies, "Iterative hard thresholding for compressed sensing," *Applied and Computational Harmonic Analysis*, vol. 27, no. 3, pp. 265–274, 2009.

[93] A. Maleki and D. L. Donoho, "Optimally tuned iterative reconstruction algorithms for compressed sensing," *IEEE J. Sel. Top. Sig. Process.*, vol. 4, no. 2, pp. 330–341, 2010.

[94] M. Mishali and E. Yonina, "Spectrum-blind sampling and reconstruction of multi-band signals," Mar. 19 2009. WO Patent App. PCT/IL2008/001,202.

[95] Y. Eldar, K. Gedalyahu, and R. Tur, "Multi-channel sampling of pulse streams at the rate of innovation," Nov. 3 2011. WO Patent App. PCT/IB2011/051,449.

[96] M. Mishali and Y. Eldar, "Efficient sampling and reconstruction of sparse multi-band signals," Aug. 26 2010. WO Patent App. PCT/IB2010/050,661.

[97] M. Mishali and E. Yonina, "Spectrum-blind sampling and reconstruction of multi-band signals," Oct. 4 2011. US Patent 8,032,085.

[98] Y. Eldar and E. Matusiak, "Sub-nyquist sampling of short pulses," July 25 2013. US Patent App. 13/824,369.

[99] J. A. Tropp, "Just relax: Convex programming methods for identifying sparse signals in noise," *IEEE Trans. Inform. Theo.*, vol. 52, no. 3, pp. 1030–1051, 2006.

[100] D. L. Donoho, M. Elad, and V. N. Temlyakov, "Stable recovery of sparse overcomplete representations in the presence of noise," *IEEE Trans. Inform. Theo.*, vol. 52, no. 1, pp. 6–18, 2006.

[101] L. Welch, "Lower bounds on the maximum cross correlation of signals," *IEEE Trans. on Inf. theory*, vol. 20, no. 3, pp. 397–399, 1974.

[102] M. Mishali and Y. C. Eldar, "Expected rip: Conditioning of the modulated wideband converter," in *IEEE Inform. Theo. Worksh.*, pp. 343–347, 2009.

[103] X. Yang *et al.*, *Research on compressed sensing and its applications in wireless communications.* PhD thesis, 2015.

[104] X. Yang, X. Tao, Y. Guo, X. Huang, and Q. Cui, "Subsampled circulant matrix based analogue compressed sensing," *Electronics letters*, vol. 48, no. 13, pp. 767–768, 2012.

[105] M. Marnat, M. Pelissier, O. Michel, and L. Ros, "Code properties analysis for the implementation of a Modulated Wideband Converter," in *25th European Sig. Proc. Conf. (EUSIPCO)*, pp. 2121–2125, IEEE, 2017.

[106] P. J. Davis, *Circulant matrices.* American Mathematical Soc., 2013.

[107] H. Akaike, "A new look at the statistical model identification," in *Sel. Papers of Hirotugu Akaike*, pp. 215–222, Springer, 1974.

[108] J. Rissanen, "Modeling by shortest data description," *Automatica*, vol. 14, no. 5, pp. 465–471, 1978.

[109] M. Wax and T. Kailath, "Detection of signals by information theoretic criteria," *IEEE Trans. on acoustics, speech, and signal processing*, vol. 33, no. 2, pp. 387–392, 1985.

[110] W. Chen, K. M. Wong, and J. P. Reilly, "Detection of the number of signals: A predicted eigen-threshold approach," *IEEE Trans. Sig. Process.*, vol. 39, no. 5, pp. 1088–1098, 1991.

[111] E. Radoi and A. Quinquis, "A New Method for Estimating the Number of Harmonic Components in Noise with Application in High Resolution Radar," *J. on Applied Sig. Process.*, pp. 1177–1188, 2004.

[112] L. A. T. C. R. P. Workgroup, "LoRaWAN 1.1 Regional Parameters," *LoRa Alliance*, 2018 January.

[113] W. Liu, X. Wang, S. Zhu, L. Zhu, and J. Yang, "Researches on the wideband spectrum sensing prototype system based on MWC," *Int. J. of Sig. Process. Sys.*, vol. 5, no. 2, pp. 70–74, 2017.

[114] W. Liu, Z. Huang, X. Wang, and W. Sun, "Design of a single channel Modulated Wideband Converter for wideband spectrum sensing: Theory, Architecture and Hardware implementation," *Sensors*, vol. 17, no. 5, p. 1035, 2017.

[115] D. Adams, Y. C. Eldar, and B. Murmann, "A mixer front end for a four-channel Modulated Wideband Converter with 62-db blocker rejection," *IEEE J. Solid-State Cir.*, vol. 52, no. 5, pp. 1286–1294, 2017.

[116] D. J. K. Adams, *A practical implementation of the Modulated Wideband Converter Compressive Sensing receiver architecture.* PhD thesis, Stanford University, 2016.

[117] E. Bedrosian and S. O. Rice, "The output properties of Volterra systems (nonlinear systems with memory) driven by harmonic and Gaussian inputs," *Proc. of the IEEE*, vol. 59, no. 12, pp. 1688–1707, 1971.

[118] A. Y. Kibangou and G. Favier, "Wiener-Hammerstein systems modeling using diagonal Volterra kernels coefficients," *IEEE Sig. Process. Letters*, vol. 13, no. 6, pp. 381–384, 2006.

[119] T. Blumensath, "Compressed Sensing with nonlinear observations and related nonlinear optimization problems," *IEEE Trans. Inf. Theory*, vol. 59, no. 6, pp. 3466–3474, 2013.

[120] D. S. Weller and V. K. Goyal, "On the estimation of nonrandom signal coefficients from jittered samples," *IEEE Trans. Sig. Proc.*, vol. 59, no. 2, pp. 587–597, 2010.

[121] "Xampling: Analog to digital at sub-nyquist rates." `http://webee.technion.ac.il/Sites/People/YoninaEldar/hardware_mwc.php`. Accessed: Oct 2019.

[122] Z. Yijiu, L. Ling, Z. Xiaoyan, and D. Zhijian, "Model calibration for compressive sampling system with non-ideal lowpass filter," in *IEEE Electron. Measur. & Instr.*, vol. 2, pp. 808–812, IEEE, 2015.

[123] K. V. Cartwright, P. Russell, and E. J. Kaminsky, "Finding the maximum magnitude response (gain) of second-order filters without calculus," *Latin American Journal of Physics Education*, p. 559, 2012.

[124] G. Bianchi and R. Sorrentino, *Electronic filter simulation & design.* McGraw-Hill New York, 2007.

[125] A. B. Williams and F. J. Taylor, *Electronic filter design handbook.* McGraw-Hill, 1995.

[126] L. D. Paarmann, *Design and analysis of analog filters: a signal processing perspective*, vol. 617. Springer Science & Business Media, 2001.

[127] R. H. Walden, "Analog-to-Digital Converter survey and analysis," *IEEE J. Sel. areas in Commun.*, vol. 17, no. 4, pp. 539–550, 1999.

[128] B. Le, T. W. Rondeau, J. H. Reed, and C. W. Bostian, "Analog-to-digital converters," *IEEE Sig. Process. Mag.*, vol. 22, no. 6, pp. 69–77, 2005.

[129] T. Instruments, "Choose the right A/D converter for your application," *Texas Instruments*, 2016.

[130] W. Kester, "ADC Architectures II: Successive Approximation ADCs," *MT-021 Tutorial, Analog Devices*, 2009.

[131] W. Kester, "ADC Architectures III: Sigma-Delta ADC basics," *Analog Devices, MT022*, 2008.

[132] A. N. Maxim, "Understanding Pipelined ADCs," 2001.

[133] W. Kester, "Which ADC architecture is right for your application," in *EDA Tech Forum*, vol. 2, pp. 22–25, 2005.

[134] "A/D Converters." `http://www.analog.com/static/imported-files/data_sheets/AD9057.pdf`. Analog Devices Corp., 2003.

[135] M. Mishali and Y. C. Eldar, "Xampling: Compressed sensing for analog signals," in *Compressed Sensing: Theory and Applications*, no. 3, Cambridge University Press, 2012.

[136] "A/D Converters." `http://www.analog.com/en/analog-to-digital-converters/ad-converters/products/index.html`. Analog Devices Corp., 2009.

[137] "Data Converters." `http://focus.ti.com/analog/docs/dataconvertershome.tsp`. Texas Instruments Corp., 2009.

[138] A. Kipnis, A. J. Goldsmith, and Y. C. Eldar, "Optimal trade-off between sampling rate and quantization precision in sigma-delta A/D conversion," in *2015 Int. Conf. Sampling Theory and Applications (SampTA)*, pp. 627–631, IEEE, 2015.

[139] "RF Agile Transceiver." `https://www.analog.com/media/en/technical-documentation/data-sheets/AD9361.pdf`. Analog Devices Corp., 2013-2016.

[140] J. C. Candy, "Oversampling methods for A/D and D/A conversion," *Oversampling Delta-Sigma Data converters*, 1991.

[141] J. Max, "Quantizing for minimum distortion," *IRE Trans. Inf. Theory*, vol. 6, no. 1, pp. 7–12, 1960.

[142] W. R. Bennett, "Spectra of quantized signals," *The Bell System Technical Journal*, vol. 27, no. 3, pp. 446–472, 1948.

[143] M. José, "Sigma-Delta Modulators: Tutorial overview, design guide, and state-of-the-art survey," *IEEE Trans. Circuits and Systems I: Regular Papers*, vol. 58, no. 1, pp. 1–21, 2011.

[144] S. Park, "Principles of Sigma-Delta modulation for Analog-to-Digital Converters," 1999.

[145] P. M. Aziz, H. V. Sorensen, and J. Vn der Spiegel, "An overview of Sigma-Delta converters," *IEEE Sig. Process. Magaz.*, vol. 13, no. 1, pp. 61–84, 1996.

DOCTORAT
BRETAGNE
LOIRE / MATHSTIC

Université de Bretagne Occidentale

Titre : Apports de la théorie de l'information et de l'échantillonnage compressé pour la surveillance du spectre

Mot clés : Modulated Wideband Converter, surveillance de spectre, acquisition compressée

Résumé : Cette thèse a pour but d'exploiter l'état de l'art du Modulated Wideband Converter (MWC) et de l'acquisition compressée afin de surveiller et de détecter un spectre radiofréquence large bande, sans aucune connaissance a priori du signal d'entrée et de son support fréquentiel. Un prototype d'échantillonnage compressé basé sur le MWC développé par l'équipe CACS/COM du Lab-STICC est brièvement présenté. Les principaux objectifs de cette thèse est d'identifier l'impact des composants analogiques du prototype sur les sorties du MWC et de proposer des solutions afin de corriger les défauts de chaque composant indépendamment des autres. Une méthode de compensation numérique en amplitude et en phase est proposée et appliquée après l'étape de filtrage passe-bas pour obtenir une sortie proche du filtre passe-bas idéal. Ensuite, plusieurs types de convertisseurs analogiques numériques faible nombre de bits ont été recensés et combinés au MWC en simulation. Les résultats de reconstruction spectrale sont ensuite évalués à partir des taux de bonne reconstruction et de fausse alarme. Cette thèse aborde également l'influence des paramètres clés d'un signal large bande (résolution fréquentielle, largeur de bande, etc.) sur la reconstruction spectrale, notamment pour des applications de l'Internet des Objets (IoT).

Title: Contributions of Information Theory and Compressed Sampling to Spectrum Monitoring

Keywords: Modulated Wideband Converter, spectrum sensing, compressed sensing

Abstract: This thesis aims to exploit the state-of-art of the Modulated Wideband Converter (MWC) and Compressed Sensing (CS) technology, to monitor and detect a wideband spectrum, without any knowledge of the input signal and its frequency support. A prototype of compressed sensing based on the MWC scheme and developed by the CACS/COM team of Lab-STICC is briefly introduced. Addressing the impacts of analog components imperfections on the MWC output, then proposing solution to overcome them by studying each component independently, are the main objectives of this thesis. A digital post-processing scheme with amplitude and phase compensation is proposed and applied after real lowpass filtering step to achieve the filtered output as close as the ideal one. Then, several real types of Analog-to-Digital Converter (ADC) with low-bit quantization are presented and combined to the MWC in simulation. The results of spectrum reconstruction are then evaluated with respect to a proposed criterion of correct reconstruction rate and false alarm rate. This thesis goes on dealing with the influence of wideband signal key parameters (frequency resolution, bandwidths, etc.) on its spectrum reconstruction, especially for Internet-of-Things (IoT) applications.